THE ROLE OF TUMOR SUPPRESSOR GENES P53 AND NF1 IN NEURAL STEM CELLS AND BRAIN TUMOR DEVELOPMENT

By

Yuan Wang

A dissertation submitted in partial fulfillment
of the requirements for the degree of
Doctor of Philosophy
(Cell and Developmental Biology)
in The University of Michigan
2011

Doctoral Committee:

Associate Professor Yuan Zhu, Chair
Professor Andrzej A. Dlugosz
Professor K. Sue O'Shea
Professor Jack M. Parent
Assistant Professor Xing Fan

Dedication

This thesis is dedicated to patients who suffer from glioma and neurofibromatosis disease.

Acknowledgements

I would like to thank Dr. Jiong Yang for his collaboration in the p53 part of this thesis. He has initially set up the mouse cross, collected tumor samples and performed extensive analysis on end-stage tumors. Dr. Xiaojing Wang should also be acknowledged for her participation in the *Nf1* part of this thesis.

This thesis would not be possible without the extensive guidance and support from my supervisor Dr. Yuan Zhu. He has been a role model throughout my Ph.D. training, and provided valuable suggestions for my scientific research and everyday life.

I would like to acknowledge my thesis committee members, who have been very supportive through the years, and particularly in the thesis defense process.

Finally, I very much appreciate the support from current and past members of the Zhu Lab. My fellow student Lou Chang made significant contributions to my thesis revision. And special thanks go to Jerry Tomasek, Dr. Huarui Zheng and Edward Kim for their participation in various experiments.

Table of Contents

List of figures

Abstract

THE ROLE OF TUMOR SUPPRESSOR GENES P53 AND NF1 IN NEURAL STEM CELLS AND BRAIN TUMOR DEVELOPMENT

By

Yuan Wang

Chair: Yuan Zhu

Glioblastoma multiforme (GBM) is the most frequent and infiltrative neoplasm among human primary brain tumors. Highly resistant to conventional radiation and chemotherapy, GBM is one of the most deadly human cancers with a median survival of 12 months that has remained unimproved over the past two decades. Recent studies have identified that tumor suppressor genes TP53 and Neurofibromatosis Type 1 (NF1) are two of the most frequently mutated genes in human GBM. However, how deficiency in these tumor suppressor genes transforms normal brain cells into malignancy is not yet understood. Further, the cell of origin for glioma remains largely unknown.

This thesis work utilizes transgenic mouse models to understand the role of p53 and *Nf1* in normal neural stem/progenitor cell function and how inactivation of these genes transforms neural stem/progenitor cells and leads to neurological diseases. In the p53 model, p53 deficiency is sufficient for glioma formation by allowing the accumulation of cooperative oncogenic alterations. In addition, the accumulation of mutant p53 protein can be used to trace the early lesions in the brain, which occur first in neural stem cells in

the subventricular zone (SVZ) stem cell niche. Subsequent expansion of mutant p53-expressing transit-amplifying progenitor-like cells in the SVZ-associated areas initiates glioma formation. This study establishes a critical role of p53 deficiency in gliomagenesis, and provides insight into the cell-of-origin for glioma. In the *Nf1* mouse model, *Nf1* deficiency alone is insufficient for glioma formation and only appears to confer a transient growth advantage to neural progenitor cells during development, which does not persist into adulthood. The critical role of *Nf1* is to regulate neuron/glia fate determination of neural progenitor cells. Bi-allelic *Nf1* inactivation causes ectopic Olig2 expression specifically in transit-amplifying progenitors, causing increased gliogenesis at the expense of neurogenesis. In addition, *Nf1*-deficient brains exhibit enlarged corpus callosum, a structural defect recently linked to NF1-associated learning disabilities. These NF1-associated developmental defects can be reversed by treatment with a MEK inhibitor during neonatal stages. Together, this study not only provides insights into fate-determination of SVZ progenitor cells, but also identifies a potential therapeutic window for treating NF1-associated brain abnormalities.

Chapter I Introduction

Glioblastoma (grade IV malignant astrocytic glioma), also known as glioblastoma multiforme (GBM), is the most frequent and malignant neoplasm among human primary brain tumors. GBM is highly infiltrative to surrounding normal brain tissues, a trait that prevents complete surgical resection. Furthermore, GBM is invariably resistant to conventional radiation and chemotherapy. As a consequence, GBM is one of the most deadly human cancers with a median survival of 12 months that has remained unimproved over the past two decades (Zhu and Parada 2002; Furnari et al. 2007; Louis 2007). It is therefore important to develop novel therapies based on a greater understanding of the cellular and molecular mechanisms underlying gliomagenesis. As reflected by its name (multiforme), GBM contains diverse cell populations with extreme morphological, genomic and transcriptional heterogeneity (Jung et al. 1999; Maher et al. 2001; Furnari et al. 2007; The Cancer Genome Atlas Research Network, 2008). This unique feature of GBM raises one of the most difficult questions regarding GBM pathogenesis: how a normal brain cell acquires genetic mutations that lead to generation of a cancer with such diverse cell populations exhibiting the characteristics of stem cells, progenitor cells and differentiated cells. The most straightforward hypothesis for this question is that the cell-of-origin of GBM is a multipotent neural stem cell, as stem cells do not need to acquire the capacities of self-renewal (replicating themselves) and multipotency (generating multilineage cells). However, it is worth noting that it is also possible for progenitor cells or fully differentiated brain cells to gain stem cell characteristics as a result of acquired mutations. One of the important recent advances in cancer research is the development of the cancer stem cell hypothesis, which is based on the observations that a subset of tumor cells exhibit stem cell characteristics, self-renewal and mulitpotency, and more importantly, possess higher tumorgenic capacities (Bonnet and Dick 1997; Reya et al. 2001; Wicha et al. 2006; Stiles and Rowitch 2008). The major objective of my thesis is to understand the mechanisms by which normal brain cells

acquires genetic mutations and become GBM cells with stem cell characteristics. A few years ago, my thesis adviser, Dr. Yuan Zhu, developed a series of genetically engineered mouse (GEM) models with mutations in p53 and Neurofibromatosis type 1 (*Nf1*) tumor suppressor genes. These p53/*Nf1* GEM models developed malignant astrocytic gliomas with nearly complete penetrance (Zhu et al. 2005b). More importantly, malignant astrocytic gliomas in the p53/*Nf1* GEM models appear to arise from and cluster around the subventricular zone (SVZ) stem cell niche, where multipotent neural stem cells and other neural progenitor cells reside (Zhu et al. 2005b). Based on these observations, we propose the hypothesis that p53 and *Nf1* tumor suppressor genes cooperatively transform cells in the SVZ stem cell lineages in adult brain. In other words, this hypothesis suggests that SVZ cells are a cell-of-origin of malignant astrocytic gliomas driven by p53 and *Nf1* mutations. To test this hypothesis, my thesis has focused on determining the role of p53 and *Nf1* in the regulation of SVZ stem cell function in the developing and adult brain. In this Chapter, I will provide important background information regarding glioma biology, cancer stem cell hypothesis and cell-of-origin of glioma, GBM core pathways, p53 and NF1 tumor suppressor genes, as well as neural stem cell biology.

1.1 Glioma and its classification

In vertebrates, the embryonic neural tube gives rise to three major cell types in the central nervous system (CNS): neurons, astrocytes and oligodendrocytes. The latter two are collectively called glial cells. Tumors that arise in the CNS are classified mainly based on the predominant cell types, determined by morphological and histological criteria. Tumors that exhibit glial cell features are therefore termed glioma which account for the majority of adult neurological tumors (Zhu and Parada 2002; Furnari et al. 2007; Louis 2007). Gliomas can be further subclassified into astrocytoma, oligodendroglioma and oligoastrocytoma (also known as mixed gliomas), which are based on the proportion of tumor cells resembling astrocytes, oligodendrocytes or both, respectively (Maher et al. 2001; Zhu and Parada 2002; Furnari et al. 2007; Louis 2007).

The World Health Organization classifies gliomas into grade I-V based on the malignancy and histopathological criteria (Zhu and Parada 2002; Furnari et al. 2007;

Louis 2007). Grade I gliomas are generally benign, whereas Grade II-V are malignant and infiltrative. Among all types of gliomas, astrocytomas are the most common CNS neoplasms, which account for more than 60% of all primary brain tumors. Grade IV malignant astrocytic glioma (glioblastoma), also known as glioblastoma multiforme (GBM), is the most frequent and infiltrative neoplasm among human primary brain tumors. There are two subtypes of glioblastoma. Primary glioblastoma arises de novo with no evidence of pre-existing lesions whereas secondary glioblastoma develops progressively from lower-grade gliomas. Despite their differences in the clinical courses and molecular lesions, primary and secondary GBMs exhibit the same histopathological and clinical features. The median survival for glioblastoma patients is less than one year, which has not improved over the past two decades (Maher et al. 2001; Zhu and Parada 2002; Furnari et al. 2007; Louis 2007). This presents a major challenge to clinical oncologists and cancer researchers and calls for a greater understanding of the cellular and molecular basis for gliomagenesis.

1.2 Strategies for glioma mouse modeling

Much of our current understanding of glioma comes from the study of glioma mouse modeling. There are four major strategies to induce glioma formation in mice: chemical mutagen-induced models, xenograft or allograft transplantation models, tissue specific genetic models and retroviral infection models. Each of these strategies has its strength and limitations. Treatment with mutagens such as DNA alkylating agents could randomly generate point mutations and induce glioma in mice histologically similar to human glioma (Barth 1998), however, it is hard to define which genetic alteration or which cell type is responsible for glioma development. Xenograft or allograft transplantation models have been widely used in preclinical trials for glioma treatment (Plate et al. 1993; Kondo et al. 1998). In these models, cultured human or rodent glioma cell lines are injected into the brain of nude mice. These cells give rise to glioma in mice at a predictable rate with high tumor penetrance. However, the treatment response in mice could not be directly applied in humans since tumor microenvironment could be drastically different in mice compared to humans. Also these transplantation models do not recapitulate the tumorigenesis process and provide little information about the *de novo* development of

glioma. Both mutagen induced models and transplantation models are modeling glioma formation with undefined genetic alterations. With the advancement in our understanding of the molecular genetics of glioma, it is applicable to model glioma through recapitulation of the genetic events during gliomagenesis by germline or tissue specific genetic modifications (Reilly et al. 2000; Zhu et al. 2005a; Alcantara Llaguno et al. 2009). Gain-of-function or loss-of-function germline modifications can be achieved by transgenic or gene targeting techniques. Gain of function mutations could be mimicked by overexpression of oncogenes, and loss of function mutations could be achieved by targeted deletion of tumor suppressors. This strategy tests the transformation competence of the activation of certain signaling pathways and allows the assessment of cooperative effects between different oncogenes and tumor suppressor genes. However, germline mutations could potentially lead to developmental defects and embryonic lethality. Tissue specific glioma models circumvent this caveat by targeting restricted population of cells with the Cre/LoxP system (Sauer 1998). This strategy could also provide significant insight into which cell type(s) is most susceptible for malignant transformation. The limitation of germline/tissue specific glioma models lies in the fact that it only mimics one possible genetic setting for gliomagenesis and may only represent a subset of gliomas driven by specific genetic mutations. The last strategy for glioma modeling is regional specific genetic modification using retroviral vectors (Holland et al. 2000; Alcantara Llaguno et al. 2009; Jacques et al. 2010). This strategy introduces genetic modifications through retroviral infection and targets the cells within a specific region of the brain (e.g. SVZ). This technique can be used to assess the relative tumorigenic capacity of cells from different regions of the brain.

1.3 Cancer stem cell hypothesis and cell-of-origin for brain tumor

The extreme heterogeneity within the tumor, along with the highly proliferative nature of cancer cells leads to a straightforward hypothesis that cancer might arise from a rare population of cells with stem cell properties: self-renewal and multipotency. This concept was first proposed about 150 years ago (Cohnheim 1867; Durante 1874; Cohnheim 1875; Wicha et al. 2006). Over 40 years ago, it was further specified that tissue-specific stem

cells may be the cell-of-origin of cancer (Till and Mc 1961; Wicha et al. 2006). *In vitro* "clonogenic assays" supported this notion by showing that a subpopulation of tumor cells isolated from tumor specimens has higher proliferative capacity in colony formation assays (Reya et al. 2001). However, this hypothesis has not been directly tested until recently due to the technical difficulties to directly measure and compare the self-renewal capacity of different sub-population of cancer cells.

Recent advances in stem cell biology and the development of new animal models allows the direct test of the validity of this hypothesis. Various studies have revealed that within tumors there are a subset of tumor cells which exhibit stem cell characteristics: self-renewal and mulitpotency (Bonnet and Dick 1997; Holyoake et al. 1999; Cobaleda et al. 2000; Al-Hajj et al. 2003; Hope et al. 2003; Singh et al. 2003) These stem-like cells, also referred to as cancer stem cells (CSCs), tumor-initiating cells or tumor-propagating cells, show higher tumor-initiating capacity in transplantation assays than non-CSCs and are more resistant to radiation therapy (Bao et al. 2006). These observations lead to the central hypothesis of cancer stem cell theory: in contrary to traditional belief that all cancer cells share the same tumorigenic capacity, solid and liquid tumors are composed of 1) a relatively small population of slowly cycling cells that undergo self-renewal to sustain and expand the tumors and 2) a larger population of cells that are fate-committed and have finite division capacity, forming a hierarchy of cells that is reminiscent of the relationship between stem cells and differentiated cells. Based on the cancer stem cell hypothesis, the reason why cancer therapies frequently fail is because they are targeting the wrong cell types. While radiation and chemotherapy could effectively eliminate large numbers of actively proliferating cancer cells, the slowly-proliferating cancer stem cells remain and could re-propagate the tumors (Wicha et al. 2006; Stiles and Rowitch 2008).

CSCs were first identified in liquid tumor leukemia (Bonnet and Dick 1997; Holyoake et al. 1999; Cobaleda et al. 2000; Hope et al. 2003), and later in solid tumors including brain tumors (Al-Hajj et al. 2003; Singh et al. 2003). Singh et al. reported that a group of cells that express the cell surface marker CD133 may represent brain tumor stem cells (Singh et al. 2003). These $CD133^{+}$ cells express neural stem cell markers and have the unique

capacity to form tumors when transplanted into immunodeficient mice and are capable of forming multipotent neurospheres in culture (Singh et al. 2004). Additional studies suggest that $CD133^+$ glioma cells are more radioresistant and angiogenic than $CD133^-$ tumor cells, which further supports the cancer stem cell hypothesis (Bao et al. 2006). The potential caveats for these studies include that $CD133^+$ cells may not represent the entire population of glioma stem cells. Some gliomas contain self-renewing, multipotent cells that are $CD133^-$ (Beier et al. 2007). Furthermore, CD133 also labels non-CSCs such as ependymal cells (Pfenninger et al. 2007). Finally, in xenograft models the recipient mouse brain may represent a selective microenvironment that favors the survival of certain cell types and the number of cells that are capable of initiating tumors is underestimated. The last argument has been supported by studies in melanoma xenograft models in which a much larger proportion of melanoma cells exhibit tumorigenic capacity in optimized host environment. Quintana et al found that while only $\sim$1 in a million melanoma cells form tumors in immunocompromised NOD/SCID mice, when co-injected with matrigel (a gelatinous protein mixture secreted by mouse sarcoma cells which mimics the complex extracellular environment), 1 in 4 melanoma cells can form tumors in NOD/SCID IL2Rγ^{null} mice which lack T, B, and natural killer cells and bypass xenogeneic immune responses(Quintana et al. 2008). Whether this happens in brain tumor xenograft models is still under investigation.

CSC hypothesis provides a novel framework to address the mechanism underlying gliomagenesis. By identifying and characterizing the CSC population in glioblastomas, novel therapies may be developed to eradicate this population of cells. Similarly, the identification of the tumor initiating cells may provide earlier diagnosis and/or prophylactic therapies to susceptible patients. Despite the controversies regarding the frequency of CSCs among human cancers, the striking similarity between brain tumor stem cells (BTSCs) and normal neural stem cells raises an interesting question whether these BTSCs, or brain tumors in general, are derived from neural stem cells. However, the stem cell characteristics of BTSCs cannot serve as direct evidence for its developmental origin, because theoretically, more differentiated cells could acquire oncogenic mutations and dedifferentiate into stem-like cells. At least three types of cells

could in principle serve as the cell-of-origin for malignant glioma: (1) mature dedifferentiated cells, (2) lineage-restricted neural progenitors that are normally unipotent, and (3) multipotent neural progenitors.

Recent studies provided several lines of evidences to suggest multipotent neural progenitors are the cell-of-origin. The first line of evidence comes from signaling analysis in neural stem cells and brain cancers. Activation of similar signaling pathways has been identified in both neural progenitors and cancer cells. Notch signaling, which promotes formation of radial glial and survival of neural stem cells (Gaiano et al. 2000; Androutsellis-Theotokis et al. 2006), is constitutively activated in high grade gliomas and glioma cell lines and is required for the maintenance of $CD133^+$ cells in GBM (Purow et al. 2005; Fan et al. 2010). Mitogenic signals that promote neural progenitor cell proliferation through EGF, FGF, PDGF and LIF, and their respective receptors, are commonly identified in gliomas (Kesari et al. 2005; Stiles and Rowitch 2008). The phosphatidylinositol-3-OH kinase (PI3K) signaling pathway, which is responsible for metabolism and survival, is also activated in high grade gliomas (Samuels et al. 2004). All these signaling analyses indicate that neural progenitors and tumors share common regulatory mechanisms. The second line of evidence comes from glioma mouse models. If multipotent neural progenitors are the cell-of-origin for gliomas, the predication will be that neural progenitors are competent for malignant transformation by mutations found in human GBMs. In 2005, Zhu et al. developed an *in vivo* glioma mouse model by targeting two tumor suppressors p53 and *Nf1* (Zhu et al. 2005b). In this model, they used a Cre transgene driven by human glial fibrillary acidic protein (hGFAP) promoter to introduce p53 and *Nf1* mutations into developing radial glia, and found high brain tumor penetrance among these mice. Under this genetic targeting strategy, all the radial-glia-derived progeny, including adult neural stem/progenitors and well differentiated neurons and glia carry the same p53/*Nf1* mutations. Nevertheless, based on Magnetic Resonance Imaging (MRI) analysis and histological studies, p53/*Nf1* gliomas appear to initiate and cluster around the SVZ stem cell niche, supporting the notion that SVZ neural progenitors are the cell-of-origin for brain tumors. The competence of SVZ progenitors to undergo malignant transformation was further demonstrated by Alcantara Llaguno et al. in 2009.

They employed adenovirus-mediated Cre expression in the adult SVZ, along with a tamoxifen (TM)-inducible Cre system, to specifically target p53/*Nf1*/Pten mutations into adult neural SVZ stem and progenitor cells. The targeted deletion of these tumor suppressors in the SVZ resulted in efficient gliomagenesis, while targeted deletion in the cortex where mature cell reside did not (Alcantara Llaguno et al. 2009). Together these observations suggest that a population of cells residing in the SVZ is the cell-of-origin for gliomas.

Although signaling analysis and glioma mouse models favor multipotent neural progenitors as the cell-of-origin, definitive evidence is lacking. The signaling comparison is flawed due to the fact that tumor cells have accumulated numerous mutations and the signaling profiles cannot be directly linked to the cell-of-origin. The study in mouse models cannot distinguish between various types of neural SVZ stem and progenitor populations, because based on current Cre/LoxP conditional knockout system, targeting the stem cells will inevitably target all the progeny derived from stem cells. In addition, there is no reliable marker to detect the earliest glioma cells in the brain, and the lack of lineage-tracing makes it extremely difficult to conclude which type(s) of cells are the cell-of-origin.

1.4 Glioma core pathways and the role of tumor suppressors in gliomagenesis

If neural stem/progenitor cells are the cell-of-origin for brain tumors, the immediate question is how normal cells undergo malignant transformation to become tumor-initiating cells. Recent large-scale cancer genome analysis [e.g. The Cancer Genome Atlas (TCGA)] has systematically identified genes and pathways that are altered in human GBM and provided significant insights into the molecular mechanism of gliomagenesis. In particular, they identified three core pathways that must be deregulated for primary GBMs to form: retinoblastoma protein RB, p53, and RTK/Ras/PI3K pathways. Rb signaling is responsible for preventing excessive cell growth by inhibiting cell cycle progression, and is altered in 78% of human glioblastomas (The Cancer Genome Atlas Research Network, 2008). In the p53 glioma core pathway, tumor

suppressor p53 is the key player, which is often referred to as “the guardian of genome” due to its critical role in regulating cell cycle progression and inducing apoptosis (programmed cell death) or senescence (cell aging, loss of replication capacity) in response to cellular stress (i.e. DNA damage and oncogenic mutations) (Vogelstein et al. 2000). In humans, p53 is encoded by the TP53 gene. 87% of human glioblastoma have mutations in the p53 pathway, and between 30 to 40% of primary glioblastomas have mutations in the TP53 gene (The Cancer Genome Atlas Research Network, 2008). Consistently, individuals with Li-Fraumeni syndrome, a familiar cancer syndrome caused by the presence of a germ-line mutation in the TP53 gene, are predisposed to development of astrocytic gliomas (Louis 2007). In secondary GBM, TP53 mutations are among the earliest genetic mutations. Importantly, the frequencies of TP53 mutations are equally high among grade II (59%), grade III (53%), and grade IV malignant gliomas (65%), suggesting that TP53 mutations play a critical role in the early stage of gliomagenesis (Ohgaki et al. 2004).

RTK/Ras/PI3K signaling, which is required for cell growth and metabolism, are hyperactivated in glioma cells and genetic alterations in this pathway occur in 88% of human GBMs (The Cancer Genome Atlas Research Network, 2008). Neurofibromin, which contains a functional domain homologous to Ras GTPase activating protein (GAP) family members, negatively regulates RTK/Ras signaling pathways by accelerating the conversion of active Ras-GTP to inactive Ras-GDP (Ballester et al. 1990; Xu et al. 1990). Neurofibromin is encoded by the NF1 gene, which is named after a familiar cancer syndrome, Von Recklinghausen’s neurofibromatosis type 1 (NF1). Each year, 1 out of 3000 newborns suffer from NF1 disease. NF1 patients are predisposed to developing benign and malignant tumors in central and peripheral nervous system (Listernick et al. 1999). Consistently, cancer genome atlas found that 15% to 20% of human primary GBMs harbor NF1 mutations (The Cancer Genome Atlas Research Network, 2008). It is worth noting that NF1 patients also develop non-tumor related phenotypes, including macrocephaly, astrogliosis and cognitive deficits (Hyman et al. 2005). In terms of cognitive deficits, NF1 belongs to a group of neurological disorders termed neuro-cardio-facial-cutaneous-syndromes (NCFC), caused by germline mutations in the Ras/ERK

signaling pathway (Bentires-Alj et al. 2006; Denayer and Legius 2007). (More information about NF1 and NCFC will be discussed in Chapter III introduction section). Therefore, investigating the role of *Nf1* in neural cells will not only advance our understanding of brain tumor development, but also provide insights into these non-tumor related brain pathology.

Of note, TP53 and NF1 are among the top five mutated genes in human GBMs (The Cancer Genome Atlas Research Network, 2008). These signaling pathways are tightly regulated in normal brain cells but apparently deregulated in tumors. How these signaling alterations singly and cooperatively contribute to gliomagenesis remains to be determined.

1.5 The significance of studying tumor suppressor function in neural stem cells

Identification of brain tumor cell-of-origin will not only facilitate early diagnosis of the tumors, but also provide a potential therapeutic target to treat the deadly disease at its infancy. Since early stage tumor cells are generally considered genetically more stable and may share the same oncogenic mutations, targeting these tumor-initiating cells will be easier than targeting end-stage tumor cells which have already accumulated numerous mutations and exhibit disruptions in various signaling pathways (Jung et al. 1999; Maher et al. 2001; Furnari et al. 2007; The Cancer Genome Atlas Research Network, 2008). However, given the technical difficulties in defining cell-of-origin of brain cancers as discussed in section 1.3, I took an indirect approach to study the hypothesis of whether neural stem cell are a cell-of-origin of malignant astrocytic gliomas. Specifically, if this hypothesis is correct, I expect that the critical tumor suppressor genes that are frequently inactivated in human glioblastoma (e.g. TP53 and NF1) must play an important role in regulating normal neural stem cell function. More specifically, my thesis attempted to address a more testable hypothesis that p53 and *Nf1* play a critical role in regulating self-renewal, proliferation, survival and differentiation of neural stem cells. This will not only provide insights into gliomagenesis but also address fundamental questions of neural stem cell biology.

To investigate how p53 and *Nf1* regulate neural stem cell function, it is essential to understand the developmental origin of neural stem cells and how they give rise to multi-lineage progeny in the brain. I will dedicate the second half of my introduction chapter to a brief review of different aspects of neural stem cell biology.

1.6 Methodology for labeling and characterization of neural stem/progenitor cells

In mammals, neural stem cells are a unique population of self-renewing, multipotent cells that are capable of generating nerve cells (neurons) and glial cells (the supporting elements) in the CNS throughout life. The advancement in neural stem cell biology is achieved through technical innovations to study neural stem cell function and neurogenesis/gliogenesis *in vitro* and *in vivo*. Major techniques widely used in the field are summarized below:

Nucleotide analog labeling: *In vivo* analysis of neural progenitor cell proliferation and differentiation is first achieved by using nucleotide analogs to label mitotic cells. In the 1950s, exogenous nucleotide [H^3]-thymidine was introduced to mark dividing cells, which incorporates into newly synthesized DNA during the S-phase of cell cycle and can be passed down to the progeny of the mitotic cells. [H^3]-thymidine could be later visualized through autoradiographic detection (Sidman et al. 1959). The generation of new neurons was first reported using [H^3]-thymidine labeling in three-day old mouse brains (Smart 1961). In the 1980s, bromodeoxyuridine (BrdU), a synthetic thymidine analog, was introduced as another S-phase marker of the cell cycle (Gratzner 1982). Since BrdU could be easily detected by immunohistochemistry and colocalized with other cell markers by immunofluorescence, BrdU has become the most commonly used method in the field for phenotypic and quantitative analysis of neural progenitors and their progeny. Short-term pulse labeling with nuclear analogs is used to analyze cell proliferation. Since the amount of analogs incorporated from a single injection is diluted during each cell cycle and may become undetectable after three or more cell divisions, in a long-term pulse-chase experiment, only cells that exit cell cycle shortly after the pulse

can retain the nucleotide analog labeling. Therefore, long-term pulse-chase with nuclear analogs can be used to label newly differentiated cells or slowing dividing cells, such as neural stem cells. The major limitation of this approach is that it cannot be used to label live cells, because the visualization of [H^3]-thymidine requires autoradiography and the detection of BrdU requires tissue fixation and DNA denaturation.

Retroviral/lentiviral labeling: Another approach to label mitotic cells is retroviral labeling. For retroviruses which lack nuclear import mechanisms, integration of viral DNA into host cell DNA can only occur in cells that undergo mitosis and break down their nuclear membrane (Lewis and Emerman 1994). Therefore, expression of transgenes carried by retroviruses may only occur in mitotic cells and their progeny. Expression of a live reporter, such as green fluorescence protein (GFP), allows live cell imaging to analyze neural progenitor cell proliferation and differentiation. In contrast to retroviruses, lentiviruses can perform viral integration into host genome at any time of the cell cycle and could be used to label relatively quiescent cells such as neural stem cells (Zufferey et al. 1998). Both retroviral and lentiviral labeling are based on genetic modifications and are thus applicable for long-term lineage tracing. In addition, retroviral/lentiviral infection could also be used to deliver Cre-recombinase or small interfering RNA (siRNA) to specifically knockout/knockdown genes in a restricted population of cells. The drawback of this techinique is that it requires invasive stereotaxic injection into specific brain regions and triggers inflammatory responses which may complicate the interpretation of the results.

Specific marker expression: The most straightforward approach to label neural progenitors and their progeny *in vivo* is to introduce transgenic reporters under the control of specific promoters that only express in desired cell population(s). For example, in Nestin-GFP transgenic mice, all the Nestin-expressing neural stem/progenitor cells can be visualized by their GFP expression (Yamaguchi et al. 2000). However, this approach only transiently labels cells that express specific markers. As the cells differentiate and lose the immature markers, it is impossible to track the same population of cells. Thus, this approach by itself cannot be used for lineage tracing.

Neurosphere assay: Neural stem cells are routinely studied *in vitro* using a method commonly referred to as the neurosphere assay, which was first developed by Reynolds and Weiss (Reynolds and Weiss 1992). Neural progenitor cells isolated from ventricular zone (VZ)/SVZ could be cultured in self-renewal medium (which contains growth factors like EGF and FGF) and form sphere-like heterogeneous cellular entities (primary neurospheres) in non-adherent culture systems. Primary neurospheres are almost entirely formed from colonial expansion of individual neural stem cells and transit-amplifying progenitor cells. Thus, the number of the total neurospheres formed reflects the frequency of neural stem/progenitor cells, and the size of neurospheres is determined by proliferation/survival status of these neural progenitors. Primary neurospheres could be physically dissociated into individual cells and cultured in self-renewal medium to form secondary neurospheres. The frequency of secondary neurospheres represents the self-renewal capacity of neural progenitors. Neurosphere assay could also be used to analyze multi-lineage differentiation of neural progenitors. Upon growth factor withdrawal, cells within neurospheres differentiate into neurons, oligodendrocytes and astrocytes, which can be marked by specific markers Tuj1, O4 and GFAP, respectively, through immunocytochemistry. The relative ratio of each differentiated progeny allows the assessment of the differentiation potential and fate specification of neural progenitors (Pacey et al. 2006).

While neurosphere assay is an ideal method for isolation, expansion and characterization of neural stem and progenitor cells, it does not distinguish between neural stem and progenitor cells (Reynolds and Rietze 2005). To discriminate these two cell populations, Louis et al recently developed a collagen-based assay, called the Neural Colony-Forming Cell Assay (NCFCA), for the quantification of neural stem cells (Louis et al. 2008). In the NCFCA, colonies $\geq$2 mm in diameter are derived from cells that meet all the functional criteria of neural stem cells, while colonies < 2mm are derived from progenitors. This technique could thereby facilitate specific analysis of neural stem cell function.

1.7 Neural stem cells: the developmental origin and their progeny

With these technical innovations, since the initial isolation of neural stem cells from rodent CNS in late 1980s and early 1990s (Temple 1989; Reynolds and Weiss 1992), characterization of neural stem cells and neural-stem-cell-derived progenitors in murine models has greatly advanced our understanding of normal brain development.

Developing neural stem cells

In mice, the developmental origins of neural stem cells are neuroepithelial cells derived from the ectoderm. Around embryonic day 9 (E9) and E10, neuroepithelial cells acquire glial features and generate radial glia, which function as the developing neural stem cells. Radial glial cells reside in the ventricular zone (VZ), a region immediately adjacent to the lateral ventricle (Kriegstein and Alvarez-Buylla 2009). This microenvironment where stem cells reside is often referred to as the neural stem cell niche. During embryonic CNS development, generation of neurons (neurogenesis) precedes the generation of glia (gliogenesis) (Miller and Gauthier 2007). Cortical neurogenesis takes place from E10 to E18 in mice. Radial glial cells, which express brain lipid-binding protein (BLBP) and Nestin, can undergo asymmetric division to directly give rise to neuron in the cortex. Alternatively, they can indirectly generate neurons through lineage-committed, transit-amplifying neural progenitors, also known as neuron-restricted intermediate progenitor cells (nIPCs). Radial glial processes function as a scaffold to guide neuronal migration during cortical neurogenesis. Oligodendrocytes are also derived from radial glial cells through glial-restricted intermediate progenitor cells (gIPCs) during late embryonic development. At perinatal stage, the majority of radial glial cells detach from the ventricle and transform into astrocytes, while the remainder continue to generate neurons and oligodendrocytes through their respective nIPCs and gIPCs (Kriegstein and Alvarez-Buylla 2009). The peak of gliogenesis occurs in the first few weeks of neonatal development (Miller and Gauthier 2007). The developmental origin of neural stem cells is illustrated in Figure 1.

Adult neural stem cells

Neurogenesis in the adult brain was traditionally considered non-existent. Ramon y Cajal suggested that neurons are generated exclusively during prenatal development based on a premise that the addition of new neurons would disrupt the existing neuronal network. This conclusion governed the field for most of the past century due to the fact that there was no good lineage tracing technique to prove the existence of adult neurogenesis (Gross 2000). Only recently has it been accepted that new neurons are constantly generated in discrete regions of adult brain. Adult neural stem cells were first isolated in 1992 from the adult rodent CNS (Reynolds and Weiss 1992) and later from humans in 1999 (Kukekov et al. 1999). In the adult brain, multipotent neural stem and progenitor cells are spatially restricted in two stem cell niches: the subventricular zone (SVZ) of the lateral ventricle and the subgranular layer (SGL) of the hippocampal dentate gyrus (Merkle and Alvarez-Buylla 2006). SVZ neural stem cells, also called type B cells, are astrocytic cells derived from neonatal radial glial cells. Type B cells give rise to transit-amplifying intermediate progenitor cells (intermediate progenitor cells, IPCs or type C cells), which are highly proliferative and generate neural progenitor cells (neuroblasts, type A cells) and oligodendrocytes precursor cells (OPCs). Neuroblasts migrate tangentially along rostral migratory stream (RMS), a tubular structure ensheathed by glial cells, until they reach the olfactory bulb (OB) and differentiate into mature interneurons, including GABAnergic granule neurons and dopaminergic periglomerular neurons. OPCs, on the other hand, migrate radially into the overlying corpus callosum and become oligodendrocytes (Ming and Song 2005; Merkle and Alvarez-Buylla 2006). Notably, gliogenesis in the adult brain is significantly reduced compared to the developing brain and the majority of SVZ progenitor cells (~95%) are later committed to the neuronal fate (Marshall et al. 2003; Merkle and Alvarez-Buylla 2006).

Based on ultra-structural analyses, Doetsch et al has calculated the relative ratio of different cell populations in the adult SVZ (Doetsch et al. 1997). Among them, about 23% are type B cells, 11% are type C cells and 33% are type A cells. There is no single specific marker available to identify SVZ neural stem cells or type B cells. While they express Nestin like embryonic radial glial cells, they also express glial fibrillary acidic

protein (GFAP) and glutamate aspartate transporter (GLAST), markers that are frequently associated with astrocytes (Doetsch et al. 1997). Meanwhile, Nestin is not a specific marker for SVZ neural stem cells since it is also expressed in SVZ type C and A cells. Therefore, SVZ neural stem cells are commonly referred to as $GFAP^+/Nestin^+$ cells. The best known marker for Type C cells is Ascl1, a basic helix-loop-helix (bHLH) transcription factor that promotes proliferation, although it is also expressed in a subset of type A cells(Parras et al. 2004; Kohwi et al. 2005). As type C cells commit to neuronal or glial lineage, they start to express transcription factors Dlx2 or Olig2, respectively. Neuronal-committed SVZ A cells can be marked by immature neuronal markers polysialylated neural cell adhesion molecule (PSA-NCAM), class III β-tubulin (Tuj1) and doublecortin (DCX), while glial-committed OPCs acquire NG2 expression (Kriegstein and Alvarez-Buylla 2009). The lineage relationship of adult SVZ progenitors and their marker expression profile is summarized in Figure 2 B and C.

The functional importance of adult neurogenesis was first demonstrated by studies in songbirds (Ming and Song 2005). The first evidence that adult-born neurons can integrate into existing neuronal network and form functional circuits came from electrophysiological studies of new neurons in adult songbird (Fan et al. 2005). During the past decade, accumulating evidence correlates adult neurogenesis to behavior both in songbirds and in mammals. For instance, in the hippocampus, increased SGZ neurogenesis in rodents is associated with enhanced spatial learning and long term potentiation (LTP) (Farmer et al. 2004), and decreased SGZ neurogenesis led to defects in behavior tests and a reduction of LTP in the dentate gyrus (Shors et al. 2001; Shors et al. 2002). In the olfactory bulb, enriched odor exposure increases the number of newborn neurons and improves odor memory (Rochefort et al. 2002), while reduced olfactory bulb neurogenesis in genetically modified mice exhibited impaired odor discrimination (Gheusi et al. 2000; Enwere et al. 2004).

1.8 Fate specification of VZ/SVZ neural stem/progenitor cells

The brain is a complicated organ that requires precise and tightly regulated events during development for proper function. The “neuron first, glia second” developmental order has

evolved for efficient patterning (Miller and Gauthier 2007). Neuronal circuitry must be formed first to determine the proper number and position of glial cells for the circuitry. This also explains why neurogenesis is so limited in adult brain, where neuron-glial network has been established during embryonic and neonatal development. For neurogenesis itself, it requires proper neuronal subtype specification to give rise to diverse populations of neurons in the brain at different developmental stages. In this section, I will review the current findings about the fate specification of VZ/SVZ neural stem/progenitor cells.

Neruon-glia fate determination

Much progress has been made in the understanding of the underlying mechanism that governs the neurogenic-gliogenic-neurogenic switch of VZ/SVZ stem cells over the course of embryonic, neonatal and adult stages. During the neurogenic period, bHLH transcription factors neurogenin 1 (ngn1) and neurogenin 2 (ngn2) promote neurogenesis and repress gliogenesis (Ross et al. 2003). Distal-less homeobox-containing (Dlx) transcription factors Dlx1 and Dlx2 repress oligodendrocyte precursor cell formation by inhibiting oligodendroglial cell fate acquisition in neuroglial common progenitors (Petryniak et al. 2007). Besides inhibition through pro-neuronal transcription factors, gliogenesis is also repressed in early neuroglial progenitors through epigenetic silencing of signaling pathways required for glia fate specification. For instance, in early neural precursors, DNA methylation leads to repression of astrocyte-specific genes, inactivation of the gp130/JAK/STAT pathway and inhibition of astrogenesis (Fan et al. 2005).

In the gliogenic period, gp130/JAK/STAT signaling plays a central role in initiating astrogenesis (Nakashima et al. 1999). Cytokines including ciliary neurotrophic factor (CNTF), leukemia inhibitor factor (LIF), and cardiotrophin-1 (CT-1) activate cytokine receptor gp130, which recruits and phosphorylates the tyrosine kinase JAK. Activated JAK then phosphorylates and activates the transcription factors STATs to regulate downstream gene expression. Early OPC development depends on Sonic hedgehog (Shh) signaling (Alberta et al. 2001). Among the downstream targets of Shh, bHLH proteins Olig1 and Olig2 are essential for OPC specification and maturation throughout the central

nervous system (Lu et al. 2002; Zhou and Anderson 2002). Kessaris et al. demonstrated that the upregulation of Olig2 through Shh is dependent on Ras/ERK signaling (Kessaris et al. 2004). In addition to Shh, fibroblast growth factor 2 (FGF2) can also promote Olig2 expression in neocortical progenitor cells and induce oligodendrogenesis (Chandran et al. 2003). Hyperactivation of other receptor tyrosine kinase (RTK) pathways (i.e. epidermal growth factor receptor EGFR, platelet-derived growth factor receptor PDGFR) can lead to overproduction of $Olig2^+$ cells (Jackson et al. 2006; Ivkovic et al. 2008), which may potentially function through the Ras/ERK signaling cascade.

Neuronal subtype specification and the heterogeneity of VZ/SVZ progenitors

Although embryonic VZ appears to be a uniform layer of proliferating progenitors, recently studies have demonstrated that it is composed of radial glial cells that are heterogeneous in terms of the neuronal subtypes they will produce. Based on their unique transcription factor expression profile, embryonic VZ could be subdivided into four major subregions: Septum, cortex, lateral ganglionic eminence (LGE), and medial ganglionic eminence (MGE). Combinatorial expression of transcription factors Pax6, Emx1, Gsh1, Gsh2, Er81, Sp8, Nkx2.1, Dlx1, Dlx2, Olig2, Ngn2 and Ascl1 is implicated in neuronal subtype specification of radial glial cells and IPCs in different subregions of the VZ (Campbell 2003; Puelles and Rubenstein 2003; Guillemot 2007).

Similar regional heterogeneity has also been observed in neonatal/adult SVZ. Merkle et al demonstrated that different types of olfactory bulb neurons are generated from different sublocations of the SVZ though adenoviral regional labeling of neonatal radial glial cells and adult SVZ type B cells (Merkle et al. 2004; Merkle et al. 2007). There are two principal types of adult-born olfactory neurons, periglomerular cells and granule cells. Periglomerular cells can be subdivided into three populations of cells that express unique markers: calretinin (CalR), calbindin (CalB) and tyrosine hydroxylase (TH). Granule cells include deep, superficial, and $CalR^+$ cells. Each subtype has distinct function in the olfactory bulb (Shepherd 2004; Ming and Song 2005). In their study, Merkle et al reveals that dorsal SVZ gives rise to TH^+ periglomerular cells and a subpopulation of the $CalR^+$ periglomerular cells, while the majority of CalB+

periglomerular cells are derived from ventrolateral SVZ. For granule cell specification, dorsal SVZ progenitors primarily generate superficial GCs, while ventral SVZ progenitors gives rise to deep GCs. The majority of CalR+ periglomerular cells and granule cells are derived from the medial wall of the lateral ventricle facing the septum. Transcriptional control of neuronal subtype specification includes the expression of Pax6 (dopaminergic periglomerular neurons and a subpopulation of superficial granule cells) and SP8 ($CalR^+$ cells) (Hack et al. 2005; Kohwi et al. 2005; Waclaw et al. 2006). These studies demonstrated that neural stem/progenitor cells in embryonic and neonatal/adult VZ/SVZ are heterogeneous and are regionally specified to generate a diverse subpopulation of neurons.

1.9 Summary and overall layout of this thesis

In summary, neural stem cells play a critical in normal brain development, and deregulation of mechanisms that maintain neural stem cell homeostasis through inactivation of tumor suppressors could lead to brain tumor development. Therefore, investigating the role of tumor suppressors in neural stem cells could not only provide us insights in basic developmental biology, but also advance our understanding of disease mechanisms. The objective of my thesis work is to understand the role of p53 and *Nf1* in normal neural stem/progenitor cell function and how inactivation of these tumor suppressor genes may transform neural stem/progenitor cells and potentially lead to brain tumor development. In Chapter II, I will present the p53 glioma mouse model, which demonstrates the central role of p53 in gliomagenesis and provides new evidence that implicates neural stem/progenitor cells as the cell-of-origin for p53-associated glioma. In Chapter III, I will present the *Nf1* mouse model and show how loss of Nf1 impacts on the fate-specification of neural progenitors and how this could relate to cognitive deficits in NF1 patients. Chapter IV will be the summary and discussion of the entire thesis.

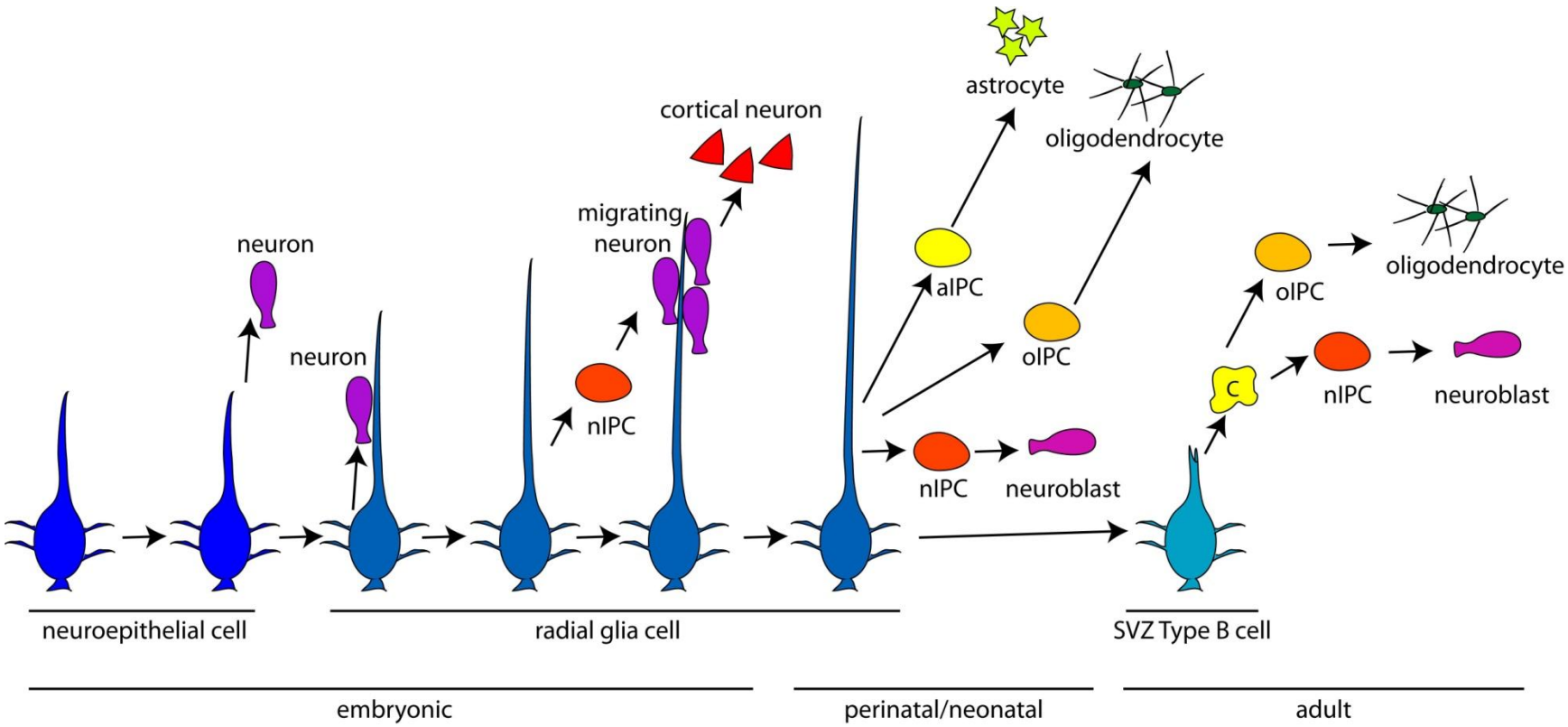
astrocyte
oligodendrocyte
cortical neuron
migrating neuron
neuron
neuron
aIPC
oIPC
oIPC
oligodendrocyte
nIPC
C
nIPC
neuroblast
nIPC
neuroblast
neuroepithelial cell
radial glia cell
SVZ Type B cell
embryonic
perinatal/neonatal
adult

Figure 1. The developmental origin of neural stem cells.
(See text for details, adapted fromKriegstein and Alvarez-Buylla, 2009).

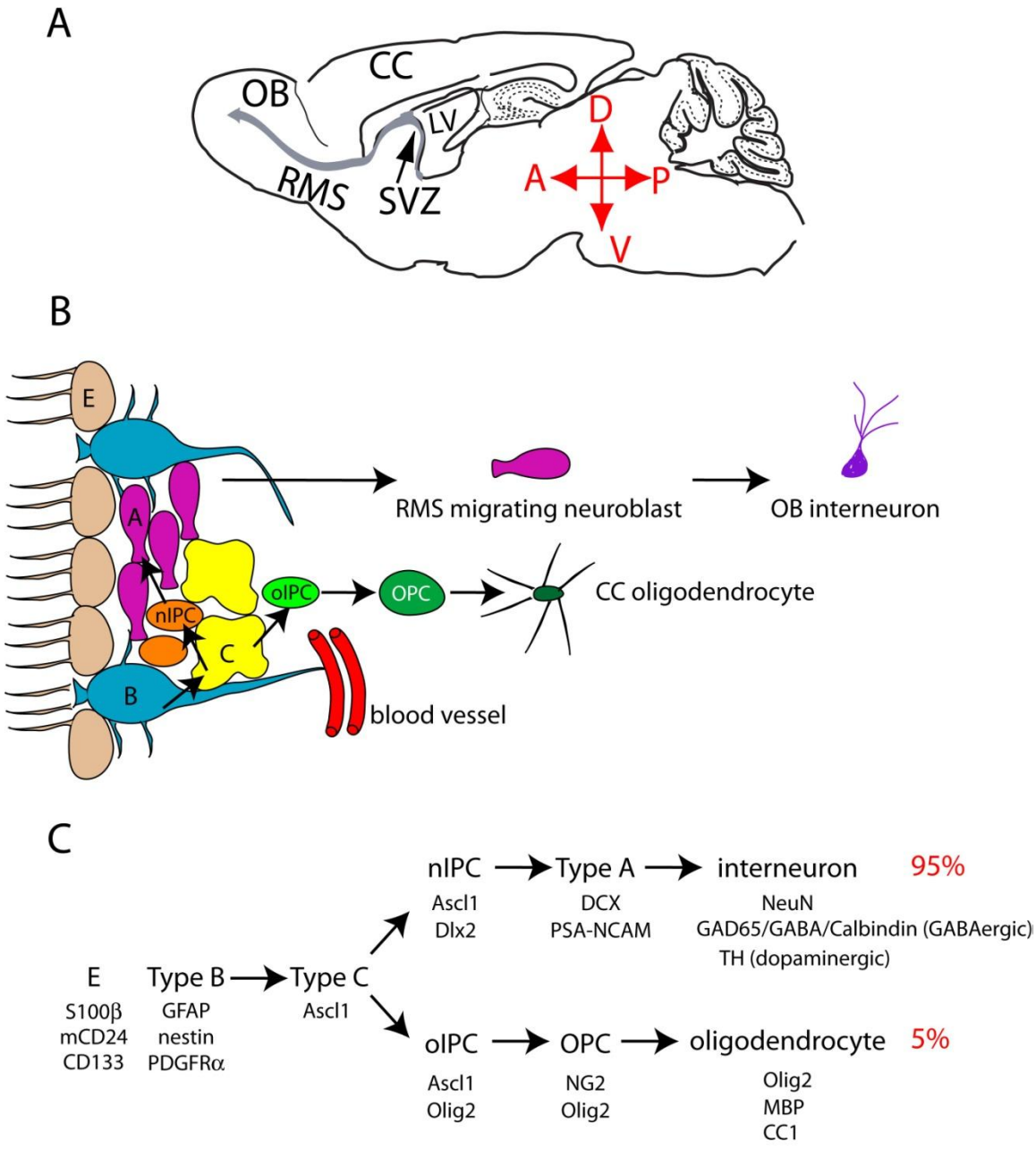

Figure 2. The lineage relationship and marker expression of adult SVZ neural progenitor cells. (See text for details).

1.10 References

The Cancer Genome Atlas Research Network. 2008. Comprehensive genomic characterization defines human glioblastoma genes and core pathways. *Nature* **455**: 1061-1068.

Al-Hajj M, Wicha MS, Benito-Hernandez A, Morrison SJ, Clarke MF. 2003. Prospective identification of tumorigenic breast cancer cells. *Proc Natl Acad Sci U S A* **100**: 3983-3988.

Alberta JA, Park SK, Mora J, Yuk D, Pawlitzky I, Iannarelli P, Vartanian T, Stiles CD, Rowitch DH. 2001. Sonic hedgehog is required during an early phase of oligodendrocyte development in mammalian brain. *Mol Cell Neurosci* **18**: 434-441.

Alcantara Llaguno S, Chen J, Kwon CH, Jackson EL, Li Y, Burns DK, Alvarez-Buylla A, Parada LF. 2009. Malignant astrocytomas originate from neural stem/progenitor cells in a somatic tumor suppressor mouse model. *Cancer Cell* **15**: 45-56.

Androutsellis-Theotokis A, Leker RR, Soldner F, Hoeppner DJ, Ravin R, Poser SW, Rueger MA, Bae SK, Kittappa R, McKay RD. 2006. Notch signalling regulates stem cell numbers in vitro and in vivo. *Nature* **442**: 823-826.

Ballester R, Marchuk D, Boguski M, Saulino A, Letcher R, Wigler M, Collins F. 1990. The NF1 locus encodes a protein functionally related to mammalian GAP and yeast IRA proteins. *Cell* **63**: 851-859.

Bao S, Wu Q, McLendon RE, Hao Y, Shi Q, Hjelmeland AB, Dewhirst MW, Bigner DD, Rich JN. 2006. Glioma stem cells promote radioresistance by preferential activation of the DNA damage response. *Nature* **444**: 756-760.

Barth RF. 1998. Rat brain tumor models in experimental neuro-oncology: the 9L, C6, T9, F98, RG2 (D74), RT-2 and CNS-1 gliomas. *J Neurooncol* **36**: 91-102.

Beier D, Hau P, Proescholdt M, Lohmeier A, Wischhusen J, Oefner PJ, Aigner L, Brawanski A, Bogdahn U, Beier CP. 2007. CD133(+) and CD133(-) glioblastoma-derived cancer stem cells show differential growth characteristics and molecular profiles. *Cancer Res* **67**: 4010-4015.

Bentires-Alj M, Kontaridis MI, Neel BG. 2006. Stops along the RAS pathway in human genetic disease. *Nat Med* **12**: 283-285.

Bonnet D, Dick JE. 1997. Human acute myeloid leukemia is organized as a hierarchy that originates from a primitive hematopoietic cell. *Nat Med* **3**: 730-737.

Campbell K. 2003. Dorsal-ventral patterning in the mammalian telencephalon. *Curr Opin Neurobiol* **13**: 50-56.

Chandran S, Kato H, Gerreli D, Compston A, Svendsen CN, Allen ND. 2003. FGF-dependent generation of oligodendrocytes by a hedgehog-independent pathway. *Development* **130**: 6599-6609.

Cobaleda C, Gutierrez-Cianca N, Perez-Losada J, Flores T, Garcia-Sanz R, Gonzalez M, Sanchez-Garcia I. 2000. A primitive hematopoietic cell is the target for the leukemic transformation in human philadelphia-positive acute lymphoblastic leukemia. *Blood* **95**: 1007-1013.

Cohnheim J. 1867. Ueber entzundung und eiterung. *Path Anat Physiol Klin Med* **40**: 1-79.

Cohnheim J. 1875. Congenitales, quergestreiftes Muskelsarkon der Nireren. *Virchows Arch* **1875**: 64.

Denayer E, Legius E. 2007. What's new in the neuro-cardio-facial-cutaneous syndromes? *Eur J Pediatr* **166**: 1091-1098.

Doetsch F, Garcia-Verdugo JM, Alvarez-Buylla A. 1997. Cellular composition and three-dimensional organization of the subventricular germinal zone in the adult mammalian brain. *J Neurosci* **17**: 5046-5061.

Durante F. 1874. Nesso fisio-pathologico tra la struttura dei nei materni e la genesi di alcuni tumori maligni. *Arch Memor Observ Chir Pract* **11**: 217-226.

Enwere E, Shingo T, Gregg C, Fujikawa H, Ohta S, Weiss S. 2004. Aging results in reduced epidermal growth factor receptor signaling, diminished olfactory neurogenesis, and deficits in fine olfactory discrimination. *J Neurosci* **24**: 8354-8365.

Fan G, Martinowich K, Chin MH, He F, Fouse SD, Hutnick L, Hattori D, Ge W, Shen Y, Wu H et al. 2005. DNA methylation controls the timing of astrogliogenesis through regulation of JAK-STAT signaling. *Development* **132**: 3345-3356.

Fan X, Khaki L, Zhu TS, Soules ME, Talsma CE, Gul N, Koh C, Zhang J, Li YM, Maciaczyk J et al. 2010. NOTCH pathway blockade depletes CD133-positive glioblastoma cells and inhibits growth of tumor neurospheres and xenografts. *Stem Cells* **28**: 5-16.

Farmer J, Zhao X, van Praag H, Wodtke K, Gage FH, Christie BR. 2004. Effects of voluntary exercise on synaptic plasticity and gene expression in the dentate gyrus of adult male Sprague-Dawley rats in vivo. *Neuroscience* **124**: 71-79.

Furnari FB, Fenton T, Bachoo RM, Mukasa A, Stommel JM, Stegh A, Hahn WC, Ligon KL, Louis DN, Brennan C et al. 2007. Malignant astrocytic glioma: genetics, biology, and paths to treatment. *Genes Dev* **21**: 2683-2710.

Gaiano N, Nye JS, Fishell G. 2000. Radial glial identity is promoted by Notch1 signaling in the murine forebrain. *Neuron* **26**: 395-404.

Gheusi G, Cremer H, McLean H, Chazal G, Vincent JD, Lledo PM. 2000. Importance of newly generated neurons in the adult olfactory bulb for odor discrimination. *Proc Natl Acad Sci U S A* **97**: 1823-1828.

Gratzner HG. 1982. Monoclonal antibody to 5-bromo- and 5-iododeoxyuridine: A new reagent for detection of DNA replication. *Science (New York, NY* **218**: 474-475.

Gross CG. 2000. Neurogenesis in the adult brain: death of a dogma. *Nat Rev Neurosci* **1**: 67-73.

Guillemot F. 2007. Cell fate specification in the mammalian telencephalon. *Prog Neurobiol* **83**: 37-52.

Hack MA, Saghatelyan A, de Chevigny A, Pfeifer A, Ashery-Padan R, Lledo PM, Gotz M. 2005. Neuronal fate determinants of adult olfactory bulb neurogenesis. *Nat Neurosci* **8**: 865-872.

Holland EC, Celestino J, Dai C, Schaefer L, Sawaya RE, Fuller GN. 2000. Combined activation of Ras and Akt in neural progenitors induces glioblastoma formation in mice. *Nat Genet* **25**: 55-57.

Holyoake T, Jiang X, Eaves C, Eaves A. 1999. Isolation of a highly quiescent subpopulation of primitive leukemic cells in chronic myeloid leukemia. *Blood* **94**: 2056-2064.

Hope KJ, Jin L, Dick JE. 2003. Human acute myeloid leukemia stem cells. *Arch Med Res* **34**: 507-514.

Hyman SL, Shores A, North KN. 2005. The nature and frequency of cognitive deficits in children with neurofibromatosis type 1. *Neurology* **65**: 1037-1044.

Ivkovic S, Canoll P, Goldman JE. 2008. Constitutive EGFR signaling in oligodendrocyte progenitors leads to diffuse hyperplasia in postnatal white matter. *J Neurosci* **28**: 914-922.

Jackson EL, Garcia-Verdugo JM, Gil-Perotin S, Roy M, Quinones-Hinojosa A, VandenBerg S, Alvarez-Buylla A. 2006. PDGFR alpha-positive B cells are neural stem cells in the adult SVZ that form glioma-like growths in response to increased PDGF signaling. *Neuron* **51**: 187-199.

Jacques TS, Swales A, Brzozowski MJ, Henriquez NV, Linehan JM, Mirzadeh Z, C OM, Naumann H, Alvarez-Buylla A, Brandner S. 2010. Combinations of genetic mutations in the adult neural stem cell compartment determine brain tumour phenotypes. *EMBO J* **29**: 222-235.

Jung V, Romeike BF, Henn W, Feiden W, Moringlane JR, Zang KD, Urbschat S. 1999. Evidence of focal genetic microheterogeneity in glioblastoma multiforme by area-specific CGH on microdissected tumor cells. *J Neuropathol Exp Neurol* **58**: 993-999.

Kesari S, Ramakrishna N, Sauvageot C, Stiles CD, Wen PY. 2005. Targeted molecular therapy of malignant gliomas. *Curr Neurol Neurosci Rep* **5**: 186-197.

Kessaris N, Jamen F, Rubin LL, Richardson WD. 2004. Cooperation between sonic hedgehog and fibroblast growth factor/MAPK signalling pathways in neocortical precursors. *Development* **131**: 1289-1298.

Kohwi M, Osumi N, Rubenstein JL, Alvarez-Buylla A. 2005. Pax6 is required for making specific subpopulations of granule and periglomerular neurons in the olfactory bulb. *J Neurosci* **25**: 6997-7003.

Kondo S, Kondo Y, Li G, Silverman RH, Cowell JK. 1998. Targeted therapy of human malignant glioma in a mouse model by 2-5A antisense directed against telomerase RNA. *Oncogene* **16**: 3323-3330.

Kriegstein A, Alvarez-Buylla A. 2009. The glial nature of embryonic and adult neural stem cells. *Annu Rev Neurosci* **32**: 149-184.

Kukekov VG, Laywell ED, Suslov O, Davies K, Scheffler B, Thomas LB, O'Brien TF, Kusakabe M, Steindler DA. 1999. Multipotent stem/progenitor cells with similar properties arise from two neurogenic regions of adult human brain. *Exp Neurol* **156**: 333-344.

Lewis P, Emerman M. 1994. Passage through mitosis is required for oncoretroviruses but not for the human immunodeficiency virus. *JVirol* **68**: 510-516.

Listernick R, Charrow J, Gutmann DH. 1999. Intracranial gliomas in neurofibromatosis type 1. *Am J Med Genet* **89**: 38-44.

Louis DN, Ohgaki, H., Wiestler, O.D., and Cavenee, W.K. . 2007. WHO Classification of Tumors of the Central Nervous System.

Louis SA, Rietze RL, Deleyrolle L, Wagey RE, Thomas TE, Eaves AC, Reynolds BA. 2008. Enumeration of neural stem and progenitor cells in the neural colony-forming cell assay. *Stem Cells* **26**: 988-996.

Lu QR, Sun T, Zhu Z, Ma N, Garcia M, Stiles CD, Rowitch DH. 2002. Common developmental requirement for Olig function indicates a motor neuron/oligodendrocyte connection. *Cell* **109**: 75-86.

Maher EA, Furnari FB, Bachoo RM, Rowitch DH, Louis DN, Cavenee WK, DePinho RA. 2001. Malignant glioma: genetics and biology of a grave matter. *Genes Dev* **15**: 1311-1333.

Marshall CA, Suzuki SO, Goldman JE. 2003. Gliogenic and neurogenic progenitors of the subventricular zone: who are they, where did they come from, and where are they going? *Glia* **43**: 52-61.

Merkle FT, Alvarez-Buylla A. 2006. Neural stem cells in mammalian development. *Curr Opin Cell Biol* **18**: 704-709.

Merkle FT, Mirzadeh Z, Alvarez-Buylla A. 2007. Mosaic organization of neural stem cells in the adult brain. *Science (New York, NY* **317**: 381-384.

Merkle FT, Tramontin AD, Garcia-Verdugo JM, Alvarez-Buylla A. 2004. Radial glia give rise to adult neural stem cells in the subventricular zone. *Proc Natl Acad Sci U S A* **101**: 17528-17532.

Miller FD, Gauthier AS. 2007. Timing is everything: making neurons versus glia in the developing cortex. *Neuron* **54**: 357-369.

Ming GL, Song H. 2005. Adult neurogenesis in the mammalian central nervous system. *Annu Rev Neurosci* **28**: 223-250.

Nakashima K, Wiese S, Yanagisawa M, Arakawa H, Kimura N, Hisatsune T, Yoshida K, Kishimoto T, Sendtner M, Taga T. 1999. Developmental requirement of gp130 signaling in neuronal survival and astrocyte differentiation. *J Neurosci* **19**: 5429-5434.

Ohgaki H, Dessen P, Jourde B, Horstmann S, Nishikawa T, Di Patre PL, Burkhard C, Schuler D, Probst-Hensch NM, Maiorka PC et al. 2004. Genetic pathways to glioblastoma: a population-based study. *Cancer Res* **64**: 6892-6899.

Pacey L, Stead S, Gleave J, Tomczyk K, Doering L. 2006. Neural stem cell culture: Neurosphere generation, microscopical analysis and cryopreservation. *Nature Protocols Online*

Parras CM, Galli R, Britz O, Soares S, Galichet C, Battiste J, Johnson JE, Nakafuku M, Vescovi A, Guillemot F. 2004. Mash1 specifies neurons and oligodendrocytes in the postnatal brain. *EMBO J* **23**: 4495-4505.

Petryniak MA, Potter GB, Rowitch DH, Rubenstein JL. 2007. Dlx1 and Dlx2 control neuronal versus oligodendroglial cell fate acquisition in the developing forebrain. *Neuron* **55**: 417-433.

Pfenninger CV, Roschupkina T, Hertwig F, Kottwitz D, Englund E, Bengzon J, Jacobsen SE, Nuber UA. 2007. CD133 is not present on neurogenic astrocytes in the adult subventricular zone, but on embryonic neural stem cells, ependymal cells, and glioblastoma cells. *Cancer Res* **67**: 5727-5736.

Plate KH, Breier G, Millauer B, Ullrich A, Risau W. 1993. Up-regulation of vascular endothelial growth factor and its cognate receptors in a rat glioma model of tumor angiogenesis. *Cancer Res* **53**: 5822-5827.

Puelles L, Rubenstein JL. 2003. Forebrain gene expression domains and the evolving prosomeric model. *Trends Neurosci* **26**: 469-476.

Purow BW, Haque RM, Noel MW, Su Q, Burdick MJ, Lee J, Sundaresan T, Pastorino S, Park JK, Mikolaenko I et al. 2005. Expression of Notch-1 and its ligands, Delta-like-1 and Jagged-1, is critical for glioma cell survival and proliferation. *Cancer Res* **65**: 2353-2363.

Quintana E, Shackleton M, Sabel MS, Fullen DR, Johnson TM, Morrison SJ. 2008. Efficient tumour formation by single human melanoma cells. *Nature* **456**: 593-598.

Reilly KM, Loisel DA, Bronson RT, McLaughlin ME, Jacks T. 2000. Nf1;Trp53 mutant mice develop glioblastoma with evidence of strain-specific effects. *Nat Genet* **26**: 109-113.

Reya T, Morrison SJ, Clarke MF, Weissman IL. 2001. Stem cells, cancer, and cancer stem cells. *Nature* **414**: 105-111.

Reynolds BA, Rietze RL. 2005. Neural stem cells and neurospheres--re-evaluating the relationship. *Nat Methods* **2**: 333-336.

Reynolds BA, Weiss S. 1992. Generation of neurons and astrocytes from isolated cells of the adult mammalian central nervous system. *Science (New York, NY* **255**: 1707-1710.

Rochefort C, Gheusi G, Vincent JD, Lledo PM. 2002. Enriched odor exposure increases the number of newborn neurons in the adult olfactory bulb and improves odor memory. *J Neurosci* **22**: 2679-2689.

Ross SE, Greenberg ME, Stiles CD. 2003. Basic helix-loop-helix factors in cortical development. *Neuron* **39**: 13-25.

Samuels Y, Wang Z, Bardelli A, Silliman N, Ptak J, Szabo S, Yan H, Gazdar A, Powell SM, Riggins GJ et al. 2004. High frequency of mutations of the PIK3CA gene in human cancers. *Science (New York, NY* **304**: 554.

Sauer B. 1998. Inducible gene targeting in mice using the Cre/lox system. *Methods* **14**: 381-392.

Shepherd GM. 2004. *The synaptic organization of the brain*. Oxford University Press, Oxford ; New York.

Shors TJ, Miesegaes G, Beylin A, Zhao M, Rydel T, Gould E. 2001. Neurogenesis in the adult is involved in the formation of trace memories. *Nature* **410**: 372-376.

Shors TJ, Townsend DA, Zhao M, Kozorovitskiy Y, Gould E. 2002. Neurogenesis may relate to some but not all types of hippocampal-dependent learning. *Hippocampus* **12**: 578-584.

Sidman RL, Miale IL, Feder N. 1959. Cell proliferation and migration in the primitive ependymal zone: an autoradiographic study of histogenesis in the nervous system. *Exp Neurol* **1**: 322-333.

Singh SK, Clarke ID, Terasaki M, Bonn VE, Hawkins C, Squire J, Dirks PB. 2003. Identification of a cancer stem cell in human brain tumors. *Cancer Res* **63**: 5821-5828.

Singh SK, Hawkins C, Clarke ID, Squire JA, Bayani J, Hide T, Henkelman RM, Cusimano MD, Dirks PB. 2004. Identification of human brain tumour initiating cells. *Nature* **432**: 396-401.

Smart I. 1961. The subependymal layer of the mouse brain and its cell production as shown by autography after [H3]-thymidine injection. *J Comp Neurol* **116**: 325-347.

Stiles CD, Rowitch DH. 2008. Glioma stem cells: a midterm exam. *Neuron* **58**: 832-846.
Temple S. 1989. Division and differentiation of isolated CNS blast cells in microculture. *Nature* **340**: 471-473.
Till JE, Mc CE. 1961. A direct measurement of the radiation sensitivity of normal mouse bone marrow cells. *Radiat Res* **14**: 213-222.
Vogelstein B, Lane D, Levine AJ. 2000. Surfing the p53 network. *Nature* **408**: 307-310.
Waclaw RR, Allen ZJ, 2nd, Bell SM, Erdelyi F, Szabo G, Potter SS, Campbell K. 2006. The zinc finger transcription factor Sp8 regulates the generation and diversity of olfactory bulb interneurons. *Neuron* **49**: 503-516.
Wicha MS, Liu S, Dontu G. 2006. Cancer stem cells: an old idea--a paradigm shift. *Cancer Res* **66**: 1883-1890; discussion 1895-1886.
Xu GF, Lin B, Tanaka K, Dunn D, Wood D, Gesteland R, White R, Weiss R, Tamanoi F. 1990. The catalytic domain of the neurofibromatosis type 1 gene product stimulates ras GTPase and complements ira mutants of S. cerevisiae. *Cell* **63**: 835-841.
Yamaguchi M, Saito H, Suzuki M, Mori K. 2000. Visualization of neurogenesis in the central nervous system using nestin promoter-GFP transgenic mice. *Neuroreport* **11**: 1991-1996.
Zhou Q, Anderson DJ. 2002. The bHLH transcription factors OLIG2 and OLIG1 couple neuronal and glial subtype specification. *Cell* **109**: 61-73.
Zhu Y, Guignard F, Zhao D, Liu L, Burns DK, Mason RP, Messing A, Parada LF. 2005a. Early inactivation of p53 tumor suppressor gene cooperating with NF1 loss induces malignant astrocytoma. *Cancer Cell* **8**: 119-130.
Zhu Y, Harada T, Liu L, Lush ME, Guignard F, Harada C, Burns DK, Bajenaru ML, Gutmann DH, Parada LF. 2005b. Inactivation of NF1 in CNS causes increased glial progenitor proliferation and optic glioma formation. *Development* **132**: 5577-5588.
Zhu Y, Parada LF. 2002. The molecular and genetic basis of neurological tumours. *Nat Rev Cancer* **2**: 616-626.
Zufferey R, Dull T, Mandel RJ, Bukovsky A, Quiroz D, Naldini L, Trono D. 1998. Self-inactivating lentivirus vector for safe and efficient in vivo gene delivery. *J Virol* **72**: 9873-9880.

Chapter II Expression of mutant p53 marks the transition from neural progenitor to malignant glioma

This part of my thesis is mainly a joint effort from former lab post-doc Dr. Jiong Yang and me. Dr. Yang collected the tumor samples and mainly focused on the end-stage analysis. I focused on the characterization of early stage $p53^{+}$ cells in the brain and the investigation of the lineage relationship between neural stem/progenitor cells and early glioma cells. Drs.Yuan Zhu and Paul E. McKeever performed the histological analysis.

2.1 Introduction

Glioblastoma (Grade IV malignant astrocytic glioma), also known as glioblastoma multiforme (GBM), is the most frequent and aggressive neoplasm among human primary brain tumors (Furnari et al., 2007; Louis et al., 2007). There are two subtypes of GBM. Primary GBM arises *de novo* with no evidence of pre-existing lesions whereas secondary GBM develops from lower-grade, albeit malignant, i.e., Grade II or III gliomas. Despite distinctive clinical courses and differing molecular lesions, primary and secondary GBMs share the same histopathological and clinical features, most notably a high propensity to diffusely infiltrate normal brain parenchyma and resistance to virtually all current therapies. Consequently, GBM is one of the most deadly human cancers with a median survival that has remained at 12 months for over the past two decades (Furnari et al., 2007; Louis et al., 2007).

Recent studies have identified genes and core pathways that are altered in human GBM (Ohgaki et al., 2004; Parsons et al., 2008; TCGA Research Network, 2008). Mutations in the components of the P53 tumor suppressor pathway have been identified in the majority of human primary GBM, approximately 30 to 40% of which have mutations in the TP53 gene (Parsons et al., 2008; TCGA Research Network, 2008). Furthermore, frequencies of

TP53 mutations are similar among lower-grade malignant gliomas and secondary GBMs, suggesting an important role of TP53 gene defects in early stages of glioma development (Ohgaki et al., 2004). Consistently, individuals with Li-Fraumeni syndrome, who carry germline P53 mutations, are predisposed to development of astrocytic gliomas (Louis et al., 2007). However, the mechanisms by which TP53 deficiency transforms normal brain cells remain poorly understood.

One critical challenge to understand the GBM pathogenesis is to identify the cell-of-origin of this disease. The cell-of-origin in most human cancers remains unknown as human tumor samples are typically acquired and analyzed at the terminal stages of the disease and thus do not provide a window to study this important question. Recent studies demonstrated that a number of brain cancers, including GBM, are driven and sustained by a subset of stem cell-like cells that exhibit the cellular characteristics of normal stem cells, including self-renewal and multipotency (Galli et al., 2004; Hemmati et al., 2003; Singh et al., 2004). However, whether a normal stem cell, a progenitor cell, or even a fully differentiated cell is the cell-of-origin for glioma stem cells remains largely unknown (Sanai et al., 2005; Stiles and Rowitch, 2008). In the adult brain, multipotent neural stem and progenitor cells are spatially restricted in two stem cell niches: the subventricular zone (SVZ) of the lateral ventricle and the subgranular zone (SGZ) of the hippocampal dentate gyrus (Merkle and Alvarez-Buylla, 2006). Genetic studies using murine glioma models and imaging analysis from a clinical study provide evidence that some GBMs may arise from the SVZ stem cell niche (Alcantara Llaguno et al., 2009; Lim et al., 2007; Zhu et al., 2005a). At the cellular level, neural stem cells in the adult SVZ (type B cells or SVZ-B) give rise to a highly proliferative cell population, transit-amplifying progenitor cells (SVZ-C cells), which then differentiate into two lineage-restricted progenitor cells, neuroblasts (SVZ-A cells) and oligodendrocyte precursor cells (SVZ-OPC) (Hack et al., 2005; Menn et al., 2006). Because of a lack of reliable markers for glioma cells, particularly at early stages of tumor development, the role of the various SVZ cell populations in gliomagenesis remains undefined.

In this study, we develop a murine glioma model in which an in-frame p53 deletion mutation is specifically targeted into the nervous system and use it to investigate the role of neural stem cells and transit-amplifying progenitors in P53-mediated gliomagenesis.

2.2 Material and methods

2.2.1 Histology and tumor analysis

Mice were aged until signs of distress appeared. Then, mice were perfused with 4% paraformaldehyde (PFA) and brains were dissected, followed by overnight post-fixation in 4% PFA at 4 ºC. Brains were divided into two hemispheres along the midline and each hemisphere was processed for either paraffin-embedded or cryostat sections. Serial sections were sagittally prepared at 5 μm for paraffin sections or 14 μm for cryostat sections. Every eleventh slide was stained by H&E. Stained sections were independently examined under a light microscope by Yuan Zhu and Paul E. McKeever. Tumor grading was determined by Yuan Zhu and Paul E. McKeever based upon the WHO grading system for malignant astrocytic glioma and medulloblastoma (Louis et al., 2007). Adjacent sections were subjected to immunohistochemical analysis (see below).

2.2.2 Histological grading of malignant astrocytic gliomas in CKO1, CKO2 and CKO3 mice

Histopathology of neoplasms that developed in these mice had to meet diagnostic criteria of the World Health Organization (WHO) for classification of tumors of the CNS (Louis et al., 2007). Tumors with neoplastic astrocytes were classified as astrocytic gliomas. Astrocytic features include extension of cellular processes from neoplastic cells. These vary from long and thick to thin and short. They are highlighted with H&E and GFAP stains. Variable nuclear shapes, particularly elongated, bent and dark staining nuclei characterize neoplastic astrocytes. Their perinuclear cytoplasm is highly variable: from imperceptible to substantial and appearing to push the nucleus to the perimeter of the cell. Astrocytic glioma is a classification that includes astrocytoma, anaplastic astrocytoma, glioblastoma, and oligoastrocytoma. To be among the first three tumors, neoplastic astrocytes must predominate. To be either an anaplastic astrocytoma (WHO grade III on a

scale of four) or glioblastoma (WHO grade V), the tumor must have mitoses. It must be crowded with malignant cells, cells with coarse nuclear chromatin, angulated and pleomorphic nuclei, or nucleolar abnormalities. To be classified as a glioblastoma and given the highest grade of malignancy, the additional feature of either necrosis or microvascular proliferation must be present. Microvascular proliferation is hypotrophy and hyperplasia of cells in the walls of tumor vessels.

2.2.3 LacZ/β-gal staining

The R26R-LacZ transgene was introduced to the CKO1 and CKO2 mice. Mice with genotypes of hGFAP-cre+;$p53^{flox/KO}$;R26R-LacZ+ (CKO1) and hGFAP-cre+;$p53^{flox/flox}$;R26R-LacZ+ (CKO2) were generated. Brains were collected from mutant mice at ages of postnatal day (P0.5), P21, and 6 months. Tumor tissues were isolated from mutant mice with high-grade brain tumors. Dissected tissues were post-fixed in PFA for 2 hours and transferred to 30% sucrose for overnight dehydration. Frozen sections cut at 10 μ were prepared and subjected to X-gal staining for 1 hour to overnight depending on the signal intensity. X-gal stained sections were then subjected to nuclear fast red for counterstaining. Co-localization of β-gal expressing cells with other lineage markers was obtained by double immunofluorescence.

2.2.4 Immunohistochemistry/ Immunofluorescence

Paraffin sections were deparaffinized through Xylene, 100% ethanol, 95% ethanol, 50% ethanol and 30% ethanol and rehydrated in distilled water. Antigen retrieval was performed with Retrieve-all antigen retrieval solution from Signet. Cryosections do not require deparaffinization or antigen retrieval steps and were directly fixed in 4% PFA for 15 minutes. Sections were then permeablized by 0.3% Triton-X (Sigma) solution for 20 minutes and blocked for 1 hour with 1.5% normal goat/horse/donkey serum (Sigma) depending on the secondary antibody to be used (e.g. use goat serum for blocking if the secondary antibody is from goat). Slides were put in humidified chamber and incubated in primary antibodies dissolved in the blocking solution at $4^{o}C$ overnight. The visualization of primary antibodies was performed with either a horseradish peroxidase

system using a diaminobenzidine-based (DAB) peroxidase substrate (Vectastain ABC kit, Vector) or immunofluorescence by using Cy2 (or Alexa 488), Cy3 (or Alexa 555) and Cy5 (Alexa 647)-conjugated secondary antibodies at 1:200 dilution for 1 hour incubation (Cy2/Cy3/Cy5, Jackson Immunoresearch; Alexa 488/555/647, Invitrogen). Slides were washed in between the steps with 1X PBS. The dilutions of primary antibodies used in this study were: p53 (1:500, rabbit, Novo Castra), BrdU (1:1000, rat, Abcam), Ki-67 (1:500, mouse, BD Pharmingen), CD133 (1:500, rat, eBiosciences), PDGFRα (1:1000, rat, eBiosciences), Olig2 (Rabbit, 1:20000, a kind gift from Dr. C. Stiles; guinea pig, 1:10000, a kind gift from Dr. B. Novitch), GFAP (1:2000, mouse, BD Pharmingen), MAP2 (1:200, mouse, Sigma), Nestin (1:100, mouse, Chemicon), PSA-NCAM (1:1000, mouse, Chemicon), NG2 (1:200, mouse, Millipore),), β-gal (1:1000, rabbit, 5 prime-3 prime) , β-gal (1:1000, goat, AbD Serotec), and CD31 (1:200, mouse, Dako). CD133 or PDGFRα staining was performed on cryostat sections, and an Invitrogen biotin/streptavidin system was used for signal amplification. Sections were examined under either a light or a fluorescence microscope (Olympus).

2.2.5 BrdU Assay

The CKO1/CKO2 mutant and control littermates were pulsed with BrdU five times a day at 2-hour intervals. The dose of BrdU was 50μg/g (gram, body weight). Mice were perfused with 4% PFA 2 hours after the last pulse. Brains were dissected and processed for either paraffin-embedded or cryostat sections. The staining for BrdU followed the regular immunofluorescence or immunohistochemistry protocol described above, except that after the Triton-X permeablization step, sliders were incubated in 2N HCl for 30 minutes followed by 0.1 M sodium borate for 20 minutes to denature the DNA.

2.3 Results

2.3.1 p53 deficiency is sufficient to induce glioma formation

To investigate the role of p53 in gliomagenesis, we used hGFAP-cre to introduce p53 mutation specifically into the central nervous system. As aforementioned, because radial

glial cells are the primary multipotent neural stem/progenitor cell populations in the developing brain, hGFAP-cre-mediated gene deletion will be transmitted to all the progeny of radial glial cells, including neurons, glia, and adult neural stem cells (Merkle and Alvarez-Buylla 2006). The p53 conditional allele (p53flox) used for this study is unlike other p53 conditional alleles. Cre-mediated recombination of this p53flox allele results in an in-frame deletion of exons 5 and 6, which encode a significant portion of the p53 DNA binding domain (Cho et al. 1994; Kitayner et al. 2006). Consistently, it has been previously shown that this p53 in-frame deletion mutant (hereafter, $p53^{\Delta E5\text{-}6}$) lacks transcriptional function (Lin et al. 2004). Thus, the $p53^{\Delta E5\text{-}6}$ allele represents a DNA binding domain-deficient loss-of-function allele. Moreover, the resultant protein of the $p53^{\Delta E5\text{-}6}$ allele is not degraded or overexpressed and mimics the levels of wildtype p53. As such, this truncated protein can be used as a surrogate marker for determining the levels of p53 in cells, which is often elevated in human tumors.

To study tumorigenic activity of the $p53^{\Delta E5\text{-}6}$ mutation in the brain, we first crossed the hGFAP-cre line with the $p53^{flox}$ mouse to generate hGFAP-cre+;$p53^{flox/+}$ mice. Ten hGFAP-cre+;$p53^{flox/+}$ mice were monitored over 12 months. These mice were healthy and behaved indistinguishably from the wild-type littermates. Moreover, there was no evidence of tumor formation in the brain of these aged mice. We then generated hGFAP-cre+;$p53^{flox/KO}$ (hereafter referred to as conditional knockout 1 or CKO1) and hGFAP-cre+;$p53^{flox/flox}$ (CKO2) mouse strains (Figure 3A). As previously shown, inactivation of p53 followed by *Nf1* loss efficiently induces malignant gliomas with complete penetrance (Zhu et al. 2005a). Thus a heterozygous *Nf1* mutation was introduced to the $p53^{\Delta E5\text{-}6}$ mutant mice and generated a third mutant strain with the genotype of hGFAP-cre+;$p53^{flox/flox}$;$Nf1^{KO/+}$ (CKO3). In CKO3 brains, p53-deficient cells are expected to inactivate the wild-type *Nf1* allele to undergo p53/*Nf1*-mediated gliomagenesis, whereas p53-deficient cells in the CKO1/2 brains could potentially cooperate with diverse oncogenic alterations to promote glioma formation (Figure 3A).

Both CKO1 and CKO2 mice were healthy, fertile, and indistinguishable from their control littermates within the first 6 months after birth (Figure 3B). However, 85% of

CKO1 (22/26) and 84% of CKO2 (43/51) mice analyzed in this study developed neurological symptoms including tremor, seizure, ataxia, or lack of balance requiring sacrifice between the ages of 6 and 14 months (Figure 3B). Each of the CKO1 and CKO2 mice with neurological deficits exhibited enlarged brains with evidence of high-grade brain tumors. The remaining CKO1 and CKO2 mice were sacrificed because of the presence of tumors outside the central nervous system (CNS). These non-CNS tumors were diagnosed as soft-tissue sarcomas, likely arising due to hGFAP-cre expression in cells outside the CNS (data not shown). A portion of the CKO1 (1/4) and CKO2 (2/8) mice with non-CNS sarcomas also exhibited enlarged brains with high-grade tumors. Together, nearly 90% of both CKO1 (23/26) and CKO2 (45/51) mutant mice developed high-grade brain tumors (Figure 3A), most of which (20/23 of CKO1 and 40/45 of CKO2) were histopathologically characterized as malignant gliomas with astrocytic characteristics and the remainder of which were medulloblastomas (Figure 3C). Because CKO1 and CKO2 mice exhibited essentially the same brain tumor phenotypes, they will be presented together as the $p53^{\Delta E5\text{-}6}$ mutant mice. Compared to CKO1 and CKO2, CKO3 mice develop tumors at much faster rate, consistent with previous findings that Nf1 mutation could accelerate glioma formation in a p53-deficient background (Zhu et al. 2005a). Together, CKO1, CKO2 and CKO3 represent highly penetrant p53-dependent models of GBM.

2.3.2 $CD133^{+}$ malignant astrocytic glioma and GBM

Malignant astrocytic gliomas observed in the advanced-stage $p53^{\Delta E5\text{-}6}$ mice diffusely infiltrated the forebrain and expressed glioma markers GFAP, Nestin, and Olig2, albeit with a high degree of heterogeneity within individual tumors and between different tumors (Figures 4A, 4B). Importantly, approximately 40% of the $p53^{\Delta E5\text{-}6}$ high-grade astrocytic gliomas exhibited the characteristics of human GBM, including the presence of necrosis, pseudopalisading tumor cells, and microvascular proliferation (Figure 4A). It is worth noting that regardless of the presence or absence of detectable necrosis, these malignant gliomas exhibited similarly high degrees of nuclear atypia (Figures 4B), resembling human primary GBM. These tumors also exhibited the defining features of

human high-grade diffuse gliomas: high levels of mitotic figures and presence of secondary structures of Scherer (Figures 4C). Furthermore, similar to human counterparts, a subpopulation of $p53^{\Delta E5\text{-}6}$ tumor cells expressed a glioma stem cell marker, CD133 (also known as prominin1), and the $CD133^{+}$ glioma cells were often located around blood vessels and expressed p53, Nestin, and Olig2 (Figure 5) (Calabrese et al., 2007; Singh et al., 2004). Taken together, the $p53^{\Delta E5\text{-}6}$ mouse model accurately recapitulates both the genetics and pathology of human high-grade astrocytic gliomas.

2.3.3 p53-deficiency does not provide any growth advantage in adult SVZ

To investigate the mechanism underlying p53-mediated gliomagenesis, we examined the brain of young adult mutant mice. At 2 months of age, no significant difference was identified between the control and $p53^{\Delta E5\text{-}6}$ brains (n = 6 for each genotype), which is consistent with the notion that p53 is dispensable for normal brain development (Donehower et al. 1992; Jacks et al. 1994). Although previous studies demonstrated that a germline p53 null mutation results in mild hyperplasia in the SVZ of the adult brain (Gil-Perotin et al. 2006; Meletis et al. 2006), we found no abnormality in the $p53^{\Delta E5\text{-}6}$ mutant SVZ stem cell niche with respect to the number or the density of the total SVZ cells (Figure 6). Furthermore, no significant difference in the number, the density, or the percentage of BrdU-positive proliferating cells was identified between the control and mutant brains including the SVZ region at 2 months (Figures 6M–3Q). Together, these results indicate that the $p53^{\Delta E5\text{-}6}$ mutation does not confer a measurable growth advantage to brain cells including SVZ stem and progenitor cells in young adult mice.

2.3.4 *Nf1* inactivation promotes p53-mediated malignant glioma formation

The fact that p53-deficiency does not provide any growth advantage to brains suggest that additional cooperative oncogenic alterations must occur to transform p53-deficient brain cells, and introduction of these oncogenic mutations to p53-deficent background could accelerate glioma formation. Consistently, despite that *Nf1* inactivation or activation of PI3K and MAPK signaling pathways appears not essential for p53-mediated gliomagenesis, all the CKO3 mice (hereafter, $p53^{\Delta E5\text{-}6}$;$Nf1^{-/-}$) analyzed (n = 36) developed

malignant astrocytic gliomas with significantly shorter latency compared to the $p53^{\Delta E5-6}$ mutant mice (Figure 3B,C). Nearly 70% of malignant gliomas observed in $p53^{\Delta E5-6}$;$Nf1^{-/-}$ mice exhibited histopathological features of human GBM, such as necrosis. These results demonstrate that *Nf1* inactivation, as one of cooperative oncogenic alterations, albeit not essential, can rapidly promote $p53^{\Delta E5-6}$-mediated gliomagenesis.

2.3.5 Mutant $p53^{\Delta E5-6}$ expression marks p53-deficient brain tumor cells

In human cancers, p53 mutations are mostly missense point mutations and in-frame deletion mutations in the DNA-binding domain (IARC TP53 DATABASE). Unlike other tumor suppressors that are typically down-regulated in tumor cells, the majority of human tumors with p53 mutations express high levels of the mutant p53 protein (Soussi and Wiman 2007). Our $p53^{\Delta E5-6}$ tumors phenocopies human tumors in this respect (Figure 7A-F). The p53 nuclear immunostaining was very specific for $p53^{\Delta E5-6}$ brain tumor cells, as no labeling was observed in the normal brain cells, including those carrying one or two $p53^{\Delta E5-6}$ alleles, or in the p53 null malignant astrocytic gliomas (the tumor model in Zhu et al., 2005a paper). In addition, we used the Rosa-LacZ reporter to confirm that p53-expressing cells have undergone Cre-mediated recombination. Indeed, all the $p53^{\Delta E5-6}$ brain tumors analyzed extensively expressed high levels of β-gal (Figure 7G a and a'). Furthermore, almost all of the $p53^{\Delta E5-6}$-positive brain tumor cells exhibited high levels of β-gal expression (Figures 7G b and b'). It is worth noting that three of five $p53^{\Delta E5-6}$ brain tumors analyzed contained a subpopulation of tumor cells with no or low β-gal staining, which often exhibited high levels of GFAP and hGFAP-cre expression (Figure 7H and data not shown). This is consistent with the previous observations that the R26R-LacZ is not expressed in most GFAP-expressing mature astrocytes, despite their expression of hGFAP-cre (Malatesta et al. 2003). In summary, p53 is stabilized in end-stage gliomas and can be used as a marker for tumor cells.

2.3.6 Expression of mutant p53$^{\Delta E5\text{-}6}$ proteins marks the earliest-stage glioma cells

The stabilization of mutant p53 exclusively in advanced stage glioma cells leads to an interesting question whether we can use the stabilization of this mutant p53 to mark glioma cells in the early stage of tumorigenesis. The first step is to identify early stage glioma precursors. In the normal adult brain, particularly after 4 months of age, virtually all the proliferating cells are restricted to the SVZ or RMS (Figure 8A). This extremely low proliferation background permits the use of BrdU immunostaining as a sensitive assay to identify glioma precursors. Based on the time course of tumor development in p53$^{\Delta E5\text{-}6}$ mice (Figure 3B), we studied the brains of 10 mutant mice at ages of 4 to 4.5 months and found that all of them exhibited abnormal proliferation in the portion of the corpus callosum immediately adjacent to the SVZ or RMS (Figures 8B and 8C). Specifically, four of these ten p53$^{\Delta E5\text{-}6}$ brains had small clusters of abnormal proliferating cells, three of which were identified in the corpus callosum immediately adjacent to the SVZ (Figures 8B' and 8C') and one was observed in the olfactory bulb (OB) (see Figure 13D). By analyzing the serial sections of these four brains, we confirmed that the identified proliferating clusters were the only proliferating cell clusters present in these brains. Thus, these results indicate that the proliferating clusters constitute the initially expanding glioma precursors. Consistently, many cells in the proliferating cell clusters exhibited a high degree of nuclear atypia (Figures 8D and 8F, arrows), a property reminiscent of malignant glioma cells. In addition to the cells in the adult neurogenic niches, glioma precursors were the only cells in mutant brains that expressed Nestin, which is never found in the normal corpus callosum (Figures 8E and 8G, top panels). Together, we conclude that glioma precursors in most mutant brains were Nestin-expressing (Nestin^{+}) cells located in the corpus callosum immediately adjacent to the SVZ.

We went on to determine whether these glioma precursor cells could be marked by mutant p53 expression. We found that about 90% of the proliferating cells revealed by BrdU staining in the corpus callosum expressed a detectable level of mutant p53$^{\Delta E5\text{-}6}$ proteins whereas no cells exhibited such expression in the similar areas of normal brains

(Figures 8E and 8G, bottom panels). Double-immunofluorescence labeling revealed that Nestin and mutant $p53^{\Delta E5\text{-}6}$ proteins were almost always co-expressed in these cells (Figures 8H and 8H'). Furthermore, the $p53^{\Delta E5\text{-}6}$-positive cells expressed Olig2, but not GFAP, CD133, or markers for lineage-restricted progenitors such as PSA-NCAM (a SVZ-A cell marker) or NG2 (a SVZ-OPC cell marker) (Figures 8I, I', K, and K' and data not shown). We further confirmed that all the Nestin+ cells in the proliferating clusters co-expressed Olig2 ($Nestin^{+}/Olig2^{+}$, Figure 8J), demonstrating that glioma precursors are distinct from $Nestin^{-}/Olig2^{+}$ normal glial progenitors or oligodendrocytes in the corpus callosum (Figures 8J and 8J', arrowheads). Taken together, these results demonstrate that the expression of mutant $p53^{\Delta E5\text{-}6}$ proteins specifically marks glioma precursors, which immunohistochemically resemble a subpopulation of transit-amplifying SVZ-C progenitor cells (hereafter, SVZ-C*) with the lineage marker expression pattern of $Nestin^{+}/GFAP^{-}/Olig2^{+}/CD133^{-}$.

To validate that the initially expanded $p53^{\Delta E5\text{-}6}$-positive SVZ-C*-like cells are glioma precursors, we analyzed 19 grossly healthy $p53^{\Delta E5\text{-}6}$ mice at older ages (6 to 9 months) along with 3 mutant mice with non-CNS sarcomas at 10 to 12 months of age. Of these 22 grossly normal $p53^{\Delta E5\text{-}6}$ brains, 15 exhibited no microscopically visible tumor mass. Compared to the mutant brains at younger ages, all the brains with no microscopically visible tumor (n = 14) analyzed between ages of 6 and 10 months had markedly increased numbers of $p53^{\Delta E5\text{-}6}$-positive cells in the corpus callosum and adjacent areas, indicating a continuous expansion of the $p53^{\Delta E5\text{-}6}$-positive cellular populations during tumor development (Figure 9). In all but two of these 14 mutant brains, the $p53^{\Delta E5\text{-}6}$-positive cells were specifically distributed in the forebrain areas that are anatomically immediately adjacent to the SVZ-associated areas (Figure 9). Importantly, most, if not all, of the continuously expanded $p53^{\Delta E5\text{-}6}$-positive cells exhibited the similar features of glioma precursors identified in younger mutant mice, which include hyperproliferation, and expression of Nestin and Olig2, but not GFAP (Figure 9 and data not shown). Together, these results suggest that the $p53^{\Delta E5\text{-}6}$-positive SVZ-C*-like cells in the corpus callosum are glioma precursors, whose continuous expansion underlying malignant glioma development. These observations also demonstrate that the histologically

homogeneous $p53^{\Delta E5\text{-}6}$-positive SVZ-C*-like glioma precursors can give rise to malignant gliomas with a high degree of heterogeneity.

2.3.7 A minor population of adult SVZ cells express mutant $p53^{\Delta E5\text{-}6}$ proteins

The observations described above raise the possibility that we might be able to identify the cell of origin for $p53^{\Delta E5\text{-}6}$-positive malignant glioma cells by determining which cell type in mutant brains first accumulates a detectable level of mutant $p53^{\Delta E5\text{-}6}$ proteins. To test this, we analyzed the brain of 11 2-month-old $p53^{\Delta E5\text{-}6}$ mice when there was no overt abnormality. Immunohistochemical analysis revealed that 1 of these 11 mutant brains lacked any $p53^{\Delta E5\text{-}6}$-positive cells and 5 of them exhibited p53 expression only in one of the two brain hemispheres. These results further confirm the notion that accumulation of a detectable $p53^{\Delta E5\text{-}6}$ protein expression is not an inherent property of this mutant allele, but rather a tumor-dependent event and hence may be used for identifying incipient tumor cells.

In the brains with $p53^{\Delta E5\text{-}6}$ expression, about 80% of $p53^{\Delta E5\text{-}6}$- positive cells were exclusively identified in the adult SVZ niche, including the anterior (SVZa1 and SVZa2), medial (SVZm), and posterior SVZ (Figures 10A and C–F'). Approximately 14% of $p53^{\Delta E5\text{-}6}$-positive cells were found in the RMS (Figures 10B and B'), and a minor population was identified in the areas of the corpus callosum just outside the SVZ (Figures 10F and 10F', arrowhead). Similar to the SVZ-B stem cells, all the $p53^{\Delta E5\text{-}6}$-positive cells expressed Nestin and about 90% of those expressed GFAP, but not markers for lineage-restricted cells (e.g., PSA-NCAM and Olig2) (Figures 10G–10J') (Merkle and Alvarez-Buylla 2006). A small population of the $p53^{\Delta E5\text{-}6}$-positive cells in the SVZ were GFAP negative, which resemble the transit-amplifying SVZ-C progenitor cells (Figures 10H and 10H', arrowhead) (Merkle and Alvarez-Buylla 2006). Together, these results suggest that a minor population of the adult SVZ cells, particularly the SVZ-B stem cells with the lineage marker expression pattern of $Nestin^{+}$/$GFAP^{+}$/ PSA-$NCAM^{-}$/$Olig2^{-}$/$NG2^{-}$/$CD133^{-}$, are the first and the primary cell types that accumulate a detectable $p53^{\Delta E5\text{-}6}$ protein expression in the young adult brain. However, it is worth noting that these $p53^{\Delta E5\text{-}}$

^{6}-positive cells morphologically were not significantly different from the surrounding SVZ cells (Figure 10).

To assess whether these p53$^{\Delta E5\text{-}6}$-positive SVZ cells manifested other tumor cell characteristics, we examined the percentage of proliferating cells in the p53$^{\Delta E5\text{-}6}$-positive and -negative cellular compartments. As revealed by BrdU staining, about 33% of the p53$^{\Delta E5\text{-}6}$-negative stem or progenitor cells were proliferating in the mutant SVZ (370/1112, n = 4 brains). Strikingly, nearly 77% of the p53$^{\Delta E5\text{-}6}$-positive SVZ cells were proliferating (36/47; n = 7 brains; p53high versus p53negative; $p < 0.0001$) (Figures 10K–L'). Because most of the p53$^{\Delta E5\text{-}6}$-positive cells were immunohistochemically identified as SVZ-B stem cells that are relatively a quiescent cell population (Merkle and Alvarez-Buylla 2006), these results suggest that the expression of mutant p53$^{\Delta E5\text{-}6}$ proteins may identify a subpopulation of SVZ stem cells as incipient tumor cells in otherwise relatively normal brains at this age.

2.3.8 Possible lineage relationship between p53$^{\Delta E5\text{-}6}$-positive cell populations

The hyperproliferative phenotypes of p53$^{\Delta E5\text{-}6}$-positive SVZ-B stem cells in the 2-month-old brain raise the possibility that these cells are the cell of origin for the p53$^{\Delta E5\text{-}6}$-positive SVZ-C*-like glioma precursors identified in the corpus callosum of the older mice. To study a possible lineage relationship between these two p53$^{\Delta E5\text{-}6}$-positive cell populations, we quantified the number of p53$^{\Delta E5\text{-}6}$-positive cells in mutant brains at these two ages. Except for the corpus callosum, the number of p53$^{\Delta E5\text{-}6}$-positive cells in mutant SVZ or RMS at 4 months was not significantly increased compared to those at a younger age (Figure 11A). However, in contrast to the p53$^{\Delta E5\text{-}6}$-positive cells that rarely expressed Olig2 in the 2-month-old SVZ, over 60% of the p53$^{\Delta E5\text{-}6}$-positive cells in the SVZ and RMS at 4 months acquired Olig2 expression and exhibited the same lineage marker expression pattern as that of the p53$^{\Delta E5\text{-}6}$-positive glioma precursors (Figure 11B). These results suggest that similar to normal stem cells, the p53$^{\Delta E5\text{-}6}$-positive SVZ-B stem cells can differentiate into Olig2^{+} SVZ-C* progenitor cells, which may function as an intermediate cell type between SVZ-B stem cells and Olig2^{+} SVZ-C*-like glioma

precursors. In support of such a transition, most of the proliferating clusters were identified in the areas immediately adjacent to the adult SVZ neurogenic niches, some of which directly involved the cells in the SVZ (Figures 11C and 11D). More importantly, within these proliferating clusters, the $p53^{\Delta E5\text{-}6}$-positive cells inside and outside the SVZ stem cell niche expressed the same lineage markers as the $Olig2^{+}$ SVZ-C* progenitors regardless of the positions at the anterior SVZ (Figure 11C) or posterior SVZ (Figure 11D) (For high magnification view, see Figure 12).

If the $p53^{\Delta E5\text{-}6}$-positive SVZ-B stem cells give rise to the $p53^{\Delta E5\text{-}6}$-positive $Olig2^{+}$ SVZ-C*-like glioma precursors, both should be p53 deficient and thus can be labeled by Cre-mediated R26R-LacZ expression. To test this, we studied the R26R-LacZ expression in the $p53^{\Delta E5\text{-}6}$ brain. In contrast to most mature astrocytes, all the $p53^{\Delta E5\text{-}6}$-positive SVZ cells expressed β-gal in the mutant brains at 2 months, confirming our lineage marker analysis that these cells were SVZ stem cells or transit-amplifying progenitors (Figure 13A). Furthermore, all the $p53^{\Delta E5\text{-}6}$-positive glioma precursors could also be identified by β-gal expression within the proliferating clusters located in the corpus callosum of older mutant brains (Figures 13B and 13C). These results indicate that both $p53^{\Delta E5\text{-}6}$-positive SVZ-B stem cells and $Olig2^{+}$ SVZ-C*-like glioma precursors are p53 deficient, supporting the notion that these neural stem and progenitor-like cells are the precursors for p53-deficient malignant glioma cells in this model. Finally, of the mutant brains identified with a proliferating cluster, one rare case contained $p53^{\Delta E5\text{-}6}$-positive glioma precursors in the neuronal layers of the OB (Figures 13Da and 13Da'). Despite their presence in the migratory destination of neuroblasts, these $p53^{\Delta E5\text{-}6}$-positive glioma precursors expressed the same lineage markers as $Olig2^{+}$ SVZ-C* progenitors (Figures 13Db–13Dd) and do not express neuronal markers PSA-NCAM, Dcx, or NeuN (data not shown).

2.4 Discussion

2.4.1 p53 glioma mouse model and clinical implications

This study demonstrates that a single p53 mutation can efficiently induce malignant astrocytic glioma formation in mice. Malignant astrocytic gliomas observed in the $p53^{\Delta E5-6}$ model recapitulate genetic, histopathological and molecular features of human GBM (Furnari et al., 2007; Louis et al., 2007). In contrast, using the same hGFAP-cre driver as described here, we previously showed that the hGFAP-cre+;$Nf1^{flox/flox}$ mice exhibited no evidence of tumor formation in the brain, even in the Nf1 heterozygous background, despite that *Nf1*-deficient brain cells had activation of both MAPK and PI3K/Akt signaling pathways (Zhu et al., 2005a; Zhu et al., 2005b). In addition, p53 deficiency can cooperate with *Nf1*- or *Pten*-deficiency to induce malignant astrocytic gliomas in mice (Reilly et al., 2000; Zheng et al., 2008; Zhu et al., 2005a). These results reveal a central role of p53 deficiency in gliomagenesis.

Compared to existing GEM glioma models that utilize multiple genetic mutations (Reilly et al., 2000; Zheng et al., 2008; Zhu et al., 2005a), the uniqueness of our mouse model is that we initially only introduce a single p53 mutation in our system, and this allows for subsequent stochastic accumulation of additional oncogenic mutations to promote glioma formation, which better mimics the "stepwise model" of human tumor development. This opens many directions for future studies. For instance, by analyzing glioma cells at different stages of glioma development in our p53 model, we could pinpoint the sequential activation of oncogenic pathways in an *in vivo* setting and identify genetic pathways that are critical for glioma initiation, progression and maintenance (for detailed discussion, see Chapter IV). In addition, since $p53^{\Delta E5-6}$ mice provide a sensitive genetic background for glioma development, this strain could be used to validate newly identified glioma genes and to generate a series of GBM models for preclinical testing of therapies that target more specific oncogenic pathways.

2.4.2 Possible oncogenic activity of $p53^{\Delta E5-6}$ protein

In human cancers, TP53-associated tumors typically contain mis-sense mutations in the TP53 gene rather than deletions of TP53. These mutant p53 proteins are highly expressed in endstage tumor cells, suggesting possible growth advantage for cells with missense mutations. The oncogenic roles of p53 mutants have been examined extensively in cell lines. Mouse models that inherit p53 mutations expressed at physiological levels have recently been generated to examine the activities of mutant p53 *in vivo*. Mice with p53 hotspot point mutations develop tumor spectrums and metastatic phenotypes different from those of mice with a p53-null allele. Mechanisms for this gain-of-function potential include increased genomic instability, increased cell migration and invasion and resistance to proapoptotic signals. Many gain-of-function effects of mutant p53 rely on its ability to bind and inactivate the p53 family members p63 and p73 (for review, see Moshe Oren and Varda Rotter, 2010).

Although the same $p53^{\Delta E5-6}$ mutation is not found in human gliomas, our mouse model phenocopies the histological features of human GBM and exhibits high level of p53 $^{\Delta E5-6}$ accumulation in tumor cells. Previous studies reported no brain tumor formation in p53 germline knockout mice (Gil-Perotin et al. 2006; Meletis et al. 2006), and $p53^{-/-}$ mice in our colony with a similar genetic background to CKO1 and CKO2 mice do not develop brain tumors. This raises the question whether p53 $^{\Delta E5-6}$ could have oncogenic activities similar to p53 missense mutations. The comparison of p53 $^{\Delta E5-6}$, p53 hotspot point mutation and p53 conditional null allele is an ongoing project in the lab carried out by Dr. Yinghua Li. His preliminary data suggest that mutant p53 could facilitate the accumulation of DNA damage and promote the survival of cells with DNA damage (personal communication).

2.4.3 Cell-of-origin for malignant astrocytic glioma

Murine models have been widely used to study the cell-of-origin of a cancer. Ideally, an oncogenic mutation can be targeted into the cells at various developmental stages of a specific cell lineage. However, this approach is often limited in the CNS due to a lack of

well-defined cell lineage-specific promoters. For example, despite being one of the best characterized and the most widely used CNS stem/progenitor cell markers, Nestin is expressed not only in multipotent SVZ-B neural stem cells and SVZ-C transit amplifying progenitors but also in lineage-restricted SVZ-A neuroblasts in the adult brain (Doetsch et al. 1997). Moreover, if a deletion-based mutational strategy (e.g., Cre/loxP system) is employed to drive tumor formation, lineage-restricted SVZ-OPC glial progenitors and oligodendrocytes, albeit expressing no Nestin, will inherit the same mutations that are targeted in Nestin^{+} SVZ-B and C cells (Menn et al. 2006). Thus, with current technologies, it is not feasible to specifically target a genetic mutation in the multipotent CNS stem/progenitor cells.

Compared to currently available p53-associated glioma models, one feature of our model is that mutant p53$^{\Delta E5\text{-}6}$ proteins are accumulated to a detectable level in all stages of glioma cells but not in normal brain cells. Combining proliferation, lineage marker expression, and morphological analysis, we used this p53 marker to study glioma precursors at the single-cell level during the earliest stages of tumor development. Although advanced-stage p53$^{\Delta E5\text{-}6}$ gliomas are extremely heterogeneous histopathologically and molecularly, the p53$^{\Delta E5\text{-}6}$-positive glioma precursors are remarkably homogeneous and exhibit a lineage marker expression pattern reminiscent of Olig2^{+} SVZ-C* transitamplifying progenitor cells. Moreover, despite that the p53$^{\Delta E5\text{-}6}$ mutation was targeted to diverse CNS cell populations throughout the brain, the p53$^{\Delta E5\text{-}6}$-positive glioma precursors were exclusively identified in the two brain areas, corpus callosum and OB, which are the migratory destinations of the two differentiated progeny of the multipotent SVZ stem cells. Therefore, the lineage marker expression pattern and anatomical location of glioma precursors suggest that the p53$^{\Delta E5\text{-}6}$-positive malignant glioma cells may arise from multipotent SVZ stem cells and/or transit-amplifying progenitors. Consistently, we demonstrate that the SVZ-B stem cells and SVZ-C progenitors are the earliest cell types that accumulate a detectable p53$^{\Delta E5\text{-}6}$ protein expression in the brains of younger mutant mice. Based on these results, we propose a model for the role of neural stem cells and transit-amplifying progenitors in p53-mediated gliomagenesis: (1) the SVZ-B stem cells are most susceptible to accumulation of

oncogenic alterations, as evidenced by high levels of mutant $p53^{\Delta E5-6}$ expression; (2) the glioma-initiating cells are the $Olig2^{+}$ SVZ-C* progenitor-like cells at the earliest stages of tumor development; (Moore et al.) the majority of differentiation-stalled $Olig2^{+}$ SVZ-C* progenitor-like cells migrate as SVZ-OPCs to the corpus callosum and a minor population migrate as SVZ-A neuroblasts to the RMS and OB; (4) $p53^{\Delta E5-6}$-positive SVZ-C*-like glioma precursors can use diverse cooperative oncogenic alterations to form high-grade gliomas with a markedly high degree of heterogeneity (Figure 14).

Although the expression of mutant p53 proteins provides a sensitive tool to monitor early-stage glioma cells at the single-cell level, the extremely low number of the $p53^{\Delta E5-6}$-positive cells in mutant brains makes it difficult to establish a definitive lineage relationship between the morphologically normal $p53^{\Delta E5-6}$-positive neural stem cells and glioma precursors. However, we obtain several independent lines of evidence supporting a lineage relationship between these two $p53^{\Delta E5-6}$-positive cell populations. First, $p53^{\Delta E5-6}$-positive cells in the SVZ are the only cells that exhibit measurable tumor cell characteristics, such as hyperproliferation, suggesting that these cells are the incipient glioma cells in otherwise normal brains at 2 months. Second, there is an intermediate cell type between $p53^{\Delta E5-6}$-positive SVZ-B stem cells and $Olig2^{+}$ SVZ-C*-like glioma precursors in the 4-month-old mutant brains. These $p53^{\Delta E5-6}$-positive intermediate cells resemble $Olig2^{+}$ SVZ-C*-like glioma precursors, but are located in the SVZ. Consistently, in some proliferating clusters, expansion of the $p53^{\Delta E5-6}$-positive SVZ-C*-like glioma precursors can be found in both the SVZ and corpus callosum. Finally, both $p53^{\Delta E5-6}$-positive SVZ-B stem cells and $Olig2^{+}$ SVZ-C*-like glioma precursors in the corpus callosum can be marked by Cre-mediated R26R-LacZ expression, indicating that these two cell populations are genetically p53 deficient.

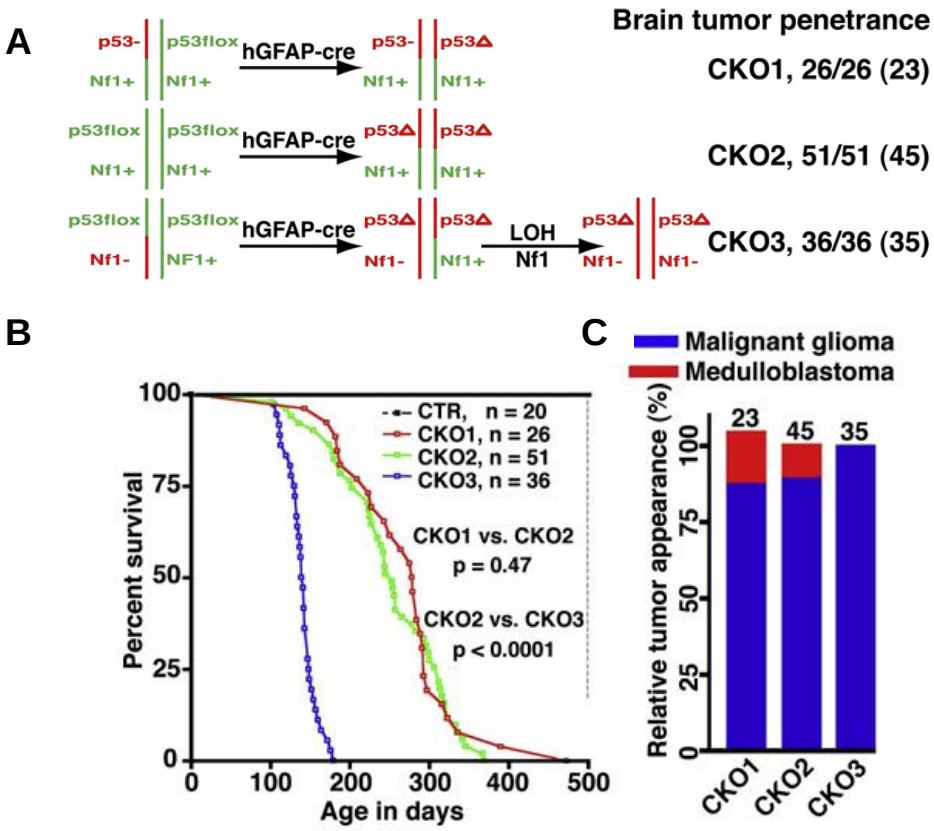

Figure 3. Tumorigenesis in CKO1, CKO2 and CKO3 mice. (A) Schematic drawing of the genetic configurations of CKO1–3 mice. All the mutant mice analyzed developed brain tumors, including those in early stages. The number in parentheses shows the number of mutant mice that developed high-grade brain tumors. (B) Survival curves of control and CKO1–3 mutant mice. p value was obtained from Kaplan-Meier survival test. (C) The percentage of malignant astrocytic gliomas and medulloblastomas observed in the mutant mice with high-grade brain tumors. Of note, 1 of 23 CKO1 mice developed both malignant glioma and medulloblastoma.

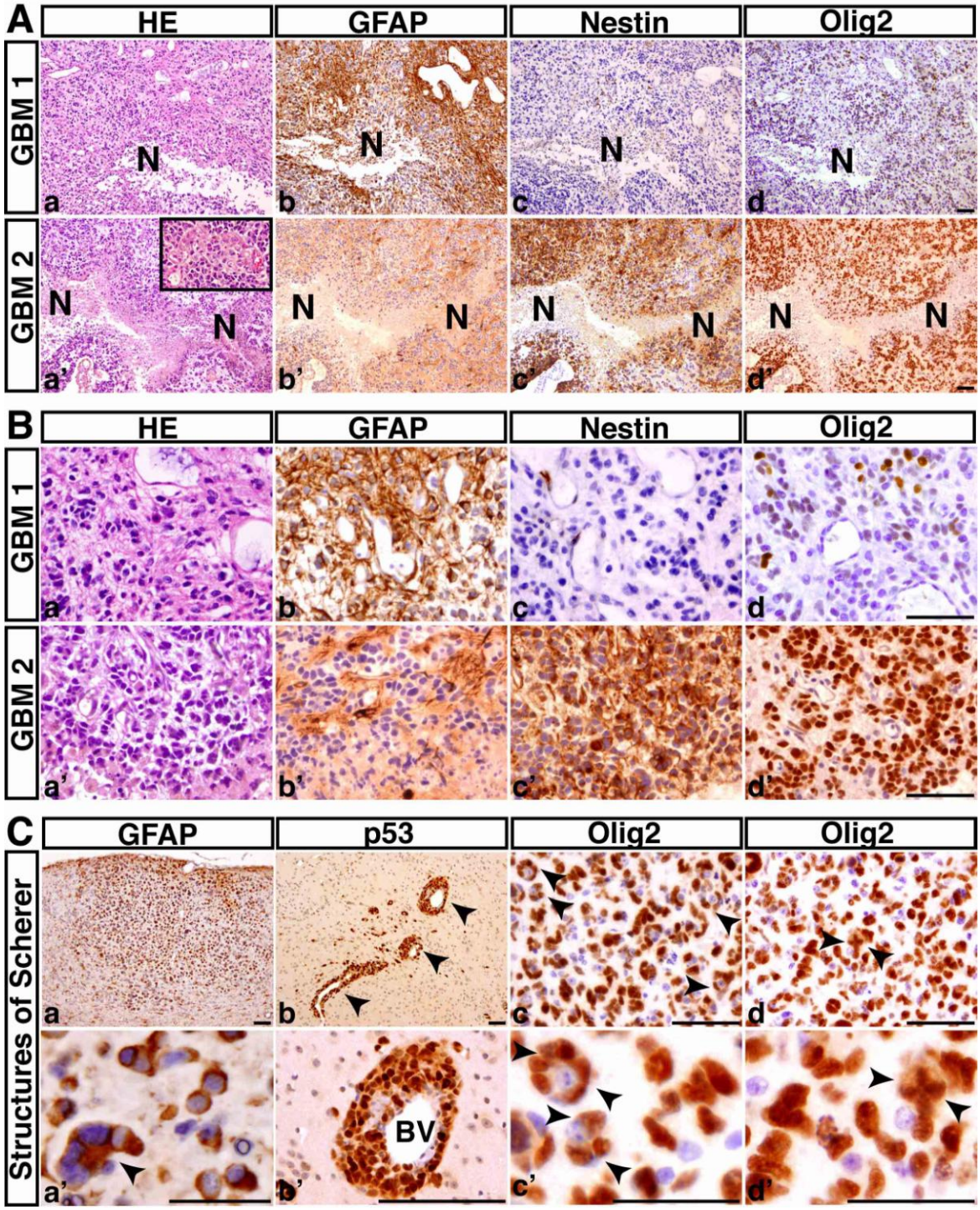
A
HE
GFAP
Nestin
Olig2
GBM 1
GBM 2
N
a
b
c
d
a'
b'
c'
d'
B
HE
GFAP
Nestin
Olig2
GBM 1
GBM 2
a'
b'
c'
d'
C
GFAP
p53
Olig2
Olig2
Structures of Scherer
a
b
c
d
a'
b'
c'
d'
BV

Figure 4. The $p53^{\Delta E5\text{-}6}$ mutant mice develop GBMs (contributed by Yuan Zhu and Jiong Yang).

(A) Serial sections from two representative $p53^{\Delta E5\text{-}6}$ GBMs (GBM1, 2) were stained with H&E (a, a'), anti-GFAP (b, b'), anti-Nestin (c, c'), and anti-Olig2 (d, d'). N, necrosis. There are regions of coagulation necrosis (a-d), and pseudopalisades of malignant GBM cells adjacent to necrosis (a'-d'). The inset in (a') shows microvascular proliferation in this GBM. (B) High-magnification views of (A) illustrate that both malignant cells and nuclei are highly pleomorphic. Many GBM cells have substantial cytoplasm and some have eccentric nuclei (a, a'). (C) The $p53^{\Delta E5\text{-}6}$ gliomas exhibit the secondary structures of Scherer: accumulation of GFAP-positive tumor cells in the subpial zone of the cerebral cortex (a, a'); perivascular satellitosis (arrowheads) (b, b'); and perineuronal satellitosis (arrowheads, c, c'). (d, d') The examples of $Olig2^{+}$ tumor cells with abnormal mitoses (arrowheads). BV, blood vessels. Scale bar, (A, B, Ca-d), 50 μm; (Ca'-d'), 25 μm.

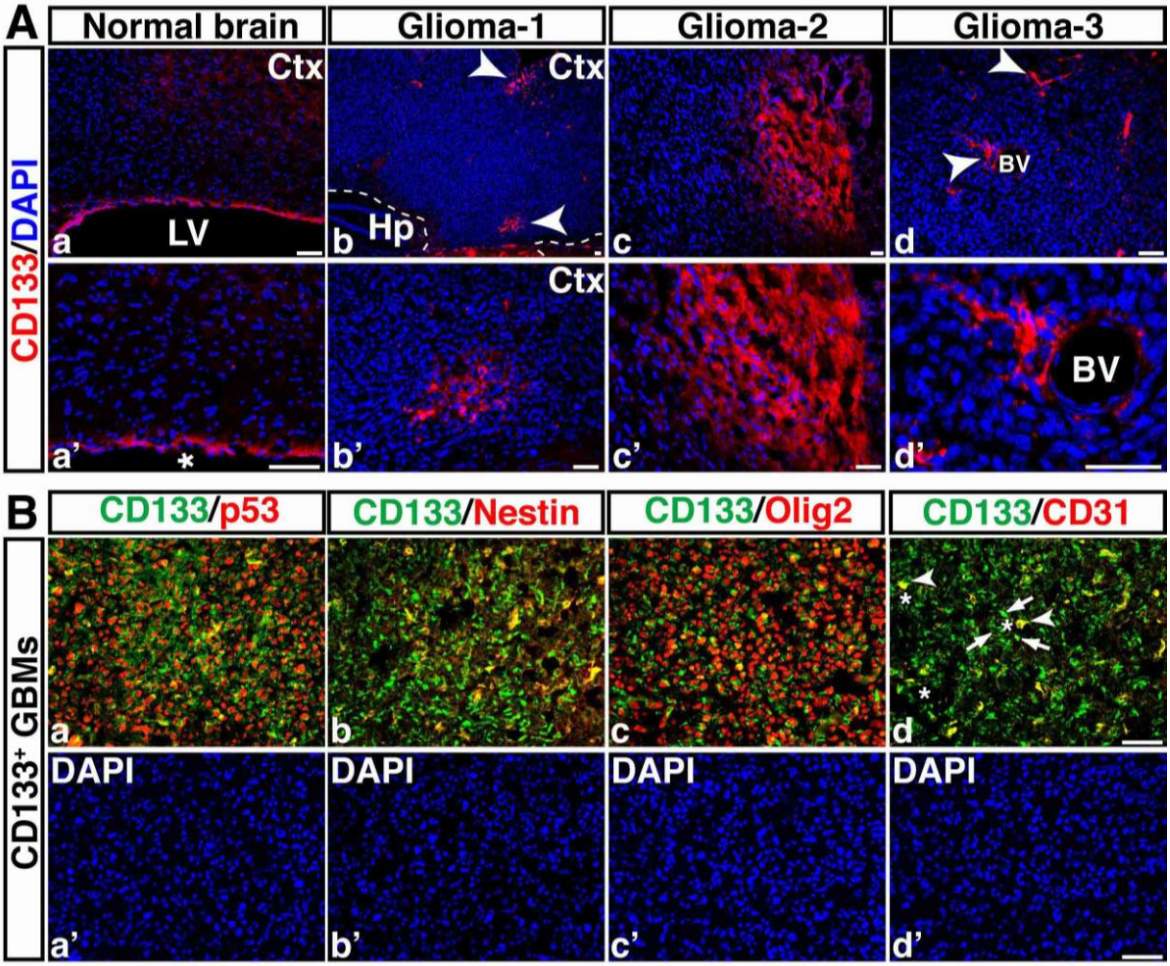

Figure 5. Expression of CD133 in normal brain and malignant astrocytic gliomas.
(A) Sections of normal brain (a) and three representative gliomas (b, c, d) were stained with anti-CD133 (red) and DAPI (blue). (a' to d') High magnification views of (a to d) illustrates that a subpopulation of glioma cells express CD133 (b, c, d) whereas only ependymal cells in normal brain were immunoreactive for CD133 (a). Arrowheads in (b, d) point to $CD133^+$ malignant glioma cells, many of which were identified around the blood vessels (BV, d, d'). The dashed lines in (b) mark the border of the tumor and normal brain tissues. Ctx, cerebral cortex; LV or "*", lateral ventricle; Hp, hippocampus. (B) Serial sections from a GBM with focal areas containing a significant number of $CD133^+$ cells were stained with anti-CD133/anti-p53 (a), anti-CD133/anti-Nestin (b), anti-CD133/anti-Olig2 (c), and anti-CD133/anti-CD31 antibodies (d). These sections were counterstained with DAPI for labeling tumor nuclei (a' to d'). Arrows in (d) show $CD133^+/CD31^-$ tumor cells and arrowheads point to a minor population of $CD133^+/CD31^+$ endothelial cells that surround the blood vessels (*) in the tumor. Scale bar, 50 μm.

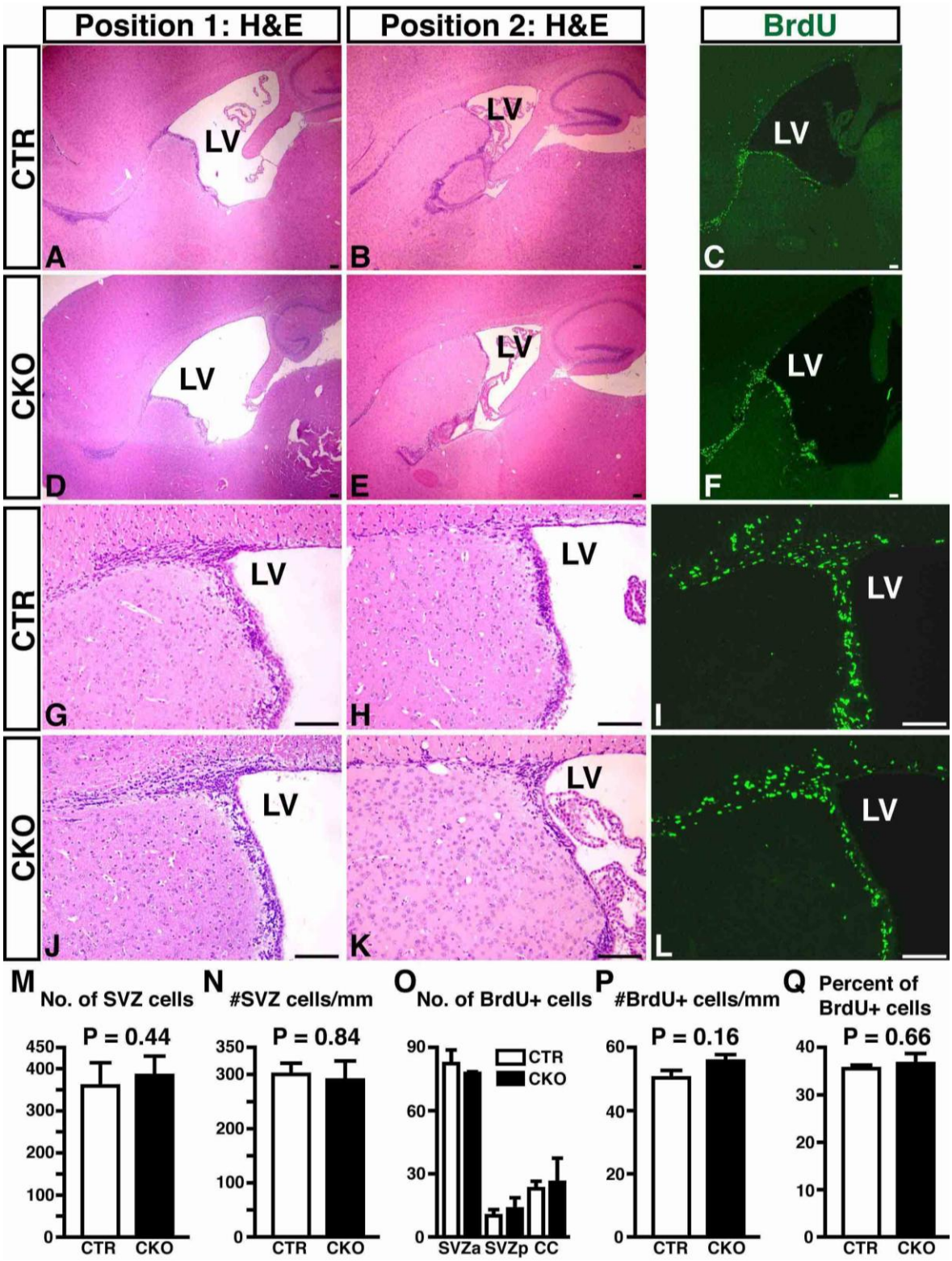
Position 1: H&E
Position 2: H&E
BrdU
CTR
CKO
LV
A
B
C
D
E
F
G
H
I
J
K
L
M No. of SVZ cells
P = 0.44
N #SVZ cells/mm
P = 0.84
O No. of BrdU+ cells
CTR
CKO
SVZa SVZp CC
P #BrdU+ cells/mm
P = 0.16
Q Percent of BrdU+ cells
P = 0.66

Figure 6. Comparison of control and $p53^{\Delta E5-6}$ mutant brains at 2 months of age. The brains of control and mutant mice at age of 2 months were sagittally sectioned, and stained with H&E (A, B and D, E) or anti-BrdU (C, F). Two independent positions (~ 100 μ apart) at sagittal planes along the midline to lateral direction were selected to compare the size and cellular density of the SVZ between control and mutant brains. (G, H, I) and (J, K, L) show the high-magnification views of the SVZ areas in (A, B, C) and (D, E, F), respectively. No significant difference in cell density and proliferation was identified between control and mutant SVZ. LV, lateral ventricle. Quantification of the number of the SVZ cells (M); the density of the SVZ cells (N) that was presented by the number of SVZ cells per unit length of the LV; the number of BrdU-positive cells in the SVZ and corpus callosum (O); and the density (P) and percentage (Q) of the BrdU-positive cells in the SVZ between control and mutant brains. Data were presented by mean ± SEM. $P < 0.05$ is considered as statistically significant. No detectable abnormality was identified in $p53^{\Delta E5-6}$ mutant brains at 2 months of age. Scale bar, 100 μ.

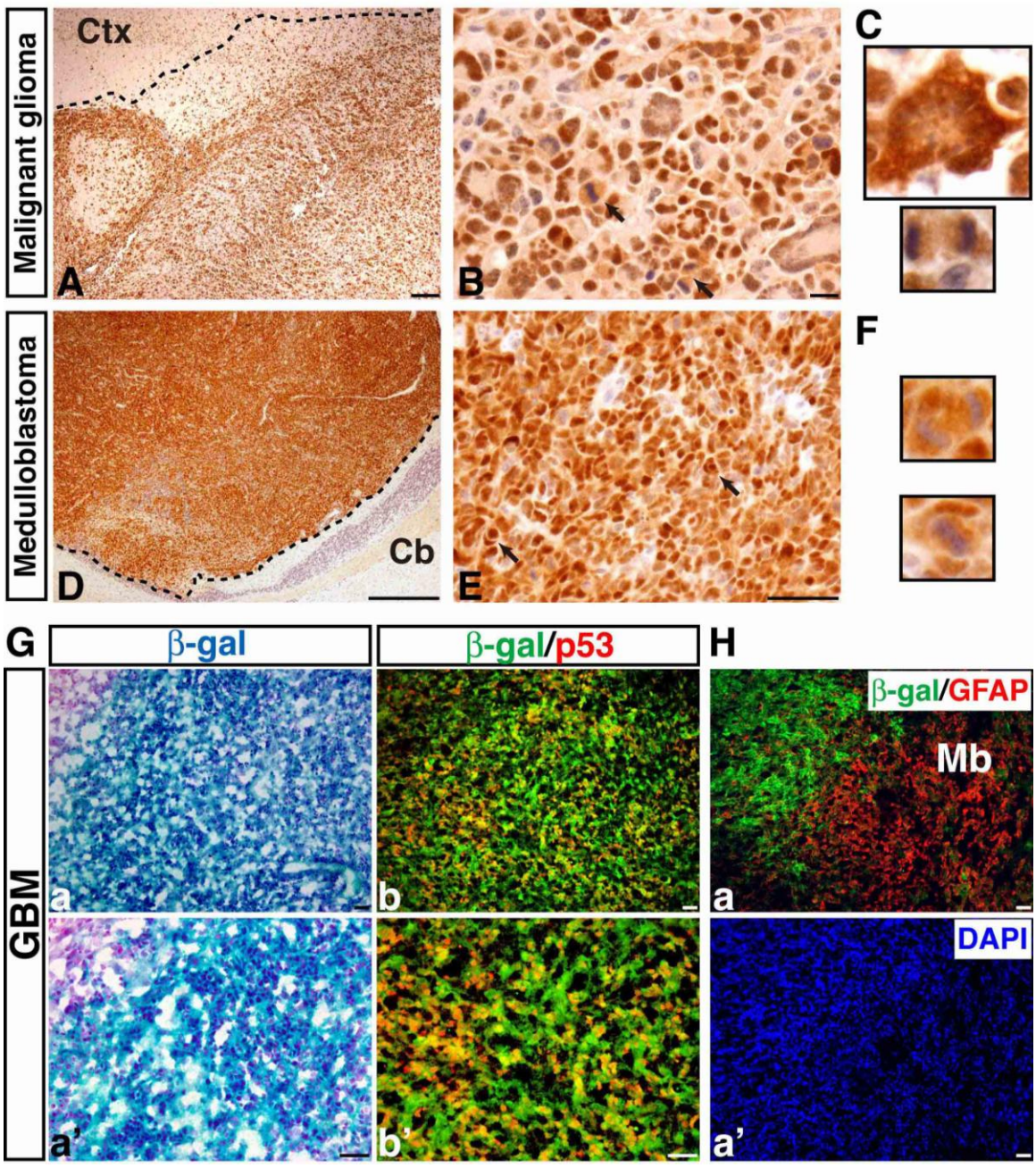
Malignant glioma
Ctx
A
B
C
Medulloblastoma
D
Cb
E
F
G
β-gal
β-gal/p53
H
GBM
a
b
β-gal/GFAP
Mb
a'
b'
DAPI
a'

Figure 7. $p53^{\Delta E5\text{-}6}$ brain tumors specifically express a detectable level of mutant p53 proteins. Representative examples showing $p53^{\Delta E5\text{-}6}$-positive malignant astrocytic gliomas (A and B) and medulloblastomas (D and E). The dashed lines roughly mark the border of the tumors and surrounding brain tissues because of the infiltrating nature of these tumors (A and D). Arrows in (B) and (E) point to mitotic figures in malignant gliomas and nuclear molding in medulloblastomas, respectively. (C) High magnification views of a $p53^{\Delta E5\text{-}6}$-positive multinucleated giant cell (top) and mitotic figure (bottom) in a malignant glioma. (F) High magnification views of a $p53^{\Delta E5\text{-}6}$-positive mitotic figure (top) and nuclear molding (bottom) in a medulloblastoma. Ctx, cerebral cortex; Cb, cerebellum. (G) Adjacent sections from $p53^{\Delta E5\text{-}6}$ brain tumors harboring the R26R-LacZ transgene were stained with X-gal (a and a') and anti-β-gal/anti-p53 antibodies (b and b'). All the $p53^{\Delta E5\text{-}6}$-positive tumor cells exhibited β-gal expression, indicating p53 deficiency. (H) A small population of tumor cells expressed little or no β-gal, but had high levels of GFAP expression (a). Tumor nuclei were counterstained with DAPI (a'). Scale bars, 50 μ.

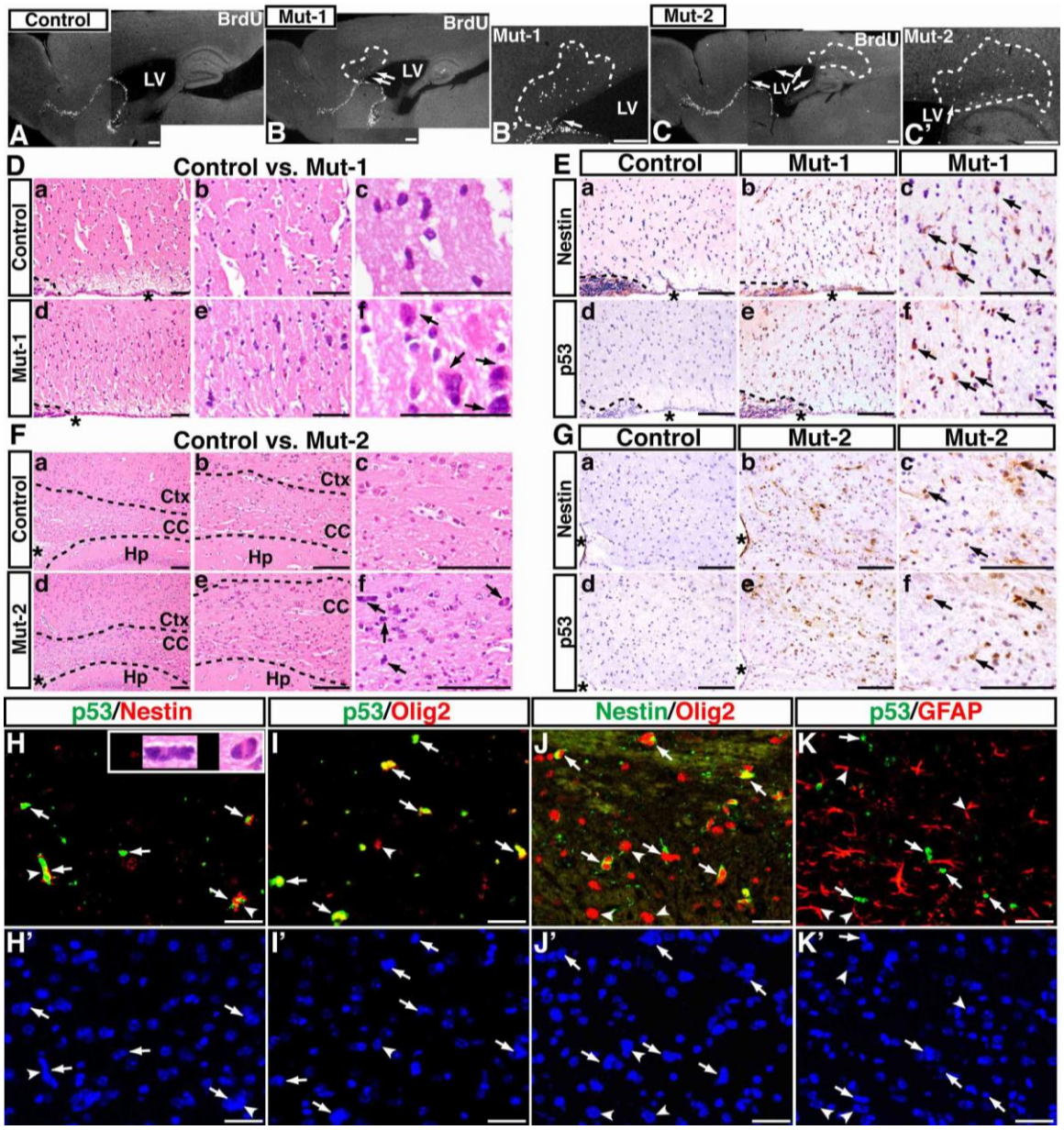
Control
BrdU
LV
A
Mut-1
BrdU
LV
B
Mut-1
LV
B'
Mut-2
BrdU
LV
C
Mut-2
LV
C'
D
Control vs. Mut-1
Control
Mut-1
a
b
c
d
e
f
E
Control
Mut-1
Mut-1
Nestin
p53
F
Control vs. Mut-2
Ctx
CC
Hp
G
Control
Mut-2
Mut-2
p53/Nestin
p53/Olig2
Nestin/Olig2
p53/GFAP
H
I
J
K
H'
I'
J'
K'

Figure 8. Expression of mutant $p53^{\Delta E5\text{-}6}$ proteins identifies the earliest-stage glioma cells. (A–C) BrdU staining was performed on sections from age-matched control (A) and two representative $p53^{\Delta E5\text{-}6}$ brains that contain proliferation clusters (marked by dashed lines) in the corpus callosum adjacent to the anterior SVZ (B and B' , Mut-1) and to the posterior SVZ (C and C' , Mut-2), respectively. Arrows in (B) through (C') point to abnormal proliferating cells in the SVZ. LV, lateral ventricle. (D) The H&E-stained sections from similar areas of control brain (a–c) and the proliferating cluster of Mut-1 brain (d–f) were imaged and shown at three different magnifications. (E) Adjacent sections of the control and Mut-1 brains (D) were stained with anti-Nestin and anti-p53 antibodies. (F and G) Similar morphological and immunohistochemical analyses of (D and E) were performed on control brain and a proliferating cluster of Mut-2 brain. Arrows in (D) and (F) point to abnormal cells with atypical nuclei in mutant brains. Arrows in (E) and (G) point to $Nestin^{+}$ and $p53^{+}$ cells in mutant brains. Asterisk in (D) to (G) denotes the lateral ventricle. The dashed lines in (D) and (E) and in (F) mark the border of the SVZ and corpus callosum and the border of the corpus callosum and surrounding tissues, respectively. Ctx, cerebral cortex; CC, corpus callosum; Hp, hippocampus. (H–K) The sections from the proliferating clusters were stained with anti-p53/anti-Nestin (H) and DAPI (H'); anti-p53/anti-Olig2 (I) and DAPI (I'); anti-Nestin/anti-Olig2 (J) and DAPI (J'); anti-p53/ anti-GFAP (K) and DAPI (K'). Arrows in (H)–(K) point to $p53^{\Delta E5\text{-}6}$-positive cells. Arrowheads in (J) and (J') point to Nestin-/$Olig2^{+}$ cells that are most likely normal glial progenitors or oligodendrocytes. Arrowheads in (K) and (K') point to the p53-negative nuclei of $GFAP^{+}$ cells. The inset in (H) shows atypical nuclei of two $p53^{+}$/$Nestin^{+}$ cells (arrowheads). Scale bars, 25 μ.

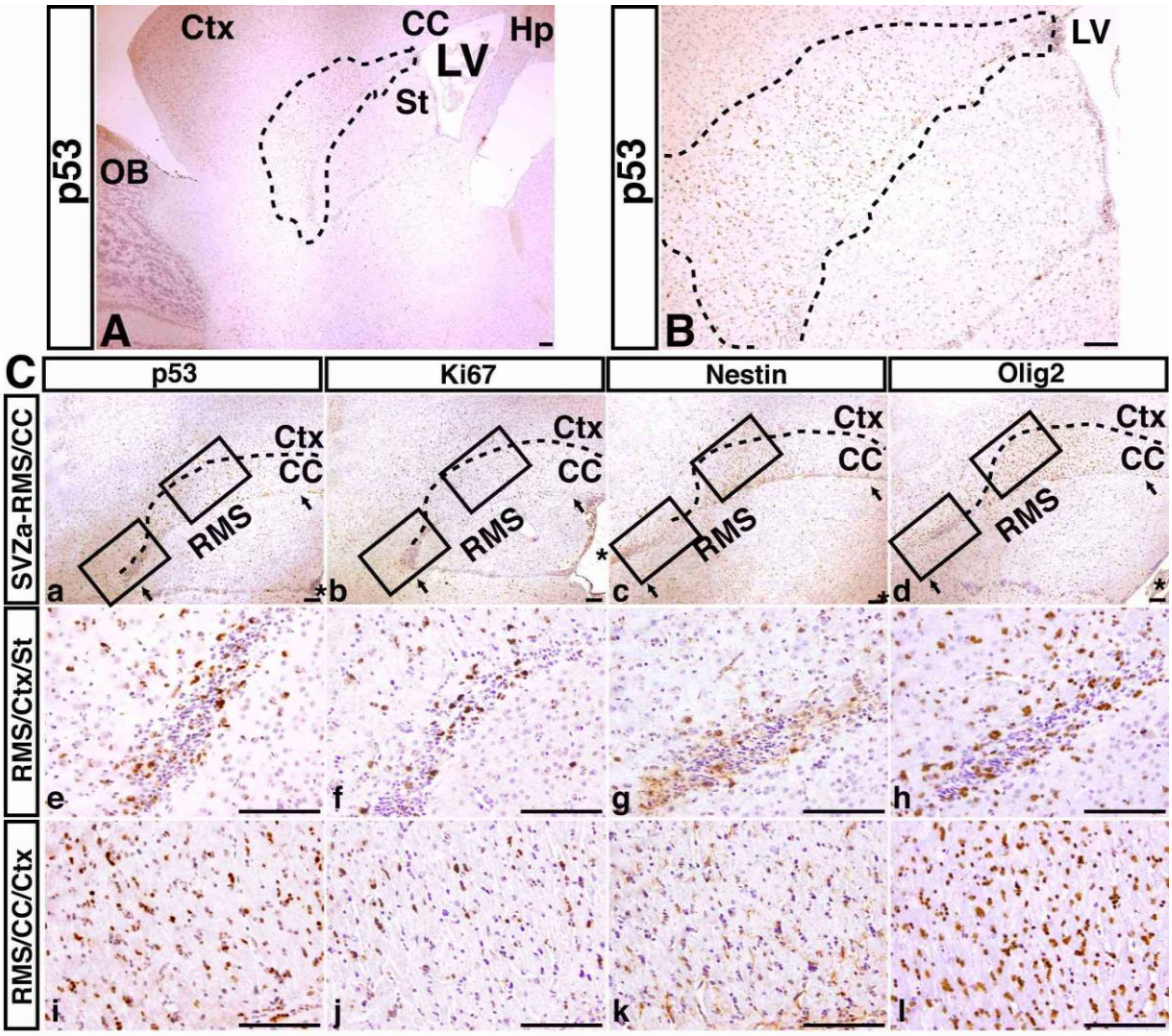

Figure 9. Continuous expansion of the $p53^{\Delta E5\text{-}6}$-positive cells underlies tumor development (Contributed by Yuan Zhu).

The images taken at two magnifications (A, B) show $p53^{\Delta E5\text{-}6}$-positive glioma cells from one representative $p53^{\Delta E5\text{-}6}$ mutant brain in the early stages of tumor development. The dashed lines in (A, B) mark the $p53^{\Delta E5\text{-}6}$-positive early lesions. (C) Adjacent sections of the mutant brain with an early lesion (A, B) were stained with anti-p53 (a, e, i), anti-Ki67 (b, f, j), anti-Nestin (c, g, k), and anti-Olig2 (d, h, l). Arrows in (a to d) mark the length of the RMS in these images. RMS, rostral migratory stream; Ctx, cerebral cortex; CC, corpus callosum. "*" marks lateral ventricle. (e, i), (f, j), (g, k), and (h, l) are the high-magnification views of the boxed areas marked in (a), (b), (c), and (d), respectively. Scale bar, 100 μm.

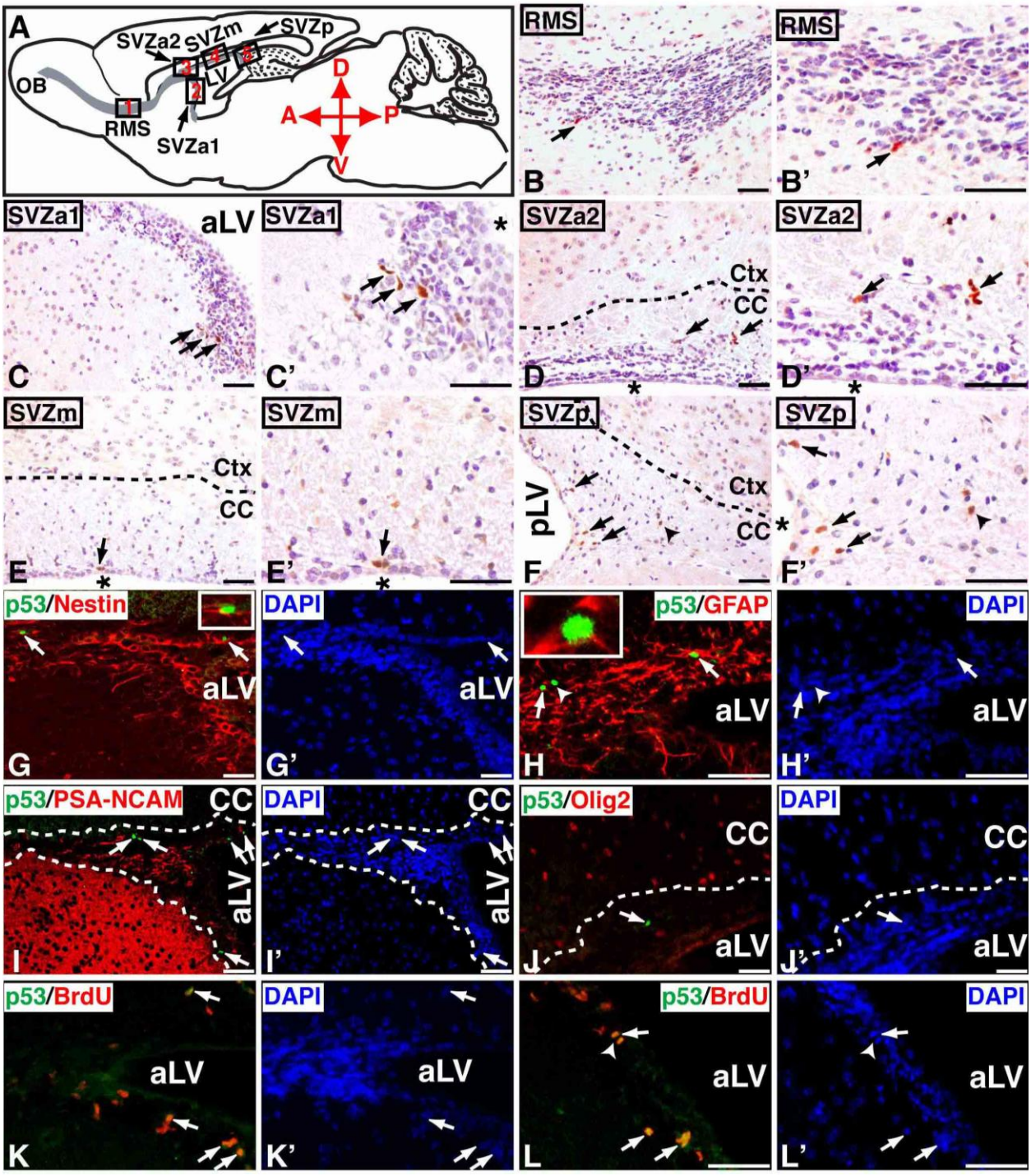
A
SVZa2
SVZm
SVZp
OB
LV
RMS
SVZa1
D
A
P
V
RMS
B
RMS
B'
SVZa1
aLV
C
SVZa1
*
C'
SVZa2
Ctx
CC
D
*
SVZa2
D'
*
SVZm
Ctx
CC
E
*
SVZm
E'
*
SVZp
pLV
Ctx
CC
*
F
SVZp
F'
p53/Nestin
aLV
G
DAPI
aLV
G'
p53/GFAP
aLV
H
DAPI
aLV
H'
p53/PSA-NCAM
CC
aLV
I
DAPI
CC
aLV
I'
p53/Olig2
CC
aLV
J
DAPI
CC
aLV
J'
p53/BrdU
aLV
K
DAPI
aLV
K'
p53/BrdU
aLV
L
DAPI
aLV
L'

Figure 10. A minor population of SVZ stem and progenitor cells exhibits a detectable mutant $p53^{\Delta E5\text{-}6}$ protein expression in young adult brain.

(A) Schematic drawing of the sagittal plane of the adult mouse brain. Except for the dentate gyrus of the hippocampus, all the Nestin+ cells in the adult brain are restrictively located in the SVZ and RMS and colored in gray. Different parts of the RMS and SVZ are shown in five designated boxed areas. At 2 months of age, most of the $p53^{\Delta E5\text{-}6}$-positive cells (B to F', arrows) are identified in the adult neurogenic areas, which include the RMS (B and B'), the anterior SVZ (C and C', SVZa1; and D and D', SVZa2), medial SVZ (E and E' , SVZm), and posterior SVZ (F and F' , SVZp). The arrowhead in (F) and (F') points to a $p53^{\Delta E5\text{-}6}$- positive cell in the adjacent corpus callosum. Sections of the anterior SVZ from 2-month-old $p53^{\Delta E5\text{-}6}$ mice were stained by anti-p53/anti-Nestin (G) and DAPI (G'); anti-p53/anti-GFAP (H) and DAPI (H'); anti-p53/anti-PSA-NCAM (I) and DAPI (I'); anti-p53/anti-Olig2 (J) and DAPI (J'); and antip53/ anti-BrdU (K and L) and DAPI (K' and L'). Arrows in (G)–(L') point to the $p53^{\Delta E5\text{-}6}$-positive cells in the SVZ. An arrowhead in (H) and (H') points to a $p53^{\Delta E5\text{-}6}$-positive/GFAP-negative progenitor cell. The insets in (G) and (H) show the high-magnification views of the $p53^{\Delta E5\text{-}6}$-positive cells expressing Nestin and GFAP, respectively. Arrowheads in (L) and (L') point to a $p53^{\Delta E5\text{-}6}$-positive cells during mitosis. aLV and pLV, anterior and posterior lateral ventricle; (*), lateral ventricle. Scale bars, 25 μ.

Figure 7

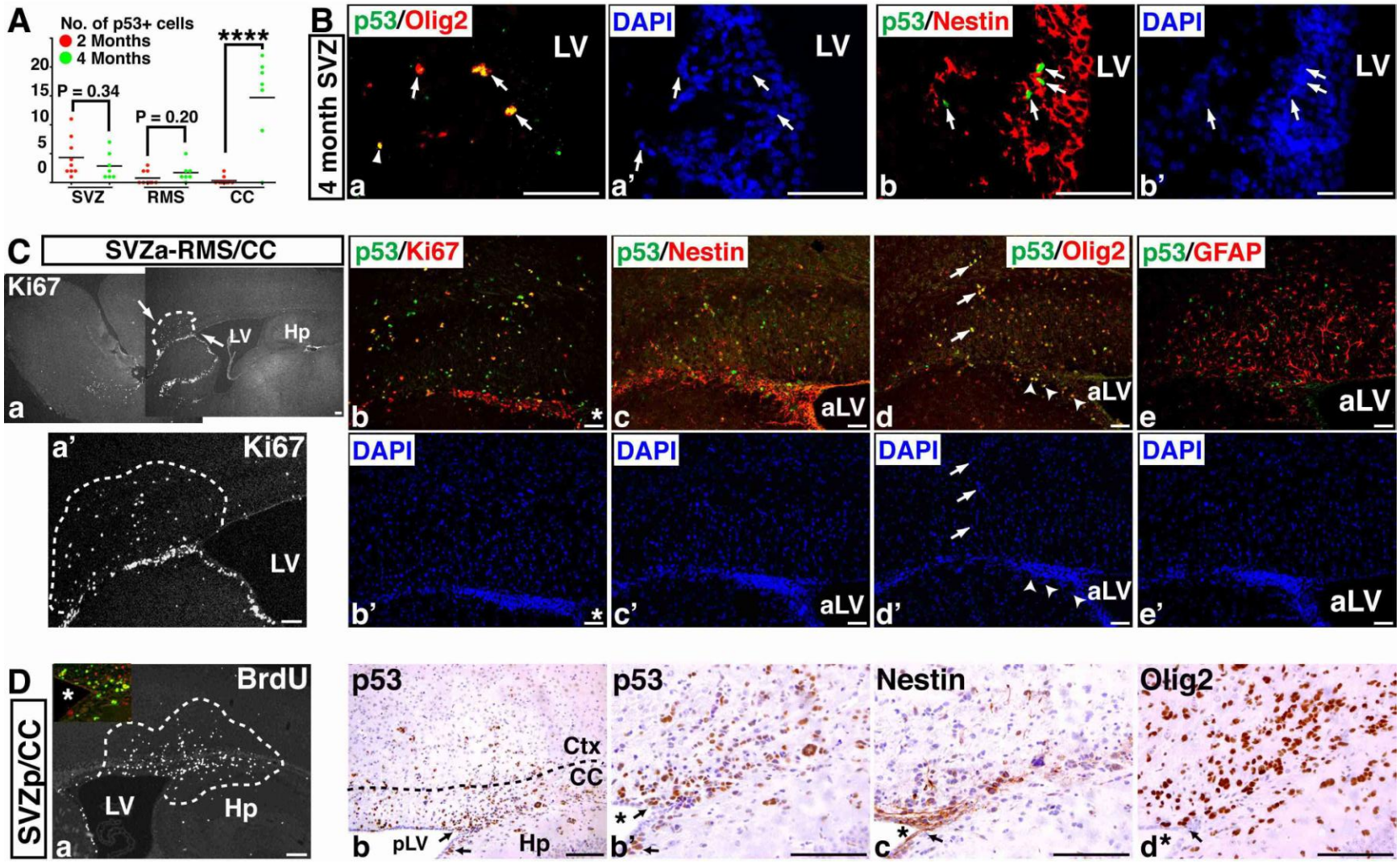
A
No. of p53+ cells
2 Months
4 Months
P = 0.34
P = 0.20
****
SVZ
RMS
CC
B
4 month SVZ
p53/Olig2
DAPI
p53/Nestin
LV
C
SVZa-RMS/CC
Ki67
Hp
p53/Ki67
p53/Nestin
p53/Olig2
p53/GFAP
aLV
D
SVZp/CC
BrdU
p53
Nestin
Olig2
Ctx
CC
pLV

Figure 11. A possible lineage relationship between p53ΔE5-6-positive SVZ-B stem cells and SVZ-C* progenitor-like glioma precursors.
(A)The quantification of $p53^{\Delta E5-6}$-positive cells in brains of mutant mice at 2 and 4 months. Each dot represents the quantification from each individual brain. ****$p < 0.0001$. (B) Sections from a 4-month-old mutant brain were stained with anti-p53/anti-Olig2 (a) and DAPI (a') and anti-p53/anti-Nestin (b) and DAPI (b'), in which arrows point to $p53^{\Delta E5-6}$-positive cells in the SVZ. (C) One representative mutant brain has proliferating clusters (marked by dashed lines) in the corpus callosum directly associated with the anterior SVZ (a and a'). Sections from this proliferating cluster were stained with anti-p53/anti-Ki67 (b) and DAPI (b'); anti-p53/anti-Nestin (c) and DAPI (c'); anti-p53/anti-Olig2 (d) and DAPI (d'); and anti-p53/anti-GFAP (e) and DAPI (e'). Arrows and arrowheads in (d) and (d') point to $p53^{\Delta E5-6}$-positive Olig2+ SVZ-C*-like glioma precursors located in the corpus callosum and SVZ, respectively. (D) Adjacent sections from one proliferating cluster identified in the posterior SVZ (a) were stained with anti-p53 (b and b'), anti-Nestin (c), and anti-Olig2 antibodies (d). Arrows in (b) to (d) point to $p53^{\Delta E5-6}$-positive glioma precursors inside the SVZ. The inset in (a) shows the high-magnification view of proliferating $p53^{\Delta E5-6}$-positive glioma precursors in the SVZ (BrdU[green]/p53[red]). aLV and pLV, anterior and posterior lateral ventricle; *, lateral ventricle. Scale bars: (Ca, Ca' , and Da) 100 μ ; (B, Cb–Ce' , and Db–Dd) 50 μ.

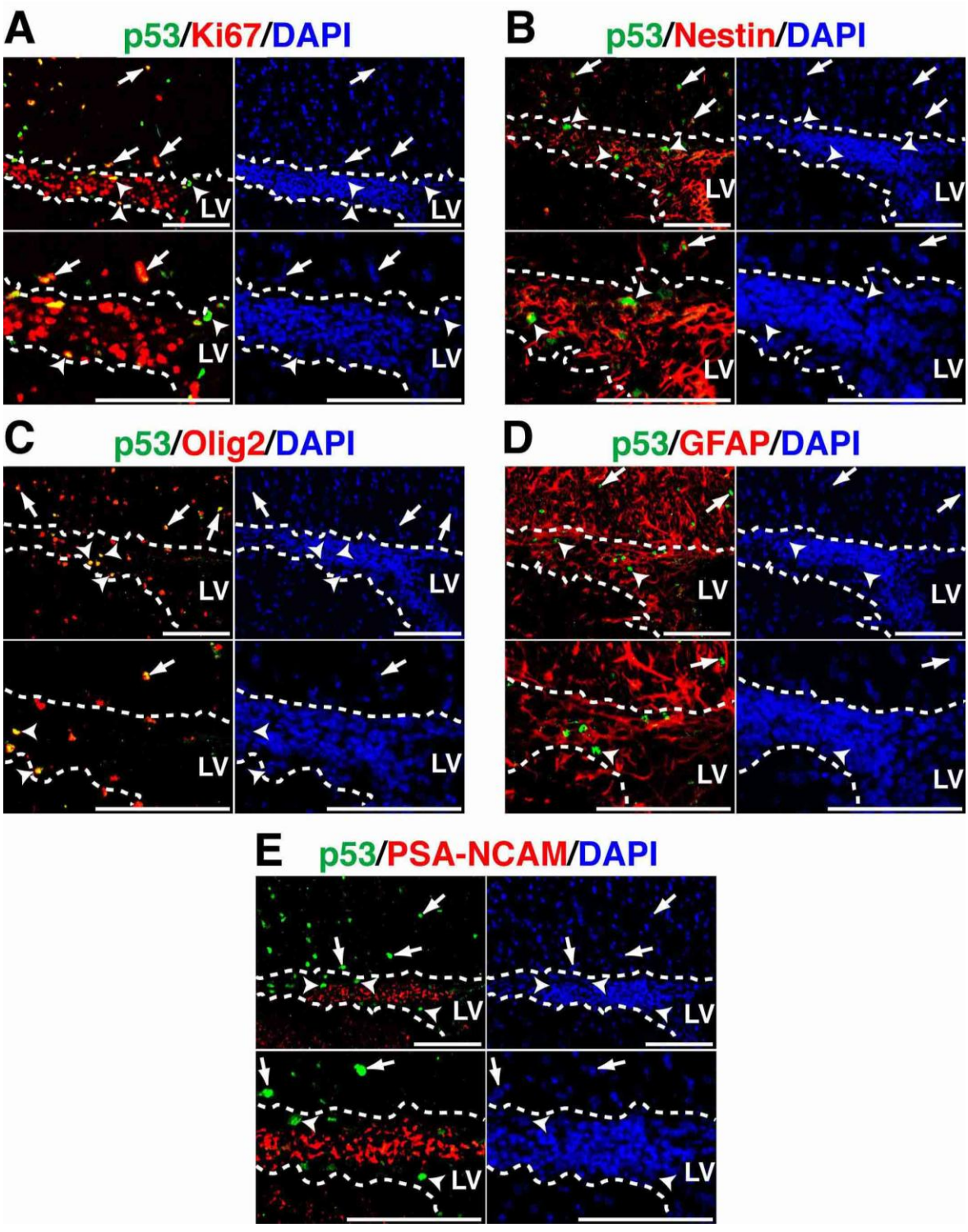
A
p53/Ki67/DAPI
B
p53/Nestin/DAPI
C
p53/Olig2/DAPI
D
p53/GFAP/DAPI
E
p53/PSA-NCAM/DAPI
LV

Figure 12. Lineage marker expression of $p53^{\Delta E5\text{-}6}$-positive glioma precursors in the corpus callosum and SVZ.

This figure shows the high-magnification views of the images shown in Figure 11C, which has a proliferating cluster involving both the corpus callosum and SVZ. Arrows and arrowheads in (A to E) point to morphologically similar $p53^{\Delta E5\text{-}6}$-positive glioma precursors in the corpus callosum and SVZ, respectively. These proliferating $p53^{\Delta E5\text{-}6}$-positive glioma precursors exhibit the lineage marker expression pattern of $Nestin^{+}/Olig2^{+}/GFAP^{-}/PSA\text{-}NCAM^{-}$, resembling SVZ-C* transit-amplifying progenitors. The dashed lines mark the SVZ. LV, lateral ventricle. Scale bar, 50μ.

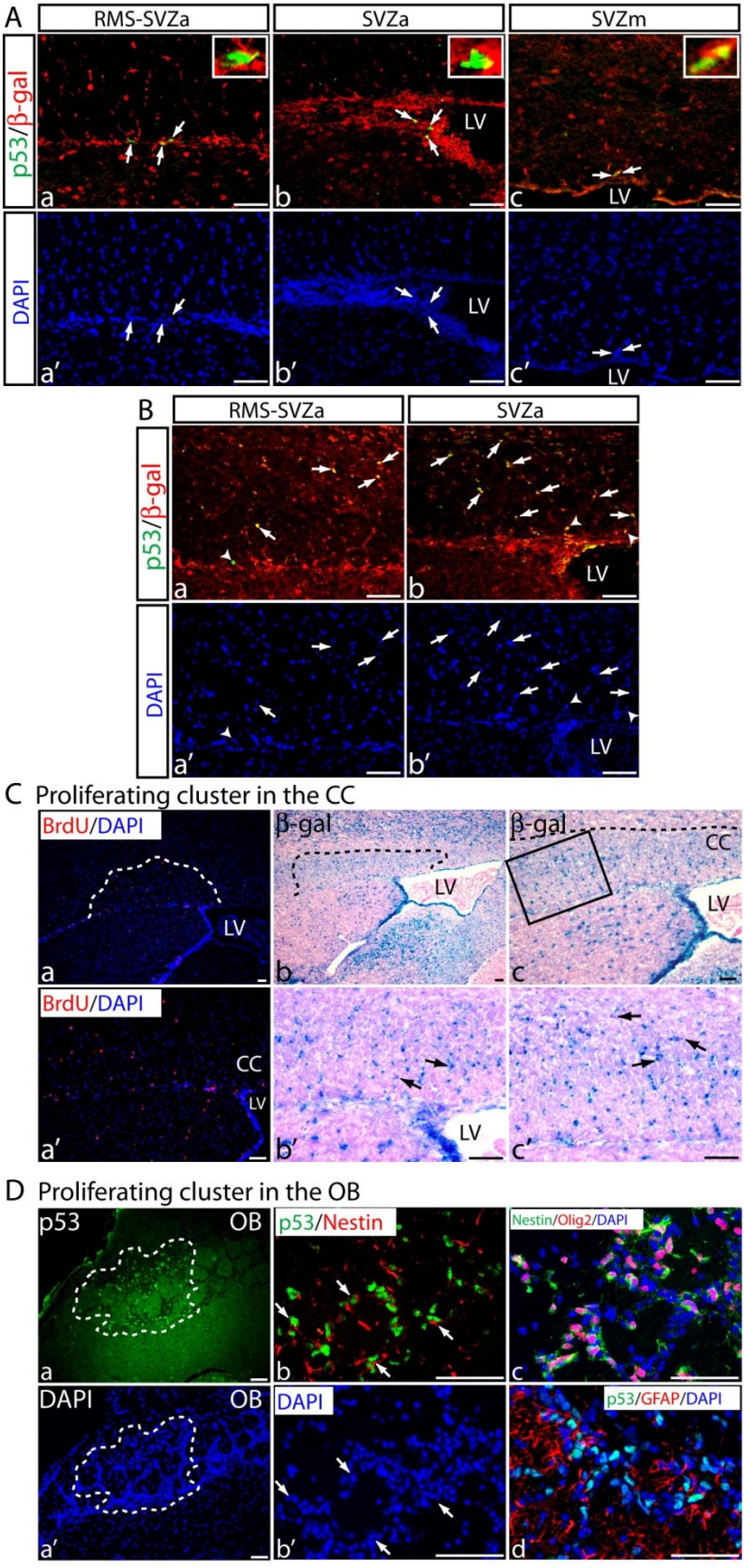
A
RMS-SVZa
SVZa
SVZm
p53/β-gal
DAPI
LV
a
b
c
a′
b′
c′
B
RMS-SVZa
SVZa
p53/β-gal
DAPI
LV
C Proliferating cluster in the CC
BrdU/DAPI
β-gal
CC
LV
D Proliferating cluster in the OB
p53
OB
p53/Nestin
Nestin/Olig2/DAPI
DAPI
p53/GFAP/DAPI

Figure 13. $p53^{\Delta E5\text{-}6}$-positive SVZ stem cells and glioma precursors express β-gal.
(A) Sections from 2-month-old $p53^{\Delta E5\text{-}6}$ brains with the R26R-LacZ transgene were stained with anti-p53/anti-β-gal antibodies (a–c) and were counterstained with DAPI for labeling nuclei (a'–c'). All the $p53^{\Delta E5\text{-}6}$-positive cells (arrows) at this age express b-gal of the R26R-LacZ regardless of their location in the RMS or anterior or medial SVZ (SVZa and SVZm). The insets in (a)–(c) show the high-magnification views of p53/β-gal double-positive cells. (B) Two representative proliferating clusters identified in the corpus callosum adjacent to either the junction of RMS and SVZa (a and a') or SVZa (b and b') were sectioned and stained with anti-p53/anti-β-gal antibodies. Within these proliferating clusters, all the $p53^{\Delta E5\text{-}6}$-positive glioma precursors in the corpus callosum (arrows) and SVZ (arrowheads) express β-gal of the R26R-LacZ. (C) Adjacent sections of a proliferating cluster were stained by BrdU/DAPI staining (a and a') and X-gal (b and c). (b' and c') High-magnification views of the boxed areas shown in (b) and (c) reveal a group of β-gal-positive cells with atypical nuclei (arrows). LV, lateral ventricle. (D) A mutant brain contains $p53^{\Delta E5\text{-}6}$-positive glioma precursors in the OB (a and a'). Sections from this proliferating cluster were stained with anti-p53/anti-Nestin (b) and DAPI (b'), anti-Nestin/anti-Olig2/DAPI (c), and anti-p53/anti-GFAP/DAPI (d). Arrows in (b) and (b') point to $p53^{\Delta E5\text{-}6}$-positive cells.

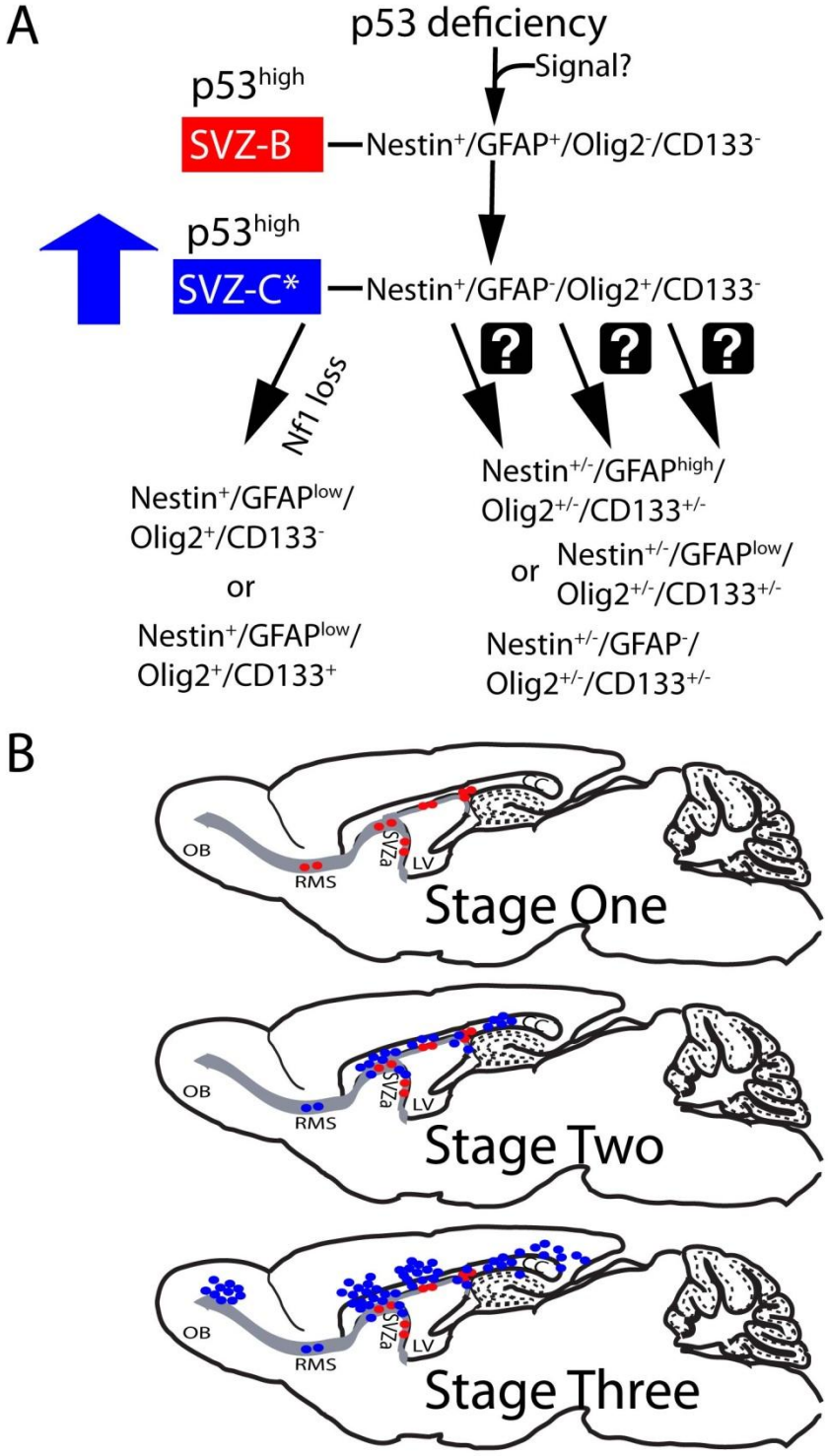
A
p53 deficiency
Signal?
p53high
SVZ-B
Nestin+/GFAP+/Olig2-/CD133-
p53high
SVZ-C*
Nestin+/GFAP-/Olig2+/CD133-
Nf1 loss
Nestin+/GFAPlow/
Olig2+/CD133-
or
Nestin+/GFAPlow/
Olig2+/CD133+
Nestin+/-/GFAPhigh/
Olig2+/-/CD133+/-
or Nestin+/-/GFAPlow/
Olig2+/-/CD133+/-
Nestin+/-/GFAP-/
Olig2+/-/CD133+/-
B
OB
RMS
SVZa
LV
Stage One
OB
RMS
SVZa
LV
Stage Two
OB
RMS
SVZa
LV
Stage Three

Figure 14. Proposed model for p53-mediated gliomagenesis.
(A) A model summarizes p53-mediated gliomagenesis (See main text).
(B) The anatomical location of $p53^{\Delta E5\text{-}6}$-positive early-stage glioma precursors during tumor development. Red dots, $p53^{\Delta E5\text{-}6}$-positive SVZ-B stem cells; blue dots, p53ΔE5-6-positive SVZ-C*-like glioma precursors. Scale bars, 50 μ.

2.5 References

Alcantara Llaguno, S., Chen, J., Kwon, C. H., Jackson, E. L., Li, Y., Burns, D. K., Alvarez-Buylla, A., and Parada, L. F. (2009). Malignant astrocytomas originate from neural stem/progenitor cells in a somatic tumor suppressor mouse model. Cancer Cell *15*, 45-56.

Brannan, C. I., Perkins, A. S., Vogel, K. S., Ratner, N., Nordlund, M. L., Reid, S. W., Buchberg, A. M., Jenkins, N. A., Parada, L. F., and Copeland, N. G. (1994). Targeted disruption of the neurofibromatosis type-1 gene leads to developmental abnormalities in heart and various neural crest-derived tissues [published erratum appears in Genes Dev 1994 Nov 15;8(22):2792]. Genes & Development *8*, 1019-1029.

Calabrese, C., Poppleton, H., Kocak, M., Hogg, T. L., Fuller, C., Hamner, B., Oh, E. Y., Gaber, M. W., Finklestein, D., Allen, M., *et al.* (2007). A perivascular niche for brain tumor stem cells. Cancer Cell *11*, 69-82.

Cho, Y., Gorina, S., Jeffrey, P. D., and Pavletich, N. P. (1994). Crystal structure of a Nf1 tumor suppressor-DNA complex: understanding tumorigenic mutations. Science *265*, 346-355.

Doetsch, F., Garcia-Verdugo, J. M., and Alvarez-Buylla, A. (1997). Cellular composition and three-dimensional organization of the subventricular germinal zone in the adult mammalian brain. J Neurosci *17*, 5046-5061.

Donehower, L. A., Harvey, M., Slagle, B. L., McArthur, M. J., Montgomery, C. A., Jr., Butel, J. S., and Bradley, A. (1992). Mice deficient for Nf1 are developmentally normal but susceptible to spontaneous tumours. Nature *356*, 215-221.

Furnari, F. B., Fenton, T., Bachoo, R. M., Mukasa, A., Stommel, J. M., Stegh, A., Hahn, W. C., Ligon, K. L., Louis, D. N., Brennan, C., *et al.* (2007). Malignant astrocytic glioma: genetics, biology, and paths to treatment. Genes Dev *21*, 2683-2710.

Galli, R., Binda, E., Orfanelli, U., Cipelletti, B., Gritti, A., De Vitis, S., Fiocco, R., Foroni, C., Dimeco, F., and Vescovi, A. (2004). Isolation and characterization of tumorigenic, stem-like neural precursors from human glioblastoma. Cancer Res *64*, 7011-7021.

Gil-Perotin, S., Marin-Husstege, M., Li, J., Soriano-Navarro, M., Zindy, F., Roussel, M. F., Garcia-Verdugo, J. M., and Casaccia-Bonnefil, P. (2006). Loss of Nf1 induces changes in the behavior of subventricular zone cells: implication for the genesis of glial tumors. J Neurosci *26*, 1107-1116.

Gutmann, D. H., Giordano, M. J., Mahadeo, D. K., Lau, N., Silbergeld, D., and Guha, A. (1996). Increased neurofibromatosis 1 gene expression in astrocytic tumors: positive regulation by p21-ras. Oncogene *12*, 2121-2127.

Hack, M. A., Saghatelyan, A., de Chevigny, A., Pfeifer, A., Ashery-Padan, R., Lledo, P. M., and Gotz, M. (2005). Neuronal fate determinants of adult olfactory bulb neurogenesis. Nat Neurosci *8*, 865-872.

Hemmati, H. D., Nakano, I., Lazareff, J. A., Masterman-Smith, M., Geschwind, D. H., Bronner-Fraser, M., and Kornblum, H. I. (2003). Cancerous stem cells can arise from pediatric brain tumors. Proc Natl Acad Sci U S A *100*, 15178-15183.

Jacks, T., Remington, L., Williams, B. O., Schmitt, E. M., Halachmi, S., Bronson, R. T., and Weinberg, R. A. (1994). Tumor spectrum analysis in Nf1-mutant mice. Curr Biol *4*, 1-7.

Kitayner, M., Rozenberg, H., Kessler, N., Rabinovich, D., Shaulov, L., Haran, T. E., and Shakked, Z. (2006). Structural basis of DNA recognition by Nf1 tetramers. Molecular cell *22*, 741-753.
Lim, D. A., Cha, S., Mayo, M. C., Chen, M. H., Keles, E., VandenBerg, S., and Berger, M. S. (2007). Relationship of glioblastoma multiforme to neural stem cell regions predicts invasive and multifocal tumor phenotype. Neuro-oncology *9*, 424-429.
Lin, S. C., Lee, K. F., Nikitin, A. Y., Hilsenbeck, S. G., Cardiff, R. D., Li, A., Kang, K. W., Frank, S. A., Lee, W. H., and Lee, E. Y. (2004). Somatic mutation of Nf1 leads to estrogen receptor alpha-positive and -negative mouse mammary tumors with high frequency of metastasis. Cancer Res *64*, 3525-3532.
Louis, D. N., Ohgaki, H., Wiestler, O. D., and Cavenee, W. K. (2007). WHO Classification of Tumors of the Central Nervous System, (Lyon IARC).
Malatesta, P., Hack, M. A., Hartfuss, E., Kettenmann, H., Klinkert, W., Kirchhoff, F., and Gotz, M. (2003). Neuronal or glial progeny: regional differences in radial glia fate. Neuron *37*, 751-764.
Mawrin, C., Diete, S., Treuheit, T., Kropf, S., Vorwerk, C. K., Boltze, C., Kirches, E., Firsching, R., and Dietzmann, K. (2003). Prognostic relevance of MAPK expression in glioblastoma multiforme. International journal of oncology *23*, 641-648.
Meletis, K., Wirta, V., Hede, S. M., Nister, M., Lundeberg, J., and Frisen, J. (2006). Nf1 suppresses the self-renewal of adult neural stem cells. Development *133*, 363-369.
Menn, B., Garcia-Verdugo, J. M., Yaschine, C., Gonzalez-Perez, O., Rowitch, D., and Alvarez-Buylla, A. (2006). Origin of oligodendrocytes in the subventricular zone of the adult brain. J Neurosci *26*, 7907-7918.
Merkle, F. T., and Alvarez-Buylla, A. (2006). Neural stem cells in mammalian development. Curr Opin Cell Biol *18*, 704-709.
Ohgaki, H., Dessen, P., Jourde, B., Horstmann, S., Nishikawa, T., Di Patre, P. L., Burkhard, C., Schuler, D., Probst-Hensch, N. M., Maiorka, P. C., *et al.* (2004). Genetic pathways to glioblastoma: a population-based study. Cancer Res *64*, 6892-6899.
Parsons, D. W., Jones, S., Zhang, X., Lin, J. C., Leary, R. J., Angenendt, P., Mankoo, P., Carter, H., Siu, I. M., Gallia, G. L., *et al.* (2008). An Integrated Genomic Analysis of Human Glioblastoma Multiforme. Science.
Reilly, K. M., Loisel, D. A., Bronson, R. T., McLaughlin, M. E., and Jacks, T. (2000). Nf1;TrNf1 mutant mice develop glioblastoma with evidence of strain-specific effects [In Process Citation]. Nat Genet *26*, 109-113.
Sanai, N., Alvarez-Buylla, A., and Berger, M. S. (2005). Neural stem cells and the origin of gliomas. The New England journal of medicine *353*, 811-822.
Singh, S. K., Hawkins, C., Clarke, I. D., Squire, J. A., Bayani, J., Hide, T., Henkelman, R. M., Cusimano, M. D., and Dirks, P. B. (2004). Identification of human brain tumour initiating cells. Nature *432*, 396-401.
Soriano, P. (1999). Generalized lacZ expression with the ROSA26 Cre reporter strain [letter]. Nat Genet *21*, 70-71.
Stiles, C. D., and Rowitch, D. H. (2008). Glioma stem cells: a midterm exam. Neuron *58*, 832-846.
TCGA Research Network (2008). Comprehensive genomic characterization defines human glioblastoma genes and core pathways. Nature *455*, 1061-1068.

Wang, H., Wang, H., Zhang, W., Huang, H. J., Liao, W. S., and Fuller, G. N. (2004). Analysis of the activation status of Akt, NFkappaB, and Stat3 in human diffuse gliomas. Laboratory investigation; a journal of technical methods and pathology *84*, 941-951.

Zheng, H., Ying, H., Yan, H., Kimmelman, A. C., Hiller, D. J., Chen, A. J., Perry, S. R., Tonon, G., Chu, G. C., Ding, Z., *et al.* (2008). Nf1 and Pten control neural and glioma stem/progenitor cell renewal and differentiation. Nature *455*, 1129-1133.

Zhu, Y., Guignard, F., Zhao, D., Liu, L., Burns, D. K., Mason, R. P., Messing, A., and Parada, L. F. (2005a). Early inactivation of Nf1 tumor suppressor gene cooperating with NF1 loss induces malignant astrocytoma. Cancer Cell *8*, 119-130.

Zhu, Y., Harada, T., Liu, L., Lush, M. E., Guignard, F., Harada, C., Burns, D. K., Bajenaru, M. L., Gutmann, D. H., and Parada, L. F. (2005b). Inactivation of NF1 in CNS causes increased glial progenitor proliferation and optic glioma formation. Development *132*, 5577-5588.

Zhuo, L., Theis, M., Alvarez-Maya, I., Brenner, M., Willecke, K., and Messing, A. (2001). hGFAP-cre transgenic mice for manipulation of glial and neuronal function in vivo. Genesis *31*, 85-94.

Chapter III *Nf1* regulates fate-specification of neural progenitor cells in developing and adult brain

3.1 Introduction

Von Recklinghausen's neurofibromatosis type 1 (NF1) is a familiar cancer syndrome that afflicts 1 in 3500 individuals worldwide (Friedman and Riccardi 1999). The hallmark feature of NF1 is the development of benign peripheral nerve sheath tumors termed neurofibromas in the peripheral nervous system (PNS) (Friedman and Riccardi 1999; Cichowski and Jacks 2001). In the central nervous system (CNS), NF1 deficiency causes tumor-related and non-tumor-related complications. Approximately15% to 20% of NF1 patients develop low-grade astrocytic tumors (gliomas) predominantly involving the optic pathway and the incidence of high-grade malignant astrocytoma development in the brain is increased by more than 5 fold compared to the general population (Listernick et al. 1997; Listernick et al. 1999). In addition, NF1 patient brains exhibit various structural defects including astrogliosis, megalencephaly (abnormal enlarged brain) and increased white matter (corpus callosum, CC) volume (Moore et al. 2000). The most common complication, however, is cognitive deficits and learning disabilities. About 40%-60% of NF1 children exhibit varying degrees of cognitive deficits associated with lower IQ scores (Hyman et al. 2005). The structural and functional defects in NF1 patients are closely related. Enlarged corpus callosum in NF1 children is found to be associated with severe forms of cognitive deficits and may serve as an early structural marker for the children at risk of learning disabilities (Dubovsky et al. 2001).

The gene responsible for this disease, *NF1*, encodes the protein neurofibromin, which contains a functional domain that shares homology with Ras GTPase activating protein (GAP) family members. Like other GAPs, neurofibromin negatively regulates the Ras/ERK signaling cascade by activating Ras GTPase and accelerating the

transformation of Ras from its active, GTP-bound form to inactive GDP-bound form (Ballester et al. 1990). NF1 belongs to a group of related developmental disorders collectively termed "neuro-cardio-facial-cutaneous (NCFC) syndromes, all of which are linked to the dysregulation of the Ras/ERK signaling pathway (Rodriguez-Viciana et al. 2006).

Since NF1 patients are heterozygous for *Nf1*, such broad spectrum of neurological deficits could be caused by two possible genetic mechanisms. The first possibility is that a single copy of the normal gene does not produce enough proteins to carry out normal function compared to two copies of the wildtype gene (haploinsufficiency). Consistently, Cui et al. reported that an *Nf1* heterozygous null mutation increases GABA release in the hippocampus, which in turn impairs hippocampal long-term potentiation (LTP) and learning (Cui et al. 2008). Additionally, pharmacological downregulation of ERK signaling reverses this phenotype. However, there is no evidence that NF1-associated brain abnormalities are solely caused by haploinsufficiency. For instance, brains of *Nf1* heterozygous mice do not exhibit the structural defects found in NF1 patients. The second possibility is that a subset of cells stochastically lose the wildtype copy of *NF1* through a genetic event termed loss of heterozygousity (LOH), and the resultant *NF1*-deficient cells fail to produce neurofibromin. In particular, in the event that LOH occurs in neural stem/progenitor cells during development, NF1-deficiency would be passed down to all the derivative progeny, potentially causing structural defects due to wide-spread NF1-deficiency altering mature cell function. Alternatively, NF1-deficiency may also have a direct effect on neural stem/progenitor cells in their ability to produce differentiated cells. Therefore, investigating the role of *NF1* in neural stem/progenitor cells could provide us a new angle to understand the disease mechanism, which could lay the foundation for developing novel therapies.

Neural stem cells are a unique population of cells in the CNS, characterized by their ability to renew themselves via mitotic cell division (self-renewal) and differentiate into both neurons and glia (multipotency). In the developing brain, neuroepithelial cells give rise to brain lipid binding protein (BLBP)-expressing radial glial cells in the ventricular

zone (VZ), which function as the developing neural stem cells (Campbell and Gotz 2002). Radial glial cells divide asymmetrically to directly generate neurons or indirectly produce neurons through neural intermediate progenitor cells (nIPCs). In late stages of embryonic development, oligodendrocytes are also derived from radial glial cells through intermediate progenitor cells that generate oligodendrocytes (oIPCs). At perinatal stage, the majority of radial glial cells transform into astrocytes while the rest of them continue to simultaneously generate neurons and oligodendrocytes through respective IPCs (Kriegstein and Alvarez-Buylla 2009). In the adult brain, multipotent neural stem and progenitor cells are spatially restricted in two stem cell niches: the subventricular zone (SVZ) of the lateral ventricle and the subgranular layer (SGL) of the hippocampal dentate gyrus (Merkle and Alvarez-Buylla 2006). SVZ NSCs, also called type B cells, are glial fibrillary acidic protein (GFAP)-expressing astrocytic cells derived from neonatal radial glial cells. Type B cells give rise to transit amplifying intermediate progenitor cells (also known as Type C cells), which are highly proliferative and generate neural progenitor cells (neuroblasts, Type A Cells) and oligodendrocytes precursor cells (OPCs). Neuroblasts migrate tangentially along rostral migratory stream (RMS), a neuronal migratory path ensheathed by glial cells, until they reach the olfactory bulb (OB) and differentiate into mature interneurons. OPCs, on the other hand, migrate radially into the overlying corpus callosum and become oligodendrocytes. Notably, gliogenesis in adult brain is significant reduced compared to the developing brain and the majority of SVZ progenitor cells (95%-97%) are later committed to the neuronal fate (Hack et al. 2005; Menn et al. 2006). Regulation of neuron-glial switch requires the interplay of a number of transcription factors. Homeobox transcription factors Dlx1 and Dlx2 have been shown to repress OPC production and favor neuronal fate (Petryniak et al. 2007), while basic helix-loop-helix (bHLH) transcriptional repressor Olig2 plays an essential role in the lineage specification of progenitor cells into oligodendrocytes and astrocytes (Marshall et al. 2005). However, the fate specification of neural progenitor cells remain incompletely understood.

A number of studies in murine models have provided significant insights into how *Nf1* could regulate neural stem/progenitor cell function in the developing brain. In *Nf1*

germline knockout mice, Dasgupta et al. found increased proliferation and self-renewal of *Nf1*-deficient embryonic neural stem cells through an *in vitro* neurosphere assay (Dasgupta and Gutmann 2005). In conditional knockout mouse models that target NSCs, Zhu et al. used hGFAP-Cre to target *Nf1* mutation into radial glial cells during development and found global astrogliosis and increased glial progenitor cells in the brain (Zhu et al. 2005). This was confirmed by a similar study from Hegedus et al. using BLBP-Cre, who also reported an abnormal increase of glial cells in *Nf1*-deficient developing brain, as well as neurite development defects (Hegedus et al. 2007). The underlying mechanisms of increased glial cell production, whether this represents glial lineage hyperproliferation or neuron-glia fate-specification switch, as well as how these developmental abnormalities could lead to the structural and functional defects in adult brains remain unclear.

In this study, by utilizing both conditional and inducible knockout mouse models, we analyzed the impact of *Nf1*-deficiency on neural stem/progenitor cells at different time points in developing and adult brain. We demonstrated that neurofibromin suppresses gliogenesis by inhibiting Olig2 expression specifically in neonatal and adult SVZ transit-amplifying progenitors in an ERK-dependent manner. The fate switch in these progenitor cell population leads to increased gliogenesis at the expense of neurogenesis, which contributes to a structural brain defect associated with learning deficits. Importantly, *Nf1*-associated developmental defects could be rescued by treatment during neonatal stages with a MEK inhibitor which prevents the activation of ERK. Thus, our finding establishes the significant role of *Nf1* in the regulation of neuron-glial fate specification and has clinical implications for the treatment of NF1-associated learning disabilities.

3.2 Material and methods

3.2.1 Control and mutant mice

The control mice used in this study are a pool of phenotypically indistinguishable mice with genotypes $Nf1^{flox/flox}$; $Nf1^{flox/+}$; and hGFAP-cre+; $Nf1^{flox/+}$. The mutant $Nf1^{hGFAP}$KO

mice include both hGFAP-cre+; *Nf1*flox/-; and hGFAP-cre+; *Nf1*$^{flox/flox}$; which have similar phenotypes. All mice in this study were cared for according to the guidelines that were approved by the Animal Care and Use Committees of the University of Michigan at Ann Arbor.

3.2.2 Tissue preparation

Mice were perfused with 4% paraformaldehyde (PFA) and brains were dissected, followed by overnight post-fixation in 4% PFA at 4 ºC. Brains were divided into two hemispheres along the midline and each hemisphere was processed for either paraffin-embedded or cryostat sections.

3.2.3 Histological analysis

Serial sections were sagittally prepared at 5 μm for paraffin sections or 10~14 μm for cryostat sections. Slides from histologically comparable positions were stained by H&E. And adjacent sections were subjected to immunohistochemical or immunofluorescence analysis. For adult brains in particular, at least three independent positions (position 1-3) that contain SVZ/RMS were selected for quantification. Each plane is approximately 100 μm apart at sagittal planes along the midline to lateral direction and was determined by histological criteria (P1: oval lateral ventricle with intact RMS; P2: triangular lateral ventricle with intact RMS; P3: triangular lateral ventricle with non-intact RMS) (Figure 23). At least three mutants and three controls were used for each analysis.

3.2.4 LacZ/β-gal staining

The R26R-LacZ transgene was used as a reporter to indicate Cre-mediated recombination in different mouse strains. Dissected tissues were post-fixed in PFA for 2 hours and transferred to 30% sucrose for overnight dehydration. Dehydrated brains were embedded in OCT and frozen on dry ice as cryostat blocks. Cryosections were cut at 10-14 μm and subjected to X-gal staining for 1 hour to overnight depending on the signal intensity. X-

gal stained sections were then counterstained by nuclear fast red for 5 minutes to visualize the nuclei.

LacZ staining solution: 1) Solution A: 5mM potassium ferricyanide crystalline; 5mM Potassium ferricyanide trihydrate; 2mM Magnesium Chloride in 1X Phosphate buffered saline (PBS) (stored at 4^{o}C, protected from light, then warm to 37^{o}C prior to using); 2) X-gal stock solution (40X):40 mg/ml in DMSO (100 mg in 2.5 ml DMSO) (stored at -20^{o}C, protected from light); 3) permeabilization solution: 10% NP-40; 2.5% sodium deoxycholate; 4) final X-gal solution: dilute X-gal stock solution 1:40 in Solution A. Add NP-40 (final concentration: 0.02%) and sodium deoxycholate (final concentration: 0.01%). All reagents were from Sigma.

Co-localization of β-gal expressing cells with other lineage markers was obtained by double immunofluorescence (See below).

3.2.5 Immunohistochemistry/immunofluorescence

Paraffin sections were deparaffinized through Xylene, 100% ethanol, 95% ethanol, 50% ethanol and 30% ethanol and rehydrated in distilled water. Antigen retrieval was performed with Retrieve-all antigen retrieval solution from Signet. Cryosections do not require deparaffinization or antigen retrieval steps and were directly fixed in 4% PFA for 15 minutes. Sections were then permeablized by 0.3% Triton-X (Sigma) solution for 20 minutes and blocked for 1 hour with 1.5% normal goat/horse/donkey serum (Sigma) depending on the secondary antibody to be used (e.g. use goat serum for blocking if the secondary antibody is from goat). Slides were put in humidified chamber and incubated in primary antibodies dissolved in the blocking solution at 4^{o}C overnight. The visualization of primary antibodies was performed with either a horseradish peroxidase system using a diaminobenzidine-based (DAB) peroxidase substrate (Vectastain ABC kit, Vector) or immunofluorescence by using Cy2 (or Alexa 488), Cy3 (or Alexa 555) and Cy5 (Alexa 647)-conjugated secondary antibodies at 1:200 dilution for 1 hour incubation (Cy2/Cy3/Cy5, Jackson Immunoresearch; Alexa 488/555/647, Invitrogen). Slides were

washed in between the steps with 1X PBS. The dilutions of primary antibodies were: Nestin (1:100, mouse, Chemicon), GFAP (1:2000, mouse, BD Pharmingen), GFAP (1:2000, mouse, DAKO), Ascl1(Mash1, 1:200, mouse, BD Pharmingen), Dlx2 (1:2000, guinea pig, a kind gift from Dr. K.Yoshikawa), Dcx (1:2000, rabbit, Abcam), Dcx (1:2000, guinea pig, Chemicon), Pax6 (1:500, rabbit, Covance), PSA-NCAM (1:1000, mouse, Chemicon), NeuN (1:400, mouse, Chemicon), TH (1:1000, rabbit, Abcam), Olig2 (1:2000, rabbit, Millipore), Olig2 (1:10000, guinea pig, a kind gift from Dr. B. Novitch), NG2 (1:200, mouse, Millipore), MBP (1:500, rat, Chemicon), BrdU (1:1000, rat, Abcam), Ki-67 (1:500, mouse, BD Pharmingen), β-gal (1:1000, rabbit, 5 prime-3 prime) , β-gal (1:1000, goat, AbD Serotec), p-ERK (1:100, rabbit, Cell Signaling), p-S6 (1:1000, rabbit, Cell Signaling), Cleaved Caspase 3 (1:500, rabbit, Cell signaling). Sections were examined under either a light or a fluorescence microscope (Olympus).

3.2.6 BrdU Assay

For BrdU assays, mutant and control littermates were pulsed with BrdU five times a day at 2-hour intervals. The dose of BrdU was 50μg/g (gram, body weight). For BrdU proliferation assay, mice were perfused with 4% PFA 2 hours after the last pulse. For BrdU differentiation assay, mice were sacrificed 30 days after the initial pulse. In both cases, brains were dissected and processed for either paraffin-embedded or cryostat sections. BrdU is a thymidine (T) analog. The staining for BrdU followed the regular immunofluorescence or immunohistochemistry protocol described above, except that after the Triton-X permeablization step, sliders were incubated in 2N HCl for 30 minutes followed by 0.1 M sodium borate for 20 minutes to denature the DNA.

When colocalizing BrdU with other protein markers through immunofluorescence labeling, sometimes the HCl treatment may have a negative impact on the staining quality of the other antigens (i.e. Olig2). To solve this problem, I used a 3-day staining procedure to first visualize the protein marker through regular immunofluorescence protocol. The stained slides were fixed in 4% PFA for 15 minutes, followed by the HCl/sodium borate treatment, and then subjected to anti-BrdU antibody incubation at 4^{o}C overnight. BrdU was visualized by fluorophore-conjugate secondary antibodies on the third day.

3.2.7 Tamoxifen administration in Nestin-Cre^{ER} inducible system

Tamoxifen was dissolved in corned oil and stored at -20^{o}C, and the concentration for TM stocks is 20mg/ml. Mice carrying the Nestin-Cre^{ER} transgene were administered with tamoxifen through intraperitoneal. injection at a dosage of 5mg per 40g body weight. Induction at P0.5 or P8 only required a single TM injection, while induction in young adult required daily TM injections for 5 constitutive days from P26-P30 (For more details, see main text).

3.2.8 MEK inhibitor treatment

MEK inhibitor PD0325901 (Selleck) was formulated in 0.5% hydroxypropyl methyl-cellulose plus 0.2% Tween 80 (Sigma) and administered by oral gavage and IP injections at the dosage of 5 mg/kg body weight every day from P0.5-P18. Mice that receive vehicle (0.5% hydroxypropyl methyl-cellulose plus 0.2% Tween 80) treatment were used as controls.

3.2.9 Neurosphere Cell culture (adapted from Sean Morrison lab protocol, by Anna Molofsky)

SVZ cells were dissected and dissociated from adult brains and was cultured in self-renewal medium. To dissect SVZ tissue, mouse brains were cut coronally at 3 different positions (the underside facing up): one to cut off the olfactory bulb, one just rostral to the optic chiasm, and one just before the hypothalamus. Slices were placed in Opti-MEM (Gibico), and SVZ was dissected out with fine forceps under the dissecting scope. The SVZ is the almost translucent, fine grey unmyelinated material that lines that lateral side of the lateral ventricle. Dissected pieces of SVZ were placed in 1 ml fresh Opti-MEM, and minced with fine forceps. The minced tissue was then transferred into a sterile conical tube, and dissociated in 3 ml pre-warmed dissociation medium (Solution C) for 20 min at 37°C. 3 ml of trypsin inhibitor solution plus 30 ul of Solution A (DNase) were added to the solution to quench trypsin activity. The mixture was spinned at 100xg for

10 minutes, and the pellet was resuspended in 400-500 µl of staining medium. The resultant solution was filtered through a 45 micron nylon mesh to get rid of debris and un-dissociated tissue. Cell density was quantified on a cell-counter plate and 2000 cells/well were plated to 6-well ultra-low binding plates for primary neurosphere culture. Each well contains 1.5 ml self-renewal medium. Neurosphere cultures were grown 10 days before analysis. The number and size of neurospheres were quantified and compared. To self-renew neurospheres, single 10-day old neurospheres were picked by pipette, centrifuged, and then mechanically dissociated and replated. 10 days into the secondary culture, we quantified self-renewal as the number of secondary neurospheres generated per primary neurosphere (2°NS/1°NS). Only spheres greater than 40 microns should be counted.

Self-renewal medium (100 ml): 1) 54 ml DMEM-low + 32 ml Neurobasal medium (Gibco); 2) 10 ml Chick embryo extract (lab preparation); 3)1 ml Penn/Strep (10,000 U/ml); 4) 1 ml N-2 Supplement (Gibco); 5) 2 ml B-27 Supplement (Gibco); 6) 100 µl of 50mM 2-mercaptoethanol stock (50uM final concentration; Sigma); 7) 80 ul FGF (25 ug/ml stock) (final concentration of 20ng/ml); 8) 80 ul EGF (25 µg/ml stock) (20ng/ml final concentration).

Solution C (200mls): 2 ml of 1 M HEPES + 192 µl of 0.5 M EDTA in 200 ml Ca/Mg free HBSS (Gibco). Adjust pH to 7.6. Dissolve 50mg Trypsin (Calbiochem) + 2mg DNase 1 (Boehringer) in above solution. Filter sterilize. Store 10 ml aliquots at -80°C.
Solution A: 10 mg DNase 1 (Boehringer) in 10 ml HBSS-free (Gibco). Filter Sterilize, store at –20°C in 0.5 ml single-use aliquots.

Trypsin Inhibitor solution: 100 ml of staining medium, with 14mg of trypsin inhibitor (Sigma) added, sterile filter.

3.2.10 Quantification and statistical analysis

Anatomically comparable sections from control and mutant brains were visualized under 40X magnification using an Olympus BX51 microscope. Images were captured and subjected to double-blinded counting. Lengths, areas and the number of cells were quantified by the NIH software, ImageJ. Control and mutant groups were compared, and statistical analysis was carried out using two-tailed Student's t-test. $p < 0.05$ was considered to be statistically significant. Comparisons among more than two groups (i.e. wildtype, heterozygous and mutant) were based on Anova test. To compare the proportions of certain types of cells from two independent cell populations (i.e. percentage of $Olig2^+$ cells in $Ascl1^+$ cells in control and mutant SVZ) and to determine if they are statistically different from one another, the number of specific cell types was quantified and subjected to Chi-Square test. $p < 0.05$ was considered to be statistically significant.

3.3 Results

3.3.1 *Nf1* suppresses Olig2 expression in neonatal SVZ stem and progenitor cells

To investigate the role of *Nf1* in neural stem and progenitor cells in the subventricular zone (SVZ), we targeted an *Nf1* mutation into radial glia at embryonic day 12.5 (E12.5) by using a Cre transgenic strain (Zhuo et al. 2001) under the control of the human glial fibrillary acidic protein promoter (hGFAP-cre). During embryonic development, radial glia are the primary neural stem cell populations, which give rise to neurons, glia as well as adult neural stem cells in the SVZ (Merkle and Alvarez-Buylla 2006). Thus, this gene targeting strategy permits us to assess the phenotypic consequence of *Nf1* inactivation in both developing and adult SVZ stem cells and their progeny. To confirm the specificity of this transgenic targeting strategy, we crossed hGFAP-cre+ mice to a mouse strain carrying Rosa26-LacZ reporter, whose expression indicates the presence of Cre-mediated recombination (Soriano 1999). Nearly all the SVZ stem and progenitor cells as well as Olig2-expressing progenitors and oligodendrocytes in the corpus callosum of the

resulting mice could be readily labeled by β-galactosidase (β-gal) expressed from the R26R-LacZ (Figures 15A and 15B). Although R26R-LacZ does not efficiently report Cre-mediated recombination in most astrocytes in the forebrain (Figure 15B b,b'), all the GFAP-expressing astrocyte express hGFAP-cre transgene (Figure 15B c, c').

For simplicity, *Nf1* mutant mice with the genotypes of hGFAP-cre+;*Nf1*$^{flox/flox}$ and hGFAP-cre+; *Nf1*$^{flox/-}$ were referred to as *Nf1*^{hGFAP}KO (*Nf1*$^{-/-}$) while age-matched littermates with genotypes of hGFAP-cre+;*Nf1*$^{flox/+}$ (*Nf1*$^{+/-}$), hGFAP-cre-;*Nf1*$^{flox/+}$ (*Nf1*$^{+/+}$) and hGFAP-cre-;*Nf1*$^{flox/flox}$ (*Nf1*$^{+/+}$) were used for control groups, as loss of one *Nf1* allele exhibited no significant *in vivo* phenotypes in the brain. First, to determine whether *Nf1* inactivation has any phenotypic consequence during embryonic development, we performed histological analysis on brains of newborn mice at postnatal day 0.5 (P0.5). We measured the size and cell number of the anterior SVZ (SVZa) and more posterior SVZ that includes a more significant contribution of stem cells in the ventricular zone (referred to as VZ/SVZ). No significant difference was identified in the SVZa and VZ/SVZ between control and *Nf1*^{hGFAP}KO neonatal brains (Figure 16Aa, a', B, C). Furthermore, the overall rate of proliferation and apoptosis in the SVZ was not significantly altered, evidenced by Ki67 and Cleaved Caspase 3 expression (Figure 16E, F, H). These results demonstrate that *Nf1* has a dispensable role in overt embryonic SVZ development. However, compared to controls, one striking phenotype observed was an over 2-fold increase in the number of cells that expressed a basic helix-loop-helix (bHLH) transcription factor Olig2 in the *Nf1*^{hGFAP}KO SVZ (Figure 16Ab, b'; Figure 2D). No increase in the percentage of Ki67^{+} proliferating cells in the Olig2^{+} lineage was observed, indicating that Olig2^{+} cells were not hyperproliferative in the *Nf1*^{hGFAP}KO SVZ (Figure 16E, G). Given that *Nf1*^{hGFAP}KO SVZ had a similar number of cells and comparable apoptotic rate to controls, we investigated the possibility of whether *Nf1* inactivation leads to ectopic Olig2 expression in SVZ stem and progenitor cells. Previous studies showed that in the embryonic SVZ, Ascl1^{+} progenitor cells selectively express the Dlx homeodomain transcription factors and Olig2, which direct neural precursors to undergo neuronal versus glial differentiation, respectively (Marshall et al. 2005; Petryniak et al. 2007). Thus, we performed Olig2/Dlx2/Ascl1 triple immunofluorescent

labeling to determine the lineage specification of Asc11$^+$ progenitors. Although the number of Ascl1$^+$ cells was comparable in mutant and control SVZ ($p = 0.104$), the percentage of Olig2-expressing cells in Ascl1$^+$ progenitors (Olig2$^+$/Ascl1$^+$) was dramatically increased from 16.7% in controls to 38.7% in mutants ($p < 0.0001$, Figure 16I, J, K). Accordingly, the Dlx2$^+$/Ascl1$^+$ progenitor populations were reduced from 82.5% to 65.3% ($p < 0.0001$, Figure 16I, J, K). Moreover, the percentage of Ascl1$^+$ cells that expressed both Olig2 and Dlx2 was increased from 5.5% to 11.7% ($p = 0.001$, Figure 16Ib, b', J, K). Taken together, these observations demonstrate that *Nf1* suppresses Olig2 expression in the neonatal Ascl1$^+$ SVZ progenitors, which otherwise would acquire Dlx2 expression and differentiate into neurons.

Unlike the SVZa, neural stem/progenitor cells and more differentiated cells in the more posterior SVZ are anatomically separated in the VZ/SVZ and overlying intermediate zone, respectively. Similarly, in the *Nf1*^{hGFAP}KO VZ/SVZ, we observed an over 2-fold increase in Olig2 expression whereas the number of Dlx2$^+$ cells was not significantly changed (Figure 17A, B). We further confirmed that the increased Olig2 expression in the VZ/SVZ was also not caused by hyperproliferation (Figure 17C, G), but instead was caused by ectopic Olig2 expression in Ascl1$^+$ and Dlx2$^+$ progenitors (Figure 17A, F, G). Of note, Olig2 expression was not expanded in Pax6$^+$ VZ and Tbr2$^+$ SVZ progenitor cells (Figure 17D, E, G). In the IZ, the expression of Olig2 and Dlx2 is almost mutually exclusive, suggesting that once cells become more differentiated, they selectively express only one of these two transcription factors. Strikingly, *Nf1*^{hGFAP}KO IZ cells exhibited a substantial loss of Dlx2 expression with a concomitant increase of Olig2 expression, suggesting that ectopic Olig2 expression results in overproduction of Olig2$^+$ lineage cells at the expense of the Dlx2$^+$ lineage (Figure 17A, B).

3.3.2 *Nf1* deficiency leads to increased gliogenesis at the expense of neurogenesis during neonatal development

To investigate the phenotypic consequence of ectopic Olig2 caused by *Nf1* deficiency during neonatal development, we analyzed the size of brains of control and *Nf1*^{hGFAP}KO

mice at P0.5 and P8. No significant difference was identified, particularly for the size of the olfactory bulb (OB) where a large number of neurons are generated from neonatal SVZ stem cells (Figure 18). While P0.5 SVZa contains a minimal number of $GFAP^+$ cells, the SVZa at P8 is comprised of a significant number of proliferating $GFAP^+$ stem cells. Compared to controls, *Nf1*^{hGFAP}KO SVZ $GFAP^+$ cells were hyperproliferative (Figure 19A, C), which was accompanied by increased number of cells in the enlarged mutant SVZ at P8 (Figure 19D). However, the proliferation rate of $Olig2^+$ cells was not significantly altered in P8 *Nf1*^{hGFAP}KO SVZa (Figure 19B, E). While the percentage of $Olig2^+$ cells in the $Ascl1^+$ progenitors remained comparable between P0.5 and P8 control SVZa (16.7% vs. 19.3%, $p = 0.269$), the percentage of $Olig2^+/Ascl1^+$ cells in *Nf1*^{hGFAP}KO SVZa was continuously increased from 38.7% at P0.5 to 46.5% at P8 ($p = 0.012$, Figure 19F). These results further support the notion that *Nf1* plays a critical role in suppressing Olig2 in neonatal SVZ $Ascl1^+$ progenitor cells.

To determine whether the altered expression pattern of Olig2 and Dlx2 lineage markers disrupts the balance of glial versus neuronal output of *Nf1*^{hGFAP}KO SVZ stem cells, we focused on the SVZa, the largest postnatal germinal zone where multipotent stem and progenitor cell populations persist into adulthood. We pulsed control and *Nf1*^{hGFAP}KO mice with bromodeoxyuridine (BrdU) at P8, a stage when most of the proliferating cells become restricted to the SVZ/RMS in the forebrain. After a 10-day BrdU chase, we analyzed the mice at P18 for SVZ-derived neurogenesis in the OB and gliogenesis in the corpus callosum (CC), respectively. As shown in Figure 20, the size and neuronal density of the *Nf1*^{hGFAP}KO OB were significantly reduced compared to controls (Figure 20A, B, C). Notably, neuronal clusters, which could be readily identified in the control OB, were largely absent in mutants (Figure 20Ac, c' and 20Ad, d'). Consistently, SVZ-derived newborn neurons labeled by BrdU and NeuN ($BrdU^+/NeuN^+$) were markedly reduced in the *Nf1*^{hGFAP}KO OB compared to controls (Figure 20A, D). Neurogenesis in the granular cell layer (GCL) and periglomerular cell layer (PGL) was equally reduced in the mutant OB (Figure 20D). It is worth noting that the number of $BrdU^+$ cells coexpressing a neuronal marker Pax6 was not significantly different in the RMS between control and *Nf1*^{hGFAP}KO brains (Figure 21A, D), suggesting that reduced neurogenesis was unlikely

caused by migratory defects. However, compared to controls, the number of $BrdU^+$ cells was increased by over 3 folds in the *Nf1*^{hGFAP}KO RMS and CC, where most of the $BrdU^+$ cells expressed glial markers, GFAP and Olig2 (Figure 21B, C, D; Figure 22A, B, C). These observations demonstrate that *Nf1* inactivation leads to increased gliogenesis at the expense of neurogenesis in the neonatal SVZ/RMS/OB/CC system. Interestingly, the ratio of newly generated $BrdU^+/GFAP^+$ astrocytes and $BrdU^+/Olig2^+$ oligodendrocytes was not significantly different in control and *Nf1*^{hGFAP}KO CC, suggesting that *Nf1* deficiency only promotes overproduction of $Olig2^+$ progenitors, but does not alter their potential to differentiate into astrocytes versus oligodendrocytes (Figure 22D).

3.3.3 *Nf1*-deficient adult brain exhibits enlarged SVZ with increased glial differentiation

To determine disease manifestations of the neonatal defects observed in *Nf1*-deficient SVZ cells, we studied adult control and *Nf1*^{hGFAP}KO SVZ at 2 months of age. Specifically, we analyzed the SVZ from these mice at three independent positions along the midline to lateral hemisphere (Figure 23). At each of these three positions, *Nf1*^{hGFAP}KO SVZ exhibited a 2- to 3-fold increase in the size of the SVZ compared to controls (Figure 24). To investigate the relative contribution of SVZ stem cells, progenitor cells and differentiated cells to the enlarged size, we determined the number of individual SVZ cell populations by using lineage markers. Compared to controls, the percentage of SVZ cells expressing glial-lineage markers including GFAP, Olig2 and NG2 was markedly increased with a concomitant reduction of Doublecortin (Dcx)-expressing neuroblasts in the *Nf1*^{hGFAP}KO SVZ (Figure 25). To determine whether increased $GFAP^+$ cells were SVZ stem cells or differentiated astrocytes in mutant brains, we double-labeled brains sections with GFAP and Nestin-a stem/progenitor cell marker. Similar to controls, *Nf1*^{hGFAP}KO SVZ contained $GFAP^+/Nestin^+$ stem cells that were closely associated with the lateral ventricle (Figure 26A). However, mutant SVZ accumulated a greater number of $GFAP^+/Nestin^-$ cells that formed a less cellular area in the anterior-dorsal parts of the SVZ, which was not observed in the normal SVZ (dotted areas in Figure 24, 25A). Furthermore, these $GFAP^+/Nestin^-$ cells exhibited the critical

features of differentiated astrocytes: the presence of multiple long cellular processes and not in the cell cycle (Figure 25A, 27D). Together, these results demonstrate that *Nf1* deficiency leads to enlarged SVZ with abnormally increased glial differentiation in the adult brain. In the adult SVZ, only 9% of multipotent Ascl1$^+$ transit-amplifying progenitors expressed Olig2 (Figure 26A-D), which is consistent with the previous studies that glial output of adult SVZ stem cells is minor (5% to 10%) (Hack et al. 2005; Menn et al. 2006). Remarkably, nearly half of Ascl1$^+$ transit-amplifying progenitors expressed Olig2 in the *Nf1*^{hGFAP}KO SVZ (48.3%, Figure 26A-D), which is comparable to the percentage of mutant Olig2$^+$/Ascl1$^+$ progenitors at P8 (46.5%). Thus, the phenotypic alteration in Olig2 expression observed in neonatal *Nf1*^{hGFAP}KO Ascl1$^+$ progenitors persists in adult SVZ transit-amplifying progenitors. Moreover, we confirmed that ectopic Olig2 expression specifically occurred in the *Nf1*^{hGFAP}KO Ascl1$^+$ transit-amplifying SVZ-C progenitors (irrespective of its expression of Dlx2), but not in GFAP$^+$ SVZ-B stem cells or Dcx$^+$ SVZ-A neuroblasts (Figure 26E and data not shown).

3.3.4 *Nf1* deficiency provides no significant growth advantage to different SVZ cell populations

We next investigated whether as a tumor suppressor gene, *Nf1* deficiency altered growth properties of *Nf1*^{hGFAP}KO SVZ cells that could also contribute to abnormal enlarged SVZ. First, we determined the overall proliferation rate in control and *Nf1*^{hGFAP}KO SVZ by using a short-term BrdU pulse assay. Although the absolute number of BrdU$^+$ cells was increased in the enlarged *Nf1*^{hGFAP}KO SVZ, the percentage of BrdU$^+$ cells was significantly reduced compared to controls (Figure 27A-C). Moreover, the differences in the number and percentage of BrdU$^+$ cells remained relatively unchanged between control and *Nf1*^{hGFAP}KO SVZ when these mice became aged (from 2 to 8 months, Figure 27B, C). These observations indicate that *Nf1*-deficient SVZ cells are not hyperproliferative or tumorigenic. Second, we measured the percentage of BrdU$^+$ cells in individual SVZ cell populations. No significant difference in proliferation was observed in Ascl1$^+$ SVZ-C cells, Olig2$^+$/NG2$^+$ SVZ-OPCs, as well as neurogenic Dlx2$^+$ progenitors and Dcx+ SVZ-A neuroblasts between control and *Nf1*^{hGFAP}KO SVZ (Figure 27D-I). Notably, due to the

presence of a large number of differentiated astrocytes in mutant SVZ, the percentage of $BrdU^+$ cells in $GFAP^+$ cell populations was significantly reduced (Figure 27D, J). Third, by using Cleaved Caspase 3 immunohistochemical staining, we found no significant difference in apoptotic rate between control and *Nf1*^{hGFAP}KO SVZ (Figure 27K, L). Finally, we performed an *in vitro* neurosphere assay to compare growth properties of multipotent control and *Nf1*^{hGFAP}KO SVZ stem and progenitor cells. No significant difference was found in the frequency of neurosphere-forming activity and the size of primary neurospheres derived from control and *Nf1*^{hGFAP}KO SVZ (Figure 28A, C, D). Surprisingly, the self-renewal capacity of SVZ stem and progenitor cells measured by the ratio of the number of secondary neurospheres to primary neurospheres was dramatically reduced in *Nf1*^{hGFAP}KO cells compared to controls (Figure 28B, E, F). It is worth noting that the self-renewal defect in culture is the only phenotype also observed in *Nf1* heterozygous cells (haploinsufficiency). Taken together, these results demonstrate that *Nf1* deficiency only leads to a transient increased proliferation in neonatal SVZ stem cells, which appears to contribute to the enlarged SVZ phenotype. However, the similar growth advantage does not persist into adult SVZ cells. Therefore, alterations in proliferation or apoptosis in adult *Nf1*^{hGFAP}KO SVZ unlikely contributes to enlarged SVZ with increased glial lineage cells.

3.3.5 *Nf1* inactivation leads to enlarged corpus callosum

To determine whether similar to neonatal SVZ, adult *Nf1*^{hGFAP}KO SVZ stem cells overproduce glial cells at the expense of neuronal production in the OB, we performed a long-term BrdU pulse-chase experiment on control and *Nf1*^{hGFAP}KO mice at 2 months of age. Thirty days after BrdU pulses, we analyzed the number and the identity of newly generated SVZ-derived cells (labeled by BrdU) in the SVZ/RMS/OB/CC system of these BrdU-treated mice (Figure 29A, B). In the *Nf1*^{hGFAP}KO OB, the number of $BrdU^+$ cells was greatly reduced compared to controls. Most of the $BrdU^+$ cells were newly generated neurons labeled by NeuN, which were reduced by 50% in mutant OB (Figure 29C, D). However, there was no significant difference in the $BrdU^+/NeuN^-$ populations, indicating that local gliogenesis was not affected by *Nf1* deficiency (Figure 29D). Accordingly, the

size and neuronal density of *Nf1*^{hGFAP}KO OB was significantly reduced compared to controls (Figure 29 E, F).

In contrast to the OB, the SVZ/RMS/CC system as well as surrounding cerebral cortex and striatum of *Nf1*^{hGFAP}KO mice contained significantly more BrdU^{+} cells compared to those of controls (Figure 29B). For example, the control RMS contained only a small number of BrdU^{+} cells, all of which expressed Pax6 or Dcx, indicating that they were migrating neuroblasts. However, we observed a 9-fold increase in BrdU^{+} cells in *Nf1*^{hGFAP}KO RMS, 44%, 15% and 41% of which expressed Olig2, GFAP and Pax6, respectively (Figure 30A-C). These results indicate that *Nf1* deficiency leads to persistent gliogenesis in the RMS, which is not existent in controls. Consistently, there was a dramatic increase in the number of RMS cells expressing glial lineage markers including Olig2 and NG2 in the absence of *Nf1* (Figure 30D). Moreover, *Nf1*^{hGFAP}KO RMS, but not controls, expressed myelin basic protein (MBP) indicative of terminal differentiation of oligodendrocytes, which altered the structure and organization of the mutant RMS (Figure 30E, F). In both control and *Nf1*^{hGFAP}KO SVZ, CC, cerebral cortex and striatum, however, all the BrdU^{+} cells expressed Olig2, but not GFAP, Pax6 or Dcx (Figure 31A and data not shown). Together, these observations indicate that similar to neonatal SVZ cells, *Nf1* deficiency only overproduces Olig2^{+} transit-amplifying progenitors, but does not alter the differentiation potentials of these adult SVZ progenitor cells that only produce oligodendrocytes, not astrocytes. Consistently, the number of Olig2^{+} cells was increased in *Nf1*^{hGFAP}KO CC (Figure 31B, C). The increase in GFAP^{+} cells is most likely due to increased gliogenesis during neonatal development (Figure 31B, C; Figure 22A). Such increase of glial cells in mutant CC is not due to increased local OPC proliferation, since we did not observe any difference in the number of BrdU^{+}/Olig2^{+} cells in control and *Nf1*^{hGFAP}KO CC (Figure 31 K,L).

To investigate the phenotypic consequence of the imbalance of glial versus neuronal production from adult *Nf1*^{hGFAP}KO SVZ, we measured the size of the CC at 4 different planes along the midline to lateral hemisphere. At all three positions that are directly associated with lateral ventricle (P1-P3), the thickness and cellular density of the CC is

significantly increased in the absence of *Nf1* (Figure 31E-G). The enlarged CC phenotype is reminiscent of what have been described in a subset of NF1 patients that exhibit severe learning disabilities. Interestingly, the size of CC from the midline section (position M, Figure 31H), which is not directly associated with the lateral ventricle, showed no increase in thickness or cellular density. These observations suggest a critical role of SVZ-mediated gliogenesis in the formation of the CC.

3.3.6 Acute inactivation of *Nf1* is sufficient to induce fate switch in the adult SVZ

To investigate whether abnormal fate-specification observed in the adult SVZ progenitors resulted from a neonatal developmental defect or ongoing requirement of *Nf1* in adulthood, we employed an inducible system in which Cre recombinase (Nestin-cre^{ER}) can be activated in Nestin-expressing SVZ stem and progenitor cells by tamoxifen (TM) treatment (Figure 32A). As revealed by activation of Cre-mediated Rosa26 LacZ reporter (R26^{LacZR}), the SVZ/RMS/OB/CC system could be efficiently targeted by TM induction at neonatal stages (Figure 32 B). From P0.5 to P8, Nestin^{+} neural stem and progenitor cells become restricted to the SVZ/RMS in the forebrain. Accordingly, compared to P0.5 induction, the Nestin-cre^{ER}-targeted cell populations at P8 were greatly restricted to the SVZ/RMS/OB/CC system (Figure 32B). These observations reveal the efficacy and specificity of this Nestin-cre^{ER} transgene. To target adult SVZ cells, we established a 5-day TM induction protocol from P26 to P30 (Figure 32C). At P31, one day after the completion of TM induction, the cells undergoing Cre-mediated recombination revealed by β-gal staining are restrictedly distributed in the SVZ and RMS, as well as SGL in the hippocampus, but not in any other brain regions (Figure 32C and data not shown), consistent with the fact that Nestin^{+} cells are restricted to the SVZ and SGL adult germinal zones. At P60, a month after TM induction, the majority of β-gal-positive cells migrated into the OB and became differentiated neurons whereas a minor population of β-gal^{+} cells was found in the overlying CC in TM-induced control brains (Figure 33A). In contrast, β-gal^{+} cells dramatically increased and formed clusters in the CC of TM-induced mutant brains (Figure 33A). Nearly all the β-gal^{+} cells in both control and mutant CC expressed Olig2, demonstrating that acute *Nf1* inactivation in the adult SVZ increased

gliogenesis (Figure 33B, C, G). Despite increased gliogenesis in the CC, there was no difference in the number of β-gal$^+$ cells or the proliferation in the SVZ (Figure 33B, F, J). The number of β-gal$^+$ cells in the RMS, however, was significantly reduced in TM-induced mutants (Figure 33B, D). Moreover, while β-gal$^+$ cells in the control RMS are Dcx$^+$/Olig2$^-$ neuroblasts, many β-gal$^+$ cells expressed Olig2 in the mutant RMS (Figure 33D, H). These results indicate that *Nf1* deficiency not only increases gliogenesis at the expense of neurogenesis, but also alters the migratory pattern of some glial progenitor cells that abnormally enter into RMS, consistent with our finding that there is continuous gliogenesis in the *Nf1*-deficient RMS (Figure 30A). Furthermore, we found increased number of Olig2-expressing cells in the *Nf1*-deficient cellular compartment (marked by β-gal expression) in the mutant SVZ compared to controls (Figure 33E, I), providing additional evidence that *Nf1* deficiency leads to ectopic expression of Olig2. Together, these results demonstrate that acute inactivation of *Nf1* confers no proliferative advantage to adult SVZ cells, but instead alters glial versus neuronal fate-specification by promoting Olig2 expression in adult SVZ cells.

3.3.7 *Nf1* regulates SVZ progenitor cell fate specification in an ERK-dependent manner

We next investigated the molecular mechanism underlying the glial versus neuronal fate switch in *Nf1*^{hGFAP}KO SVZ progenitors. Since *Nf1* functions as a negative regulator of Ras-mediated signaling pathways, we analyzed three major downstream effectors of Ras signaling pathways: ERK/MAPK, PI3K/AKT and mTORC1. Specifically, we used phospho-specific antibodies of ERK (pERK), AKT (pAKT) and S6 (pS6) kinases to evaluate the activation status of these pathways in control and *Nf1*^{hGFAP}KO brains. In paraffin-embedded sections, pAKT antibody failed to detect specific signals in either control or *Nf1*^{hGFAP}KO brains (data not shown). However, both pERK and pS6 antibodies readily detected positive cells on these brain sections, though only pERK-positive (pERK$^+$) cells were significantly increased in both neonatal and adult *Nf1*^{hGFAP}KO brains (Figure 34A-E and data not shown). Under this relatively stringent condition (paraffin sections), the majority of pERK robust staining was identified in the SVZ of both control

and *Nf1*^{hGFAP}KO brains at neonatal (Figure 34A, B) and adult stages (Figure 34C-E). Consistent with the finding that *Nf1* inactivation causes ectopic Olig2 expression specifically in Ascl1^{+} transit-amplifying progenitors, pERK expression was restricted to Ascl1^{+} and/or Olig2^{+} cells in the SVZ of both P0.5 (Figure 34A, B) and adult *Nf1*^{hGFAP}KO brains (Figure 26C, D). Over 80% and 90% of pERK^{+} cells expressed Ascl and Olig2, respectively. This observation indicates that a large proportion of pERK^{+} cells expressed both Ascl and Olig2 (Figure 26C, D). Consistently, in the *Nf1*^{hGFAP}KO, the majority of neurogenic Dlx2^{+} cells did not express pERK, and no pERK expression was found in GFAP^{+} cells (Figure 34F, G). Together, these results are most consistent with the model that *Nf1*-mediated negative regulation of ERK signaling suppresses Olig2 expression in neurogenic Ascl1^{+} transit-amplifying progenitors.

To directly test this hypothesis, we treated the mice from P0.5-P18 with a potent MEK inhibitor (MEKi), PD0325901 (Barrett et al. 2008). The level of ERK activation in MEKi-treated *Nf1*^{hGFAP}KO mice at P18 was reduced to the level of control SVZ, and more importantly, the number of Olig2^{+} cells in the mutant SVZ was now comparable to vehicle-treated control (Figure 35A, D). Furthermore, in the Ascl1^{+} progenitors, the percentage of Olig2^{+} cells in MEKi-treated mutants was also reduced to the control level (Figure 35A, E). We further analyzed the glial and neuronal production of SVZ progenitor cells. In the CC, the density of Olig2^{+} cells in MEKi-treated *Nf1*^{hGFAP}KO brains was rescued to the level of vehicle-treated controls; the density of GFAP^{+} cells, albeit not completely rescued, was significantly reduced compared to that of vehicle-treated mutants (Figure 35B, F). In the OB, neuronal density was significantly increased after MEKi treatment (Figure 35C, F). Finally, the size defects of CC and OB were also partially rescued. These MEKi treatment experiments demonstrate a potential therapeutic window for treating NF1-associated brain structural defects.

3.4 Discussion

By analyzing two *Nf1* mouse models driven by different Cre transgenes, my study demonstrated the pivotal role of *Nf1* in the regulation of SVZ progenitor fate

specification both during neonatal development and in adulthood. Moreover, these observations provide a potential mechanism underlying the neurocognitive defects observed in NF1 patients.

3.4.1 *Nf1* specifically regulates fate specification of SVZ Asc11$^+$ cells through Ras/ERK signaling

Previous studies have reported an abnormal increase of glial cells in *Nf1*-deficient mouse brain, yet the cellular and molecular mechanism has not been fully revealed (Dasgupta and Gutmann 2005; Zhu et al. 2005; Hegedus et al. 2007). One possibility is that *Nf1*-deficiency leads to overproliferation of glial progenitor cells. However, in their BLBP-Cre conditional knockout mice, Hegedus et al. found no increase in the proliferation rate of glial progenitor cells in the neonatal brain (Hegedus et al. 2007), which is consistent with our quantification in P0 and P8 SVZ. We further confirmed that glial progenitor cells do not overproliferate in adult SVZ and CC. These findings rule out overproliferation of glial progenitor cells as a major underlying mechanism for overabundance of glia. Alternatively, overproduction of glial cells could be attributed to fate specification alteration in neuroglial progenitor cells. Indeed, we found ectopic expression of Olig2 in neonatal and adult SVZ Ascl1$^+$ cells. Olig2 expression has been demonstrated both necessary and sufficient to act as a master regulator in directing SVZ progenitors toward glial fates, while preventing neuronal differentiation, in neonatal and adult brain (Marshall et al. 2005; Menn et al. 2006). Consequently, in *Nf1*-deficient brains more Ascl1$^+$ cells are specified to the glial lineages at the expense of neuronal lineage specification, leading to increased gliogenesis in the SVZ/RMS/CC system and reduced neurogenesis in the OB. This alteration of fate specification is very specific to SVZ Ascl1$^+$ progenitors (type C cells in adult SVZ). Despite our genetic targeting strategy of introducing *Nf1* mutation to all cell types in the brain, no ectopic Olig2 expression was found in SVZ-B cells (neural stem cells), SVZ-A cells (neuroblasts) or differentiated neurons. Thus, *Nf1* appears to function as a negative regulator of Olig2 specifically in SVZ Ascl1$^+$ cells to repress glial fate determination.

There are several signaling pathways known to regulate Olig2 expression in the CNS. BMP/Smad signaling plays a crucial role in establishing dorsal neural identity and its inhibition is sufficient to generate OPCs both *in vitro* and *in vivo* (Bilican et al. 2008). Sonic hedgehog (Shh), which opposes BMP signaling in ventral neural tube, can promote Olig2 expression in neocortical progenitor cells and induce oligodendrocyte progenitor production (Lu et al. 2002; Zhou and Anderson 2002). Kessaris et al. demonstrated that Shh activity is dependent on ERK signaling (Kessaris et al. 2004). In cultured dorsal spinal cord cells, fibroblast growth factor 2 (FGF2) could induce Olig2 expression, which can be inhibited by a MEK inhibitor *(Bilican et al. 2008)*. This observation suggests that FGF2-induced Olig2 expression depends on Ras/ERKsignaling pathway. In the forebrain, overexpression of growth factors (i.e. epidermal growth factor EGF, platelet-derived growth factor PDGF) can lead to overproduction of $Olig2^+$ cells in SVZ and CC (Chandran et al. 2003; Jackson et al. 2006; Ivkovic et al. 2008). However, the specific cell type(s) that are responsive to EGF/PDGF overexpression are yet to be determined. In addition, these studies did not provide conclusive mechanism whether the increase of Olig2-expressing cells is due to hyperproliferation or fate specification alterations. Our study demonstrates that *Nf1* regulates Olig2 expression in SVZ $Ascl1^+$ cells through Ras/ERK signaling, which plays an important role in SVZ progenitor fate specification and regulates the overall output of neurogenesis and gliogenesis. Consistently, we found that in control brains, activation of Ras/ERK signaling corresponds to the dynamic change of gliogenesis. While pERK level is very low in adult brain where there is minimal gliogenesis in adult, we found a number of $pERK^+$ cells colocalizing with Olig2 in the SVZ at neonatal stages (the peak of gliogenesis in the brain), indicating the involvement of Ras/ERK signaling in normal gliogenesis process. In addition, MEK inhibitor treatment on *Nf1*-deficient mice not only repressed Olig2 expression in SVZ progenitors, but also rescued the neuron-glial output in the brain, suggesting that *Nf1* indeed inhibits Olig2 expression by inactivating Ras/ERK signaling. Based on these findings we propose a model for the fate specification of SVZ $Ascl1^+$ cells. $Ascl1^+$ cells are bipotent and can undergo specification to acquire a neuronal or glial fate. Upon commitment to glial intermediate progenitors (gIPCs), $Ascl1^+$ cells downregulate *Nf1* and activate Ras/ERK signaling to promote Olig2 expression, while neuronal committed

progenitors (nIPCs) maintain high level of *Nf1* to inhibit Ras/ERK signaling and prevent misexpression of Olig2. In *Nf1*^{hGFAP}KO brains, Ras/ERK signaling transduction activity is dysregulated in Ascl1^{+} cells and nIPCs due to the loss of its negative regulator, *Nf1*. Overactive Ras/ERK activity leads to expression of Olig2 in these cells, ultimately resulting in fate switch from the neuronal lineage to the glial linage (Figure 36).

This new model, while addresses important questions concerning neural progenitor fate specification, opens up many directions for follow-up studies. First, the relationship between Ras/ERK signaling and increased Olig2 expression in Ascl1^{+} cells has yet to be defined. A recent publication by Bilican et al. demonstrated that in dorsal spinal cord, FGF-induced ERK signaling could counteract with BMP signaling by deactivating Smad1, the major effecter in the BMP signaling pathway. ERK signaling phosphorylates the linker region of Smad1 and prevents its nuclear translocation, which inhibits Smad1 transcriptional activity (Bilican et al. 2008). It is possible that this is a conserved mechanism for different types of progenitors in the CNS. Second, the upstream signal that activates Ras/ERK signaling cascade in SVZ cells is yet to be determined. As aforementioned, Shh signaling, as well as activation of RTK signaling through growth factors FGF/EGF/PDGF could all be likely candidates. Finally, how Ras/ERK activity is dynamically regulated in neuronal committed nIPCs and glial committed gIPCs still remains to be uncovered. One possible mechanism could be that these two cell populations have different neurofibromin level. This could be achieved through differential transcriptional or post-transcriptional regulation of *Nf1* gene expression. Alternatively, the level of neurofibromin could be regulated by protein degradation. One candidate molecule that regulates neurofibromin degradation is FBW7 (F-box and WD repeat domain-containing 7). FBW7 is a substrate-recognition component of the SCF complex (SKP1, CUL1 and F-box), an E3 ubiquitin ligase. Dr. Yi Sun at the University of Michigan has recently identified that FBW7 recognizes neurofibromin and mediates neurofibromin degradation through ubiquitination (personal communication). In addition, Dr. Huarui Zheng from our lab found reduced Olig2^{+} cells in FBW7 knockout mice (personal communication). These findings lead to an intriguing possibility that FBW7 specifically degrades neurofibromin in gIPCs to maintain high level of Ras/ERK

signaling in these cells. Assessment of the protein level of FBW7 and neurofibromin in different progenitor cells will be the key to test this hypothesis. These possible directions will be further explored in Chapter IV.

3.4.2 Clinical implications for NF1-associated learning disabilities

One unique feature of our mouse model is that *Nf1*^{hGFAP}KO mice exhibit enlarged corpus callosum that recapitulates the structural abnormalities in the brains of a subset of NF1 patients. Enlarged corpus callosum in NF1 children is associated with severe cognitive deficits and may serve as an early structural marker for the children at risk of learning disabilities. A recent publication compared the IQ score and white matter enlargement index among NF1 children with varying degree of cognitive deficits. Their results indicate that NF1 children with larger white matter volume tend to suffer from more severe learning disabilities (Pride et al. 2010). My study demonstrates that bi-allelic inactivation of *Nf1* in SVZ stem/progenitor cells is sufficient to induce excessive gliogenesis in the corpus callosum and increase corpus callosum size, providing the cellular basis for such structural defects. Since NF1 patients are heterozygous for *NF1*, enlarged corpus callosum is most likely due to loss of heterzygosity in a subset of neural stem/progenitor cells, and the number of cells that undergo LOH determines the degree of corpus callosum enlargement and the severity of cognitive impairment. Our mouse model could therefore serve as a valuable tool to study the structure-function relationship in NF1-associated learning disabilities. Importantly, the MEK inhibitor treatment studies have reversed the corpus callosum defect, suggesting that targeting Ras/ERK pathway during neonatal development could potentially be used as a therapy in NF1 patients to alleviate associated neurocognitive defects. In addition, these observations might have a broader clinical implication in NCFC syndromes caused by germline mutations in the oncogenic Ras/ERK signaling pathway, which all share a variable degree of cognitive impairment (Rodriguez-Viciana et al. 2006).

The remaining questions include why enlarged corpus callosum leads to learning disabilities and whether rescuing the structural defect could rescue the cognitive deficits.

Since *Nf1*^{hGFAP}KO mice are paralyzed due to the widespread genetic recombination in CNS and PNS, we were not able to carry out behavioral analysis on these mice. The optimal model for future studies will be the Nestin-Cre^{ER} inducible model, which only targets a small number of cells and could avoid defects caused by *Nf1*-deficiency during embryonic development. By inducing around P0.5, we could very likely induce the corpus callosum phenotype without paralyzing the mice. This will allow us to analyze the electrophysiological and behavioral alterations in *Nf1* mutant mice and treatment studies on these mice will provide the appropriate platform for future clinical trials. This possibility will be explored further in Chapter IV.

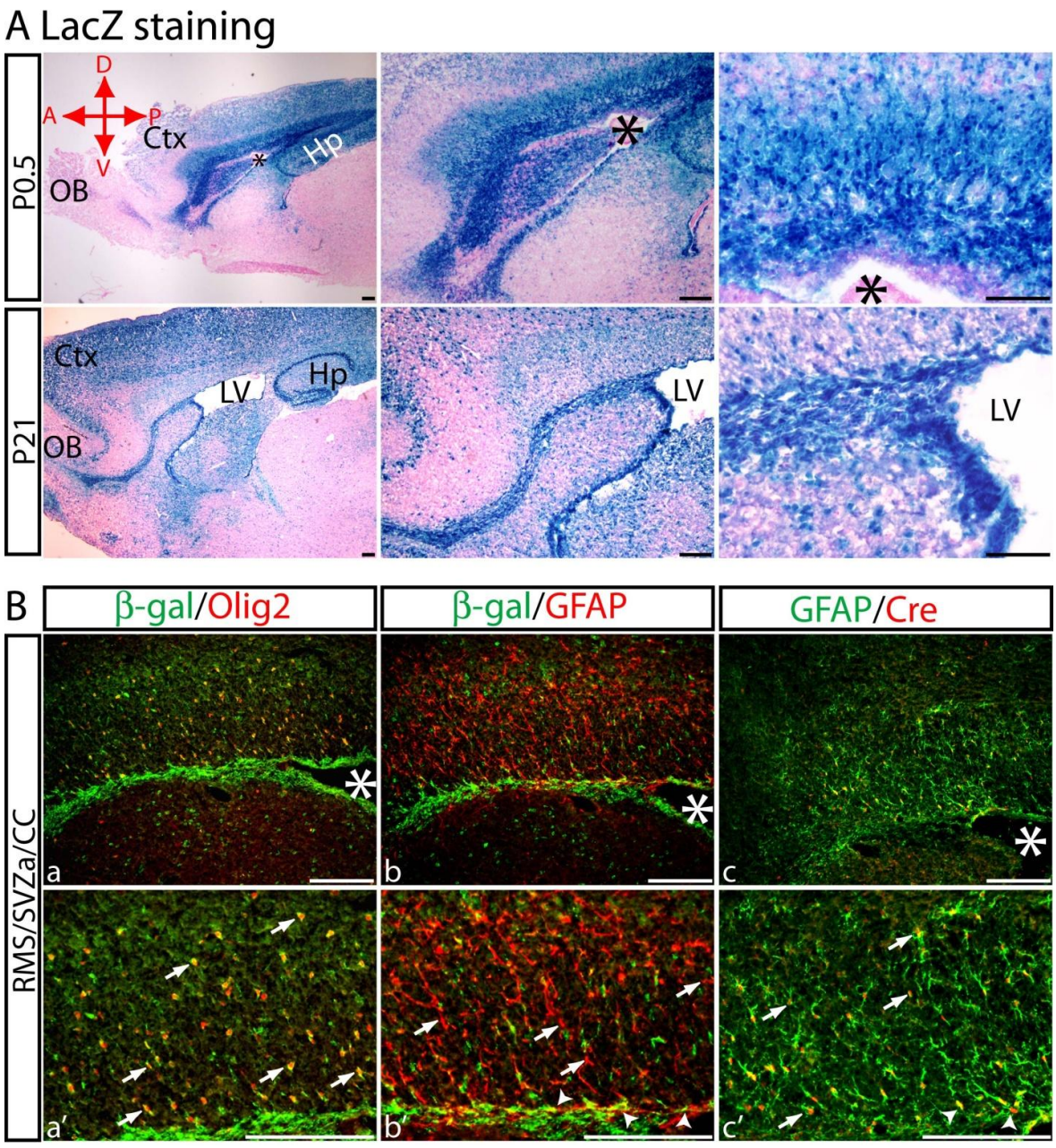
A LacZ staining
P0.5
P21
D
A
P
V
Ctx
Hp
OB
LV
B
β-gal/Olig2
β-gal/GFAP
GFAP/Cre
RMS/SVZa/CC
a
b
c
a′
b′
c′

Figure 15. hGFAP-cre-mediated genetic recombination in the developing and neonatal brain. (A) Brain sections from hGFAP-cre+; R26R-LacZ transgenic mice at ages of neonatal day 0.5 (P0.5, upper panels) and P21 (lower panels) were stained with X-gal and imaged at three different magnifications. (B) Brain sections from adult hGFAP-cre+;R26R-LacZ double transgenic mice were stained with anti-β-gal/anti-Olig2 (a, a'), anti-β-gal/anti-GFAP (b, b'), anti-β-gal/anti-Cre (c, c'). Arrows mark the co-localizing cells. Ctx, cerebral cortex; OB, olfactory bulb; Hp, hippocampus; LV and "*", lateral ventricle. Scale bar, 100μ.

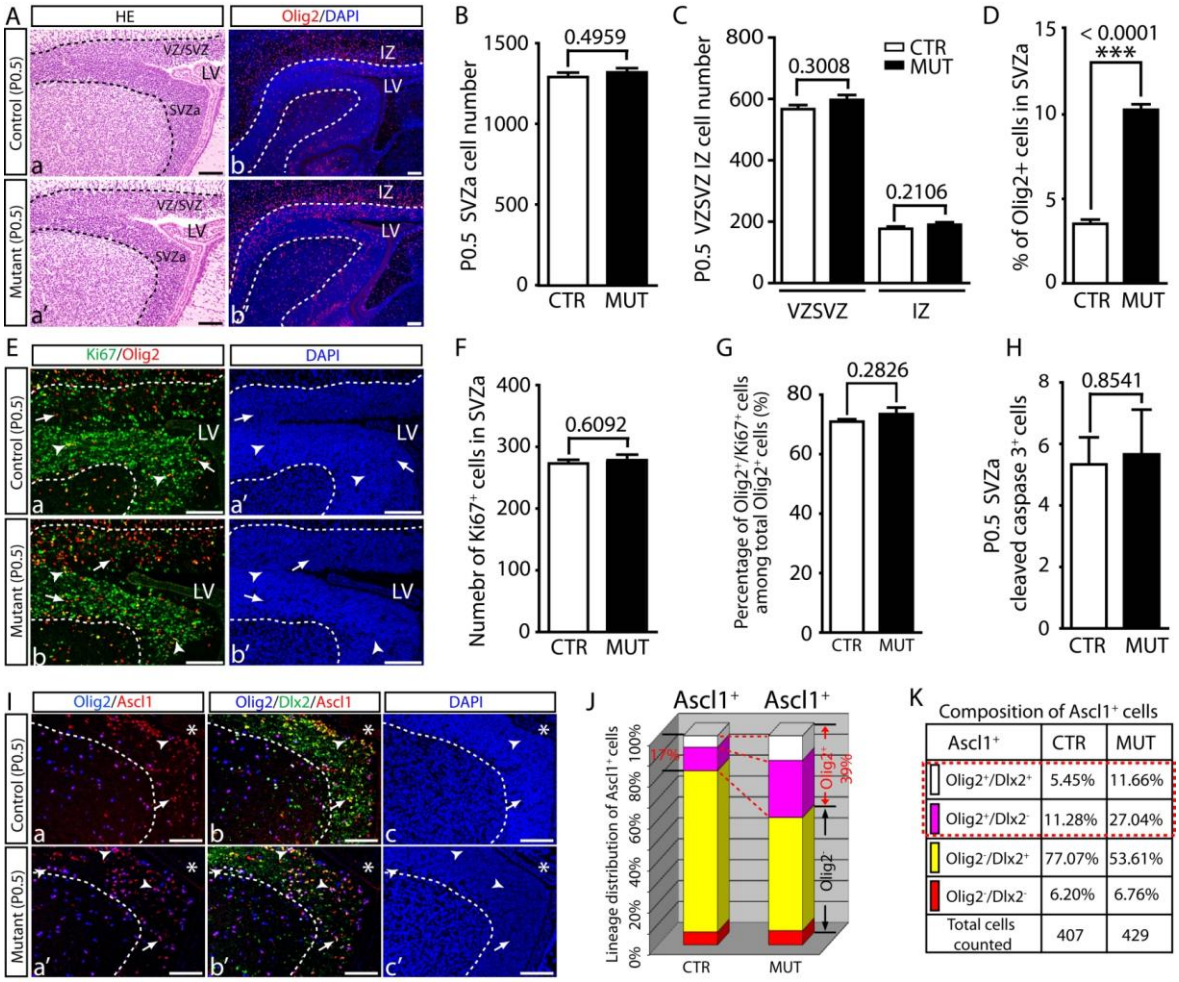
A
HE
Olig2/DAPI
Control (P0.5)
Mutant (P0.5)
VZ/SVZ
LV
SVZa
IZ
a
a′
b
b′
B
P0.5 SVZa cell number
0.4959
CTR
MUT
C
P0.5 VZSVZ IZ cell number
0.3008
0.2106
CTR
MUT
VZSVZ
IZ
D
% of Olig2+ cells in SVZa
< 0.0001
***
E
Ki67/Olig2
DAPI
F
Numebr of Ki67+ cells in SVZa
0.6092
G
Percentage of Olig2+/Ki67- cells among total Olig2+ cells (%)
0.2826
H
P0.5 SVZa cleaved caspase 3+ cells
0.8541
I
Olig2/Ascl1
Olig2/Dlx2/Ascl1
DAPI
c
c′
J
Ascl1+
Ascl1+
Lineage distribution of Ascl1+ cells
17%
Olig2+
39%
Olig2-
CTR
MUT
K
Composition of Ascl1+ cells
Ascl1+
CTR
MUT
Olig2+/Dlx2+
5.45%
11.66%
Olig2+/Dlx2-
11.28%
27.04%
Olig2-/Dlx2+
77.07%
53.61%
Olig2-/Dlx2-
6.20%
6.76%
Total cells counted
407
429

Figure 16. Loss of *Nf1* leads to misexpression of Olig2 in neural stem/progenitor cells in the neonatal SVZa.

(A)-(D) P0.5 brains from control and *Nf1*^{hGFAP}KO mice were sectioned and stained for H&E (A, left column) and Olig2 immunofluorescence labeling (A, right column). The numebr of cells in SVZa and VZ/SVZ was quantified in (B) and (C), respectively. The percentage of Olig2+ cells among SVZa cells was quantified in (D). While SVZ size and cell number are comparable at this stage, the absolute number and percentage of Olig2^{+} cells were dramatically increased in *Nf1*^{hGFAP}KO SVZa.

(E)-(G) Olig2 and Ki67 double immunofluorescence (E) revealed no difference in the total number of Ki67+ cells that were in the cell cycle (F), or the percentage of Olig2+ cells that colocalized with Ki67 (G). Arrowheads point to the colocalizing cells and arrows indicate the non-colocalizng Olig2^{+} cells.

(H) The number of cleaved caspase 3^{+} cells that underwent apoptosis was quantified and compared. No difference was identified between control and mutants.

(I) Olig2, Ascl1 and Dlx2 triple immunofluorescence labeling to analyze the cellular composition of SVZa Ascl1+ cells. Arrowheads point to the triple-labeled cells and arrows indicate the non-colocalizng Ascl1^{+}/Dlx2^{+}/Olig2^{-} cells.

(J) and (K) The quantification for the percentage of different types of cells in SVZa Ascl1^{+} cell compartment from 3 controls and 3 mutants. 39% of mutant Ascl1^{+} cells were Olig2^{+}, compared to 17% in controls.

Dashed lines roughly demarcate the SVZa or VZ/SVZ regions. LV, *, lateral ventricle. Scale bars, 50μ.

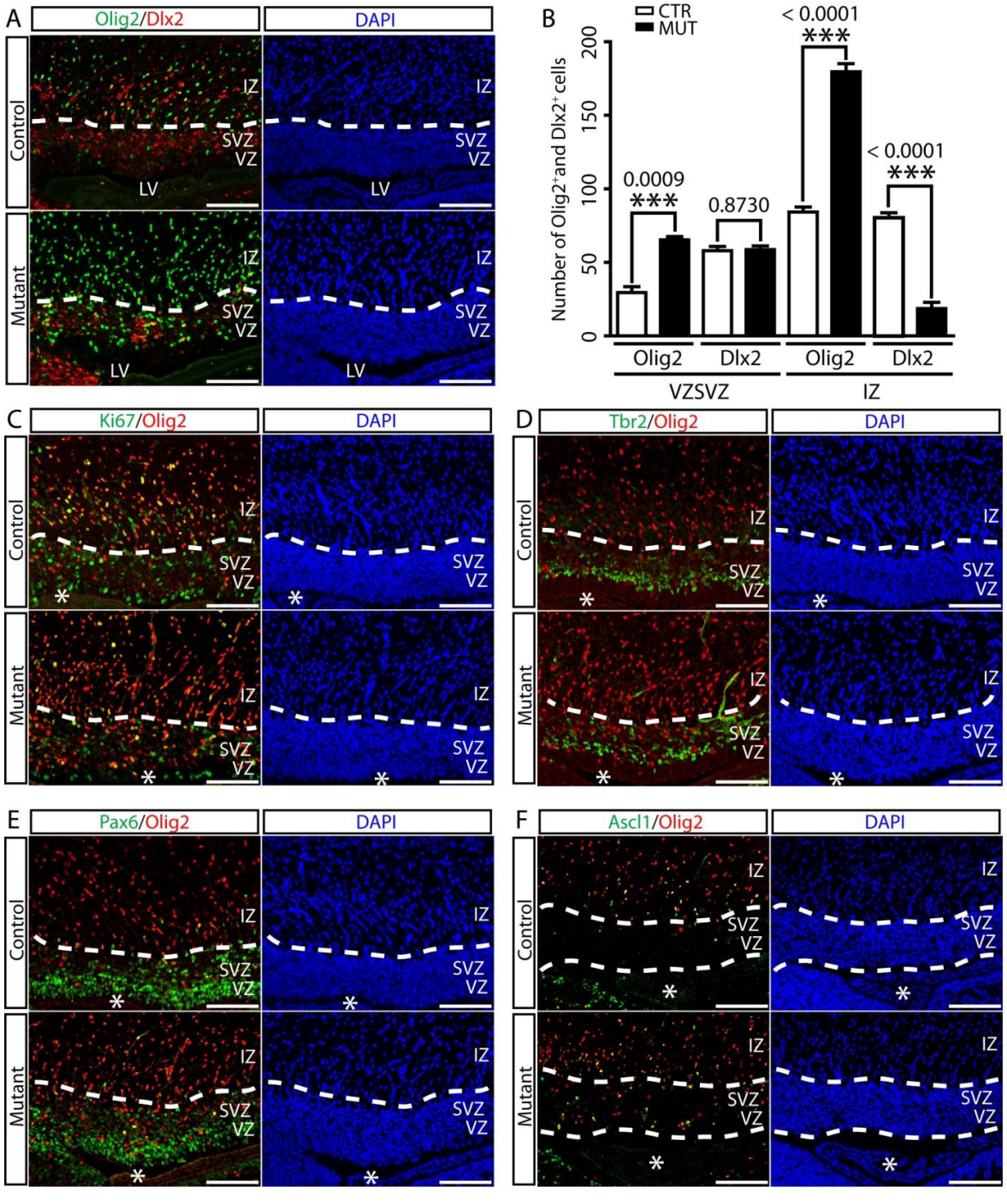

G Characterization of Olig2⁺ cells in VZ/SVZ

	CTR (n = 3)	MUT (n = 3)	p value
Ki67⁺	27/57 (47.37%)	99/237 (41.77%)	0.2692
Tbr2⁺	0/66	0/200	N. A.
Pax6⁺	12/60 (20%)	51/190 (26.7%)	0.1913
Ascl1⁺	9/51 (17.65%)	70/184 (38.04%)	0.0052
Dlx2⁺	6/55 (10.91%)	59/204 (26.96%)	0.0104

H Characterization of Olig2⁺ cells in IZ

	CTR (n = 3)	MUT (n = 3)	p value
Ki67⁺	93/209 (14.42%)	138/483 (4.03%)	< 0.0001
Tbr2⁺	0/194	0/425	N. A.
Pax6⁺	15/188 (7.98%)	27/401 (6.73%)	0.3527
Ascl1⁺	52/180 (28.89%)	99/421 (23.52%)	0.098
Dlx2⁺	12/190 (6.32%)	10/410 (2.44%)	0.017

Figure 17. Characterization of Olig2$^+$ cells in P0.5 VZ/SVZ/IZ.
(A) Olig2, Dlx2 doublelabeling for cells in VZ/SVZ/IZ. Note that Dlx2$^+$ cells were almost depleted in the mutant IZ with a significant increase of Olig2$^+$ cells.
(B) The quantification for these two cell populations in VZ/SVZ and IZ.
(C)-(F) Characterization of Olig2$^+$ cells through doublelabeling with different markers. (G) and (H) are the quantifications for colocalization. The ratio of Olig2$^+$ cells colocalizng with Ki67 was comparable in mutant and controls (C), and Olig2 expression was not expanded in Tbr2$^+$ SVZ and Pax6$^+$ VZ progenitor cells (D, E). Instead, ectopic expression of Olig2 was found in Ascl1$^+$ (F) and Dlx2$^+$ cells (See G, H).
Dashed lines roughly demarcate the VZ/SVZ. LV, *, lateral ventricle. Scale bars, 50μ.

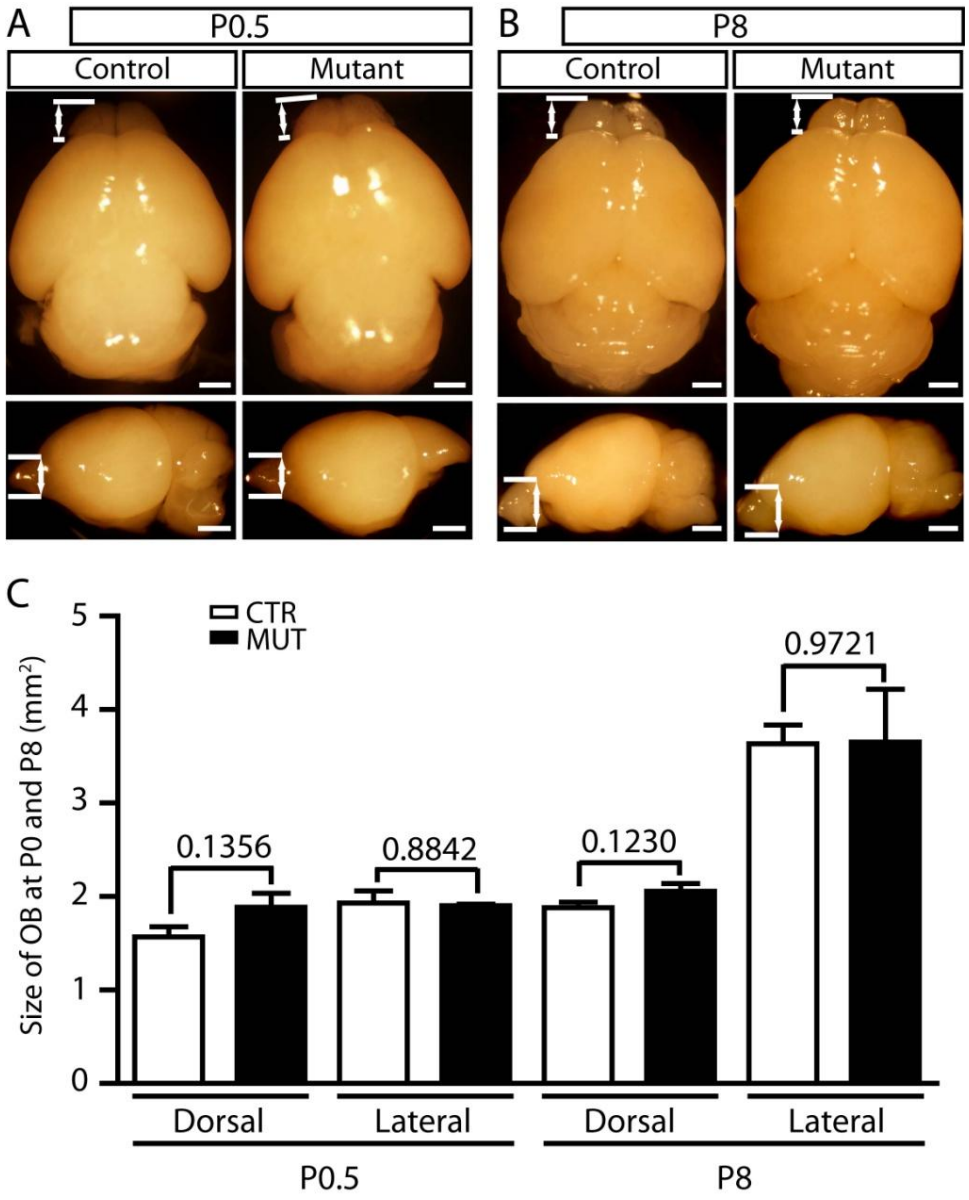

Figure 18. Whole mount analysis for P0.5 and P8 brains.
Whole mount brains from control and *Nf1*^{hGFAP}KO mice were dissected, fixed in 4% PFA and imaged under the dissection microscope. Olfactory bulb size from P0.5 (panel A) and P8 (panel B) brains were measured and compared from dorsal view (A, B upper panels) and lateral view (A, B lower panels) in (C). There was no obvious difference in olfactory bulb size in P0.5 and P8 brains. Scale bars, 1 mm

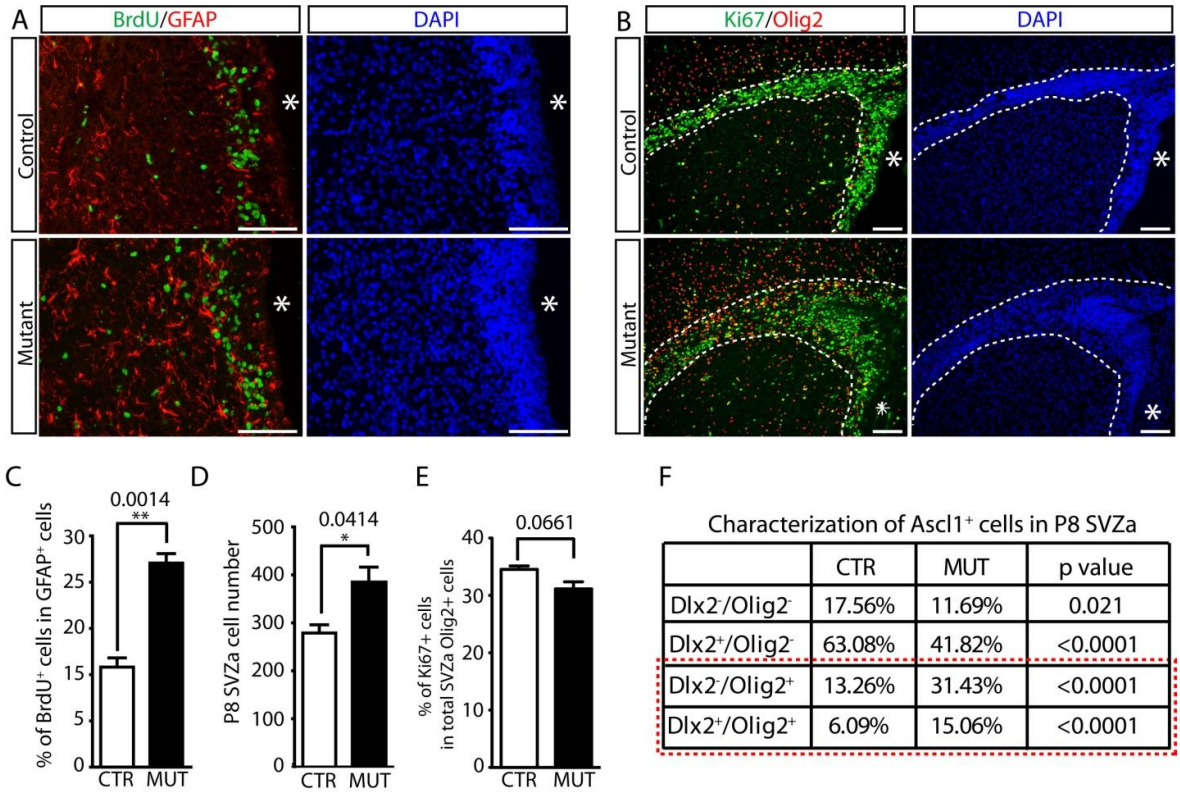

Figure 19. *Nf1* deficiency results in a transient increase of GFAP$^+$ cells at P8.
(A) GFAP$^+$ cells in *Nf1*^{hGFAP}KO SVZ exhibit increased proliferation as demonstrated by GFAP/BrdU doublelabeling, which was quantified in (C).
(B) Ki67/Olig2 double-labeling demonstrating that Olig2$^+$ cells did not overproliferate in P8 *Nf1*^{hGFAP}KO SVZ. (E): the quantification for Ki67$^+$/Olig2$^+$ cells among total SVZ Olig2$^+$ cell population.
(D) The total cell number was increased in P8 *Nf1*^{hGFAP}KO SVZ.
(F) Quantification and characterization of Ascl1$^+$ cells in P8 SVZa based on their colocalization with Dlx2 and Olig2.
Dashed lines roughly demarcate the SVZa and RMS in (B). *, lateral ventricle. Scale bars, 50μ.

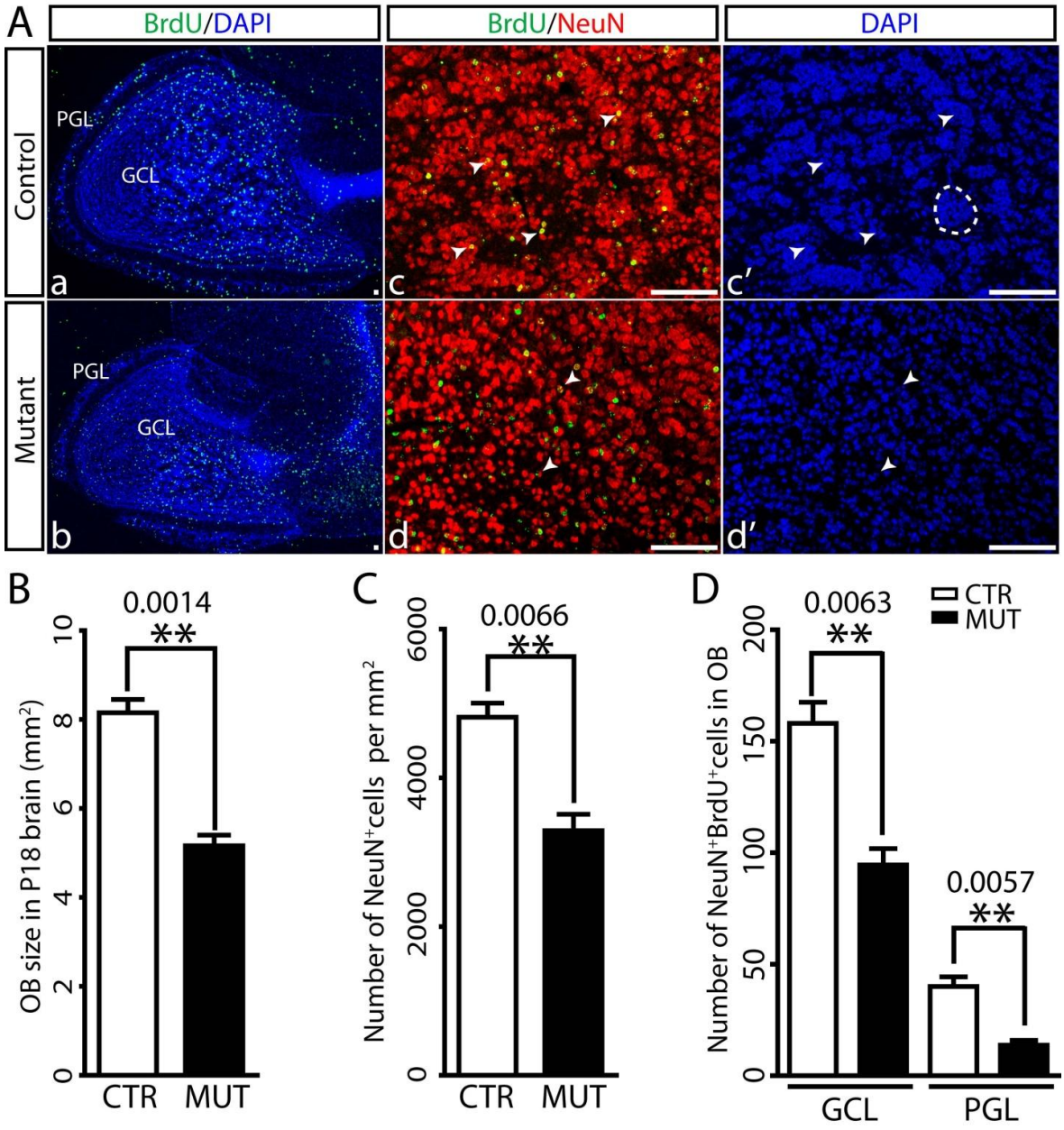
A
BrdU/DAPI
BrdU/NeuN
DAPI
Control
Mutant
PGL
GCL
a
b
c
d
c′
d′
B
0.0014
**
OB size in P18 brain (mm²)
0
2
4
6
8
10
CTR
MUT
C
0.0066
**
Number of NeuN⁺cells per mm²
0
2000
4000
6000
CTR
MUT
D
0.0063
**
0.0057
**
CTR
MUT
Number of NeuN⁺BrdU⁺cells in OB
0
50
100
150
200
GCL
PGL

Figure 20. *Nf1* deficiency leads to reduced neurogenesis during neonatal development.
Control and *Nf1*^{hGFAP}KO mice were pulsed with BrdU at P8 and analyzed at P18 after a 10-day BrdU chase to quantitatively analyze SVZ-derived neurogenesis in the OB and gliogenesis in the corpus callosum.
(A) SVZ-derived newborn neurons labeled by BrdU and neuronal marker NeuN ($BrdU^+/NeuN^+$) were markedly reduced in the *Nf1*^{hGFAP}KO OB compared to controls. (a,b) Low magnification view for the distribution of $BrdU^+$ cells. (c-d') High magnification view of NeuN/BrdU colocalizing cells, some of which are marked by arrowheads. Dashed lines mark the neuronal clusters in control OB which were largely absent in mutants.
(B) and (C): The size (B) and neuronal density (C) of control and *Nf1*^{hGFAP}KO OB were measured and compared. *Nf1*^{hGFAP}KO OB exhibited significant reduction.
(D) Quantification of $BrdU^+/NeuN^+$ cells in the granular cell layer (GCL) and periglomerular cell layer (PGL). Neurogenesis was reduced in both regions in mutant OB.
Scale bars, 50μ.

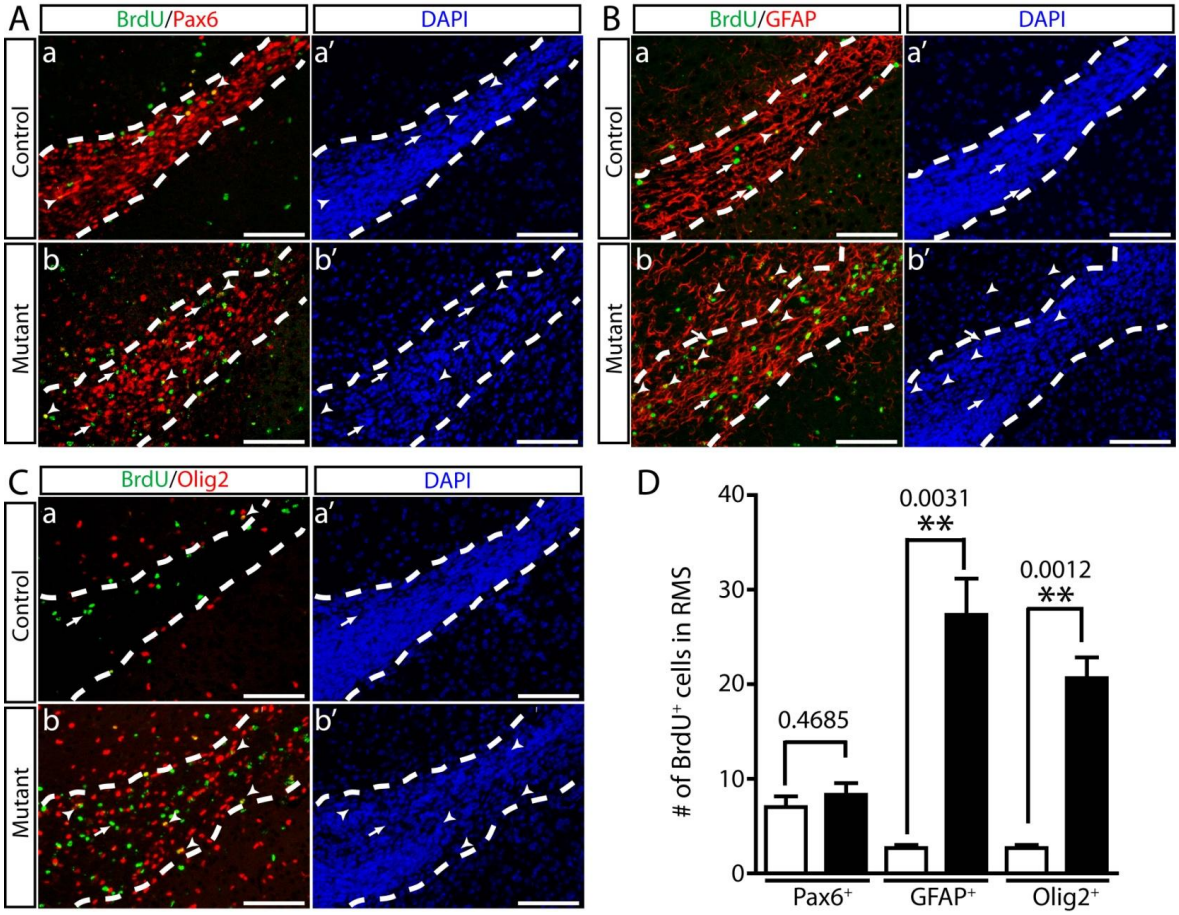

Figure 21. *Nf1*^{hGFAP}KO mice exhibit ectopic gliogenesis in the RMS during neonatal development.

In the P8-P18 BrdU differentiation assay, BrdU^{+} cells in the RMS were characterize by colocalization with neuronal/glial markers.

(A) The number of BrdU^{+} cells coexpressing neuronal marker Pax6 was not significantly different between control and *Nf1*^{hGFAP}KO brains.

(B) and (C) Gliogenesis is significantly increased compared to controls, marked by BrdU^{+}/GFAP^{+} (B) and BrdU^{+}/Olig2^{+} (C).

(D) Quantification of the number of BrdU^{+} cells that colocalize with Pax6, GFAP and Olig2.

Arrowheads point to colocalizing cells and arrows label the non-colocalizing cells. Dashed lines roughly demarcate the RMS. Scale bars, 50μ.

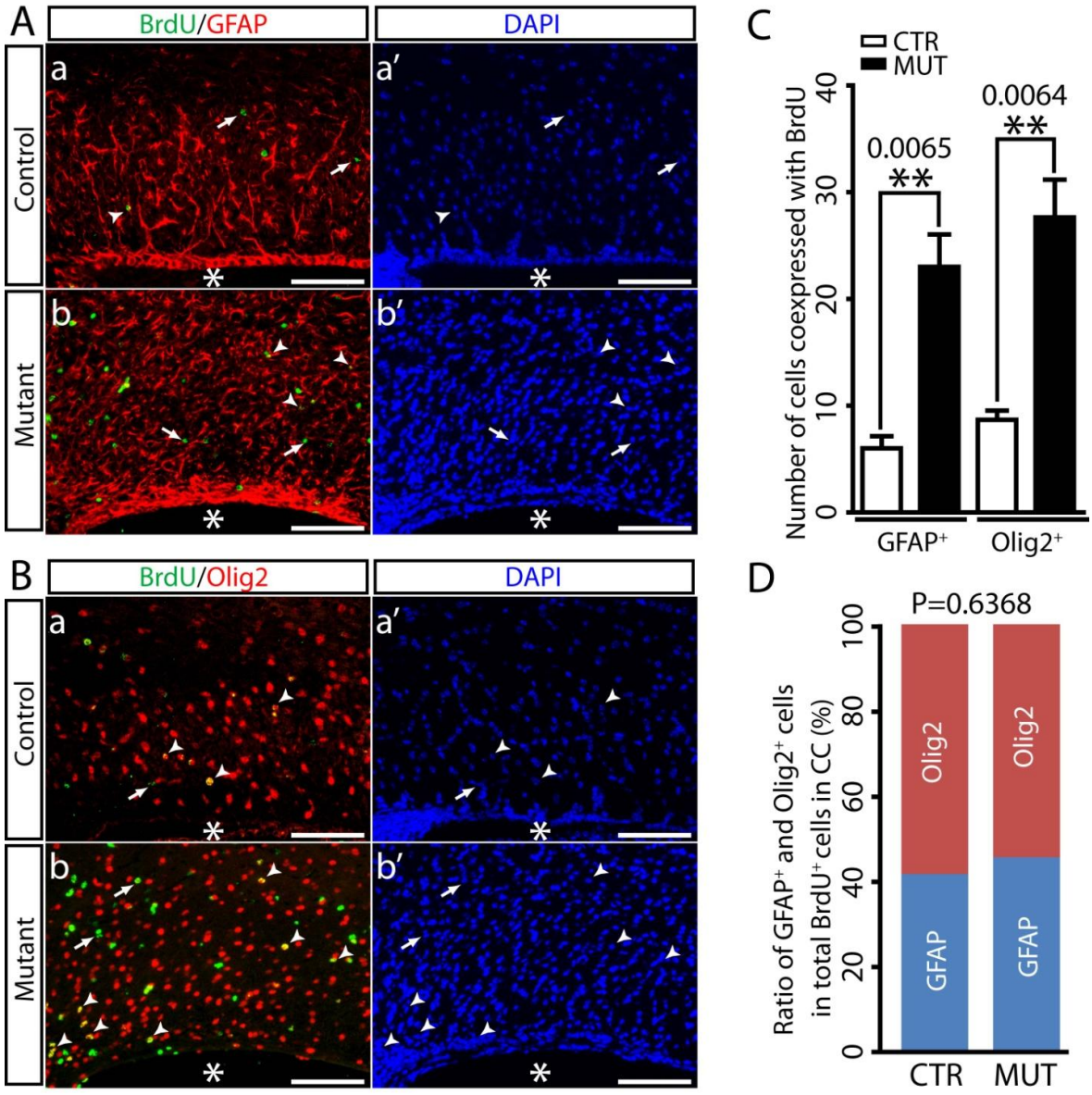

Figure 22. *Nf1*^{hGFAP}KO mice exhibit increased gliogenesis in the CC during neonatal development.

(A)-(C) In the P8-P18 BrdU differentiation assay, BrdU^{+} cells in the CC were colocalized with glial markers GFAP (panel A) and Olig2 (panel B). The number of newly generated astrocytes (BrdU^{+}/GFAP^{+}) and oligodendrocytes (BrdU^{+}/Olig2^{+}) was quantified and compared in (C).

(D) The relative ratio of astrogenesis versus oligodendrogenesis (BrdU^{+}/GFAP^{+} versus BrdU^{+}/Olig2^{+}) was unchanged.

Arrowheads in point to colocalizing cells and arrows label the non-colocalizing cells. *, lateral ventricle. Scale bars, 50μ.

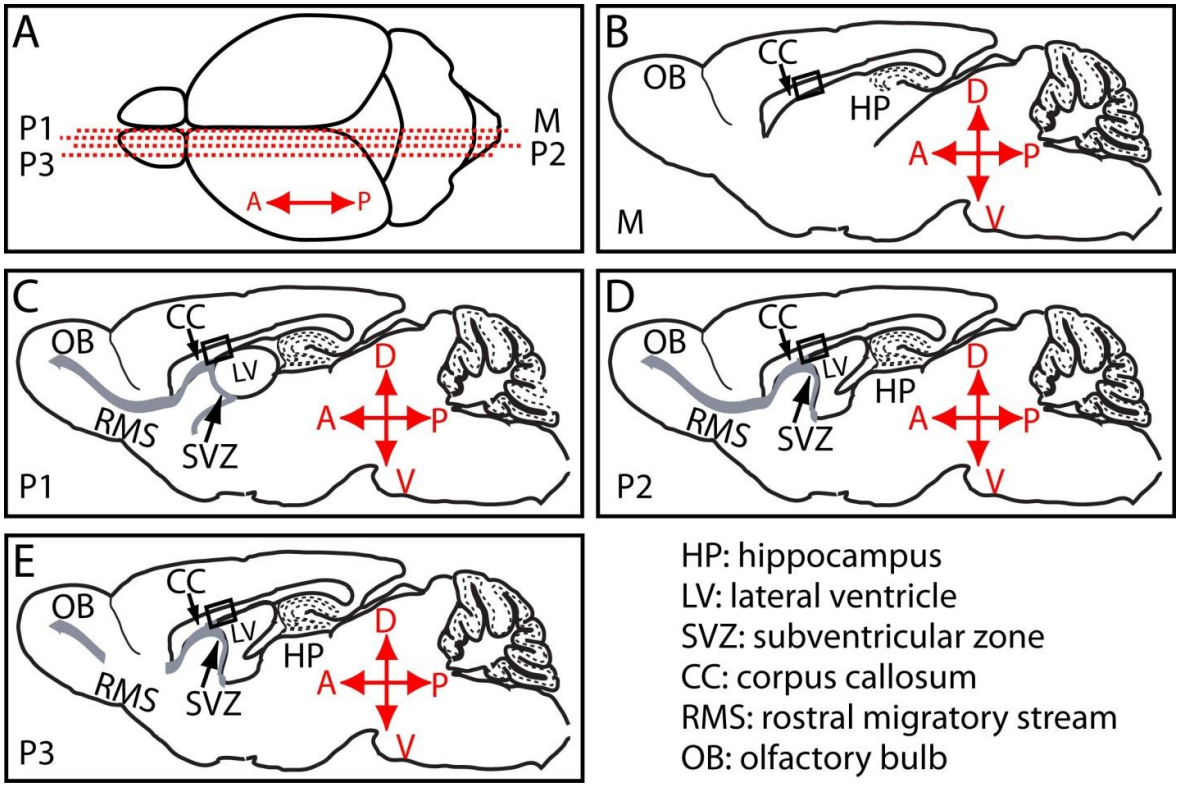

Figure 23. Schematic demonstration of different histological planes used for adult analysis.

For adult brains in particular, at least three independent positions (position 1-3) that contain SVZ/RMS were selected for quantification. Each plane is approximately 100μ apart at sagittal planes along the midline to lateral direction (A) and was determined by the following histological criteria: P1: oval lateral ventricle with intact RMS (C); P2: triangular lateral ventricle with intact RMS (D); P3: triangular lateral ventricle with non-intact RMS) (E). For CC analysis, we also compared the midline position as demonstrated in (A) and (B).

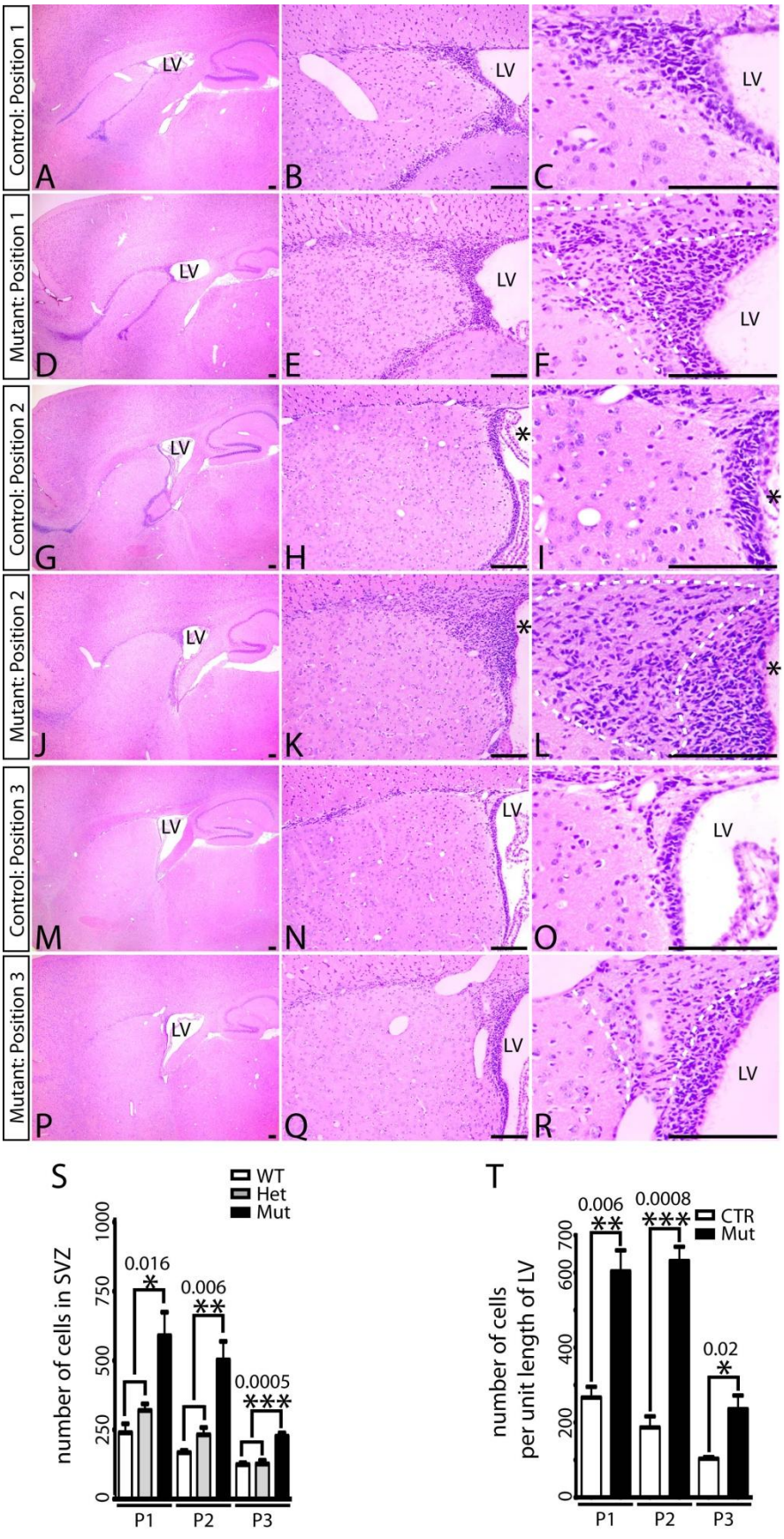
Control: Position 1
Mutant: Position 1
Control: Position 2
Mutant: Position 2
Control: Position 3
Mutant: Position 3
LV
A
B
C
D
E
F
G
H
I
J
K
L
M
N
O
P
Q
R
*
S
WT
Het
Mut
number of cells in SVZ
0
250
500
750
1000
0.016
*
0.006
**
0.0005
***
P1
P2
P3
T
CTR
Mut
number of cells
per unit length of LV
0
200
400
600
700
0.006
**
0.0008
***
0.02
*
P1
P2
P3

Figure 24. Enlarged SVZ in adult Nf1hGFAPKO mice at all three histological positions.
(A)-(R) H&E staining of 2 month old control and mutant SVZ at different magnifications. Position 1: (A)-(F); Position 2: (G)-(L); Position 3: (M)-(R); Mutant SVZ was significantly enlarged. Dashed lines demarcate the less cellular area uniquely identified in mutant SVZ.
(S) Quantification of the absolute cell number in wildtype, heterozygous and mutant SVZ.
(T) Normalized quantification of the number of cells per unit length of LV (number of cells divided by the length of LV). Wildtype and heterozygous mice were combined as controls.
Scale bars, 50μ.

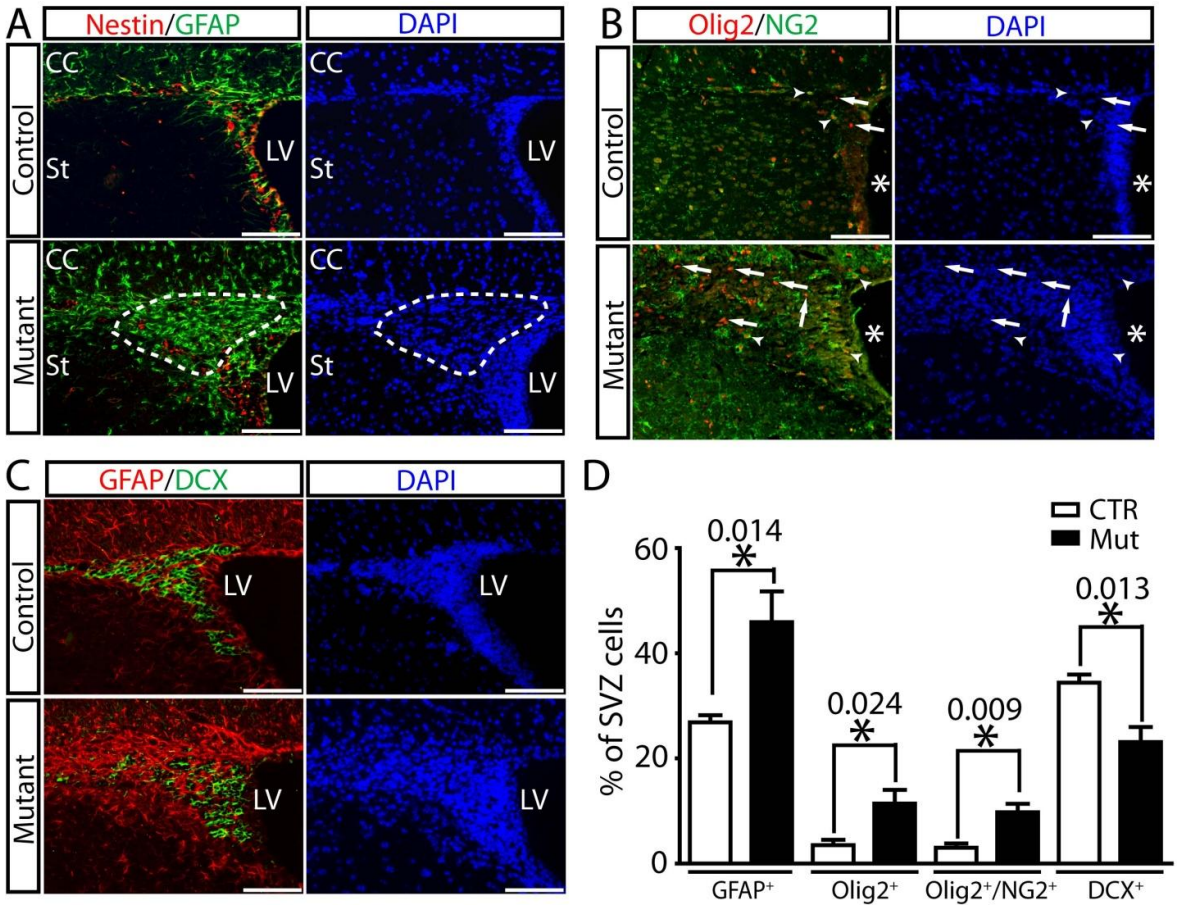

Figure 25. *Nf1*^{hGFAP}KO SVZ has disproportionally increased glial differentiation.
Sections from 2 month old control and mutant brains were stained for SVZ lineage markers. In mutant SVZ, the percentage of cells that expressed glial lineage markers GFAP (panel A), Olig2, and NG2 (panel B) was significantly increased, while the percentage of DCX^{+} neuroblasts is reduced (panel C). The less cellular area marked by dashed lines in mutant SVZ was largely composed of differentiated astrocytes that are Nestin^{-}/GFAP^{+}.
(D) Quantification of the cellular composition of SVZ. The percentage of cells expressing GFAP, Olig2, Olig2/NG2 and DCX was quantified and compared.
*, lateral ventricle. Scale bars, 50μ.

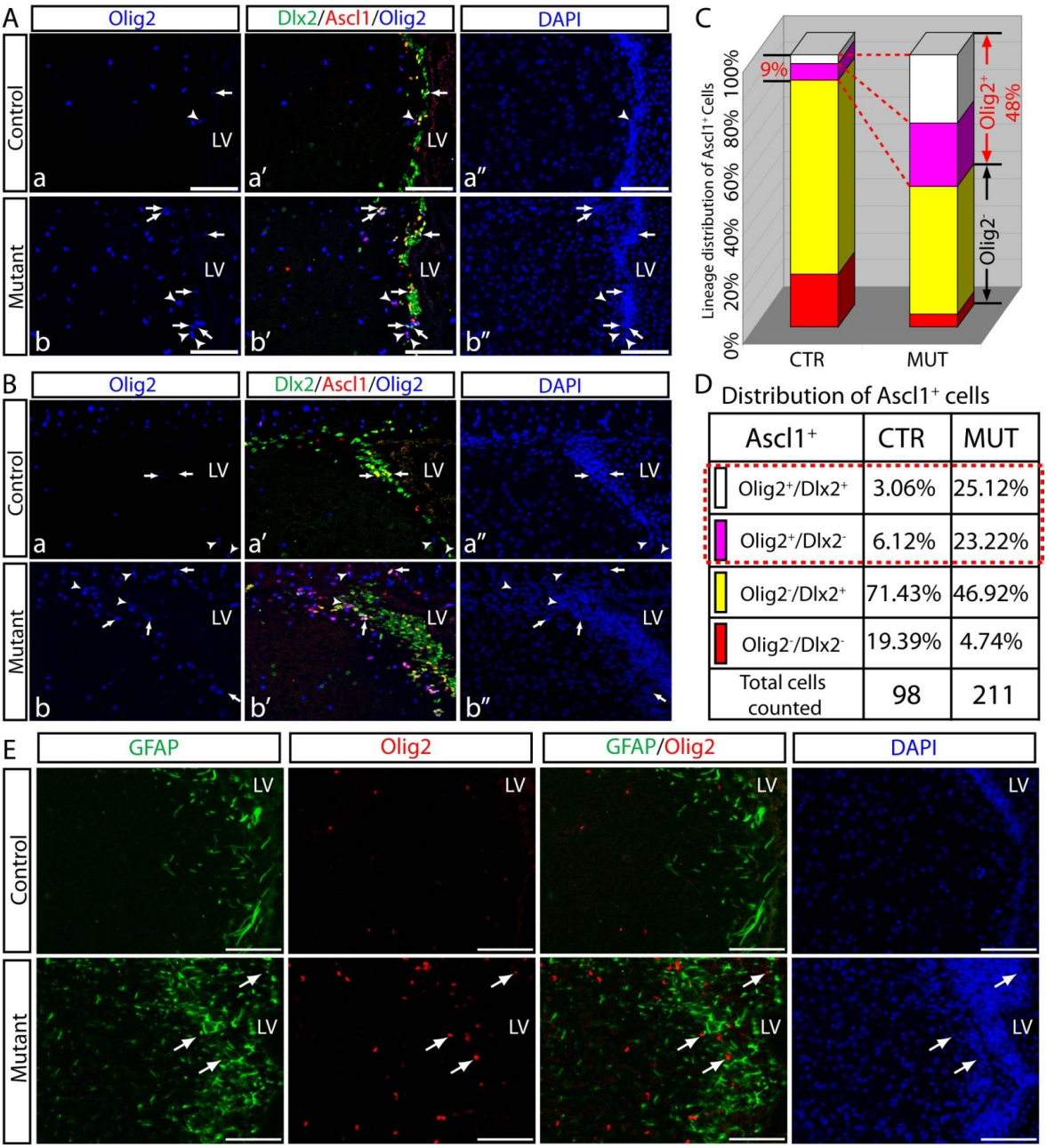

Figure 26. *Nf1* deficiency specifically alters fate specification of SVZ Ascl1$^+$ cells. (A)–(D) Lineage distribution of SVZ Ascl1$^+$ transit amplifying cells. (A) and (B) Olig2/Dlx2/Ascl1 triple labeling in ventral (A) and dorsal anterior (B) regions of control and mutant SVZ. Arrows label Olig2$^+$/Dlx2$^+$/Ascl1$^+$ triple positive cells; Arrowheads point to Olig2$^+$/ Ascl1$^+$ double-positive cells. Of note, Olig2$^+$/Dlx2$^+$/Ascl1$^+$ triple positive cells were not found in the dorsal anterior area of control SVZ (Ba) and the arrows point to Dlx2$^+$/Ascl1$^+$ double-positive cells. (E) The specificity of ectopic Olig2 expression in SVZ progenitors. Olig2 misexpression was not found in GFAP$^+$ SVZ B cells or mature astrocytes based on GFAP/Olig2 double-immunofluorescence. Scale bars, 50μ.

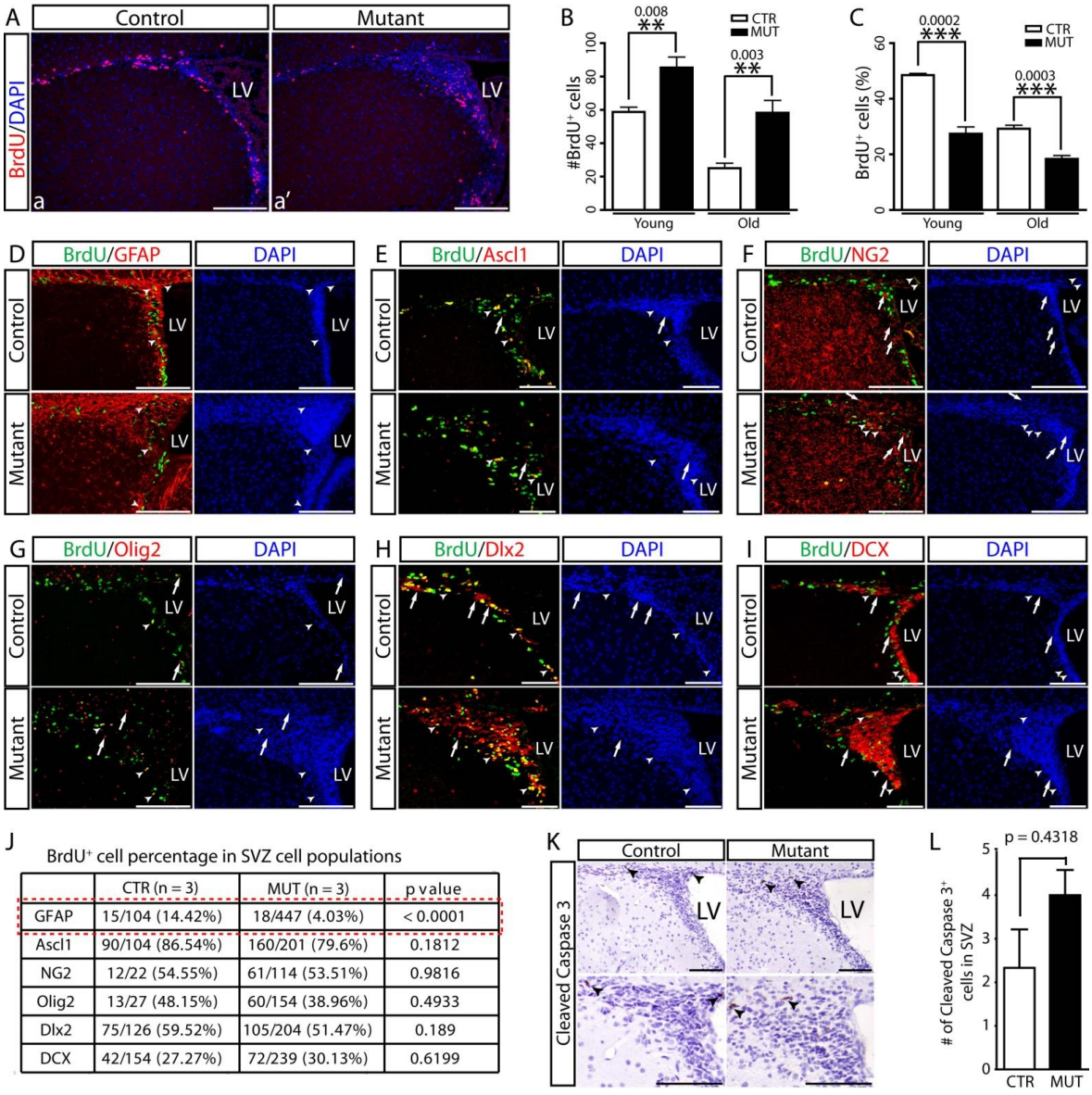

J

BrdU⁺ cell percentage in SVZ cell populations

	CTR (n = 3)	MUT (n = 3)	p value
GFAP	15/104 (14.42%)	18/447 (4.03%)	< 0.0001
Ascl1	90/104 (86.54%)	160/201 (79.6%)	0.1812
NG2	12/22 (54.55%)	61/114 (53.51%)	0.9816
Olig2	13/27 (48.15%)	60/154 (38.96%)	0.4933
Dlx2	75/126 (59.52%)	105/204 (51.47%)	0.189
DCX	42/154 (27.27%)	72/239 (30.13%)	0.6199

Figure 27. *Nf1* deficiency provides no significant growth advantage to different SVZ progenitors.

(A)-(C) BrdU proliferation assay on 2 month old mouse brains. Although the absolute number of $BrdU^+$ cells was increased in the enlarged $Nf1^{hGFAP}$KO SVZ, the percentage of $BrdU^+$ cells was significantly reduced compared to controls. Such difference in the number and percentage of $BrdU^+$ cells was also identified in aged control and mutant SVZ.

(D, E) Prolfieration marker BrdU was colocalized with different lineage markers to determine the proliferation ratio in different SVZ progenitor populations. No difference was found in $Ascl1^+$ SVZ-C cells (E), $Olig2^+/NG2^+$ SVZ-OPCs (F,G), as well as neurogenic $Dlx2^+$ progenitors (H) and DCX^+ SVZ-A neuroblasts (I). Proliferation in $GFAP^+$ cells was significantly in reduced $Nf1^{hGFAP}$KO SVZ due to the presence of a large number of differentiated astrocytes (D). Arrowheads point to the colocalizing cells and arrows indicate the non-colocalizing cells. The colocalization was quantified and summarized in (J).

(K)-(L) No difference in apoptosis was detected through Cleaved Caspase 3 IHC. Arrowheads represent cleaved caspase 3^+ cells.

Scale bars, 50μ.

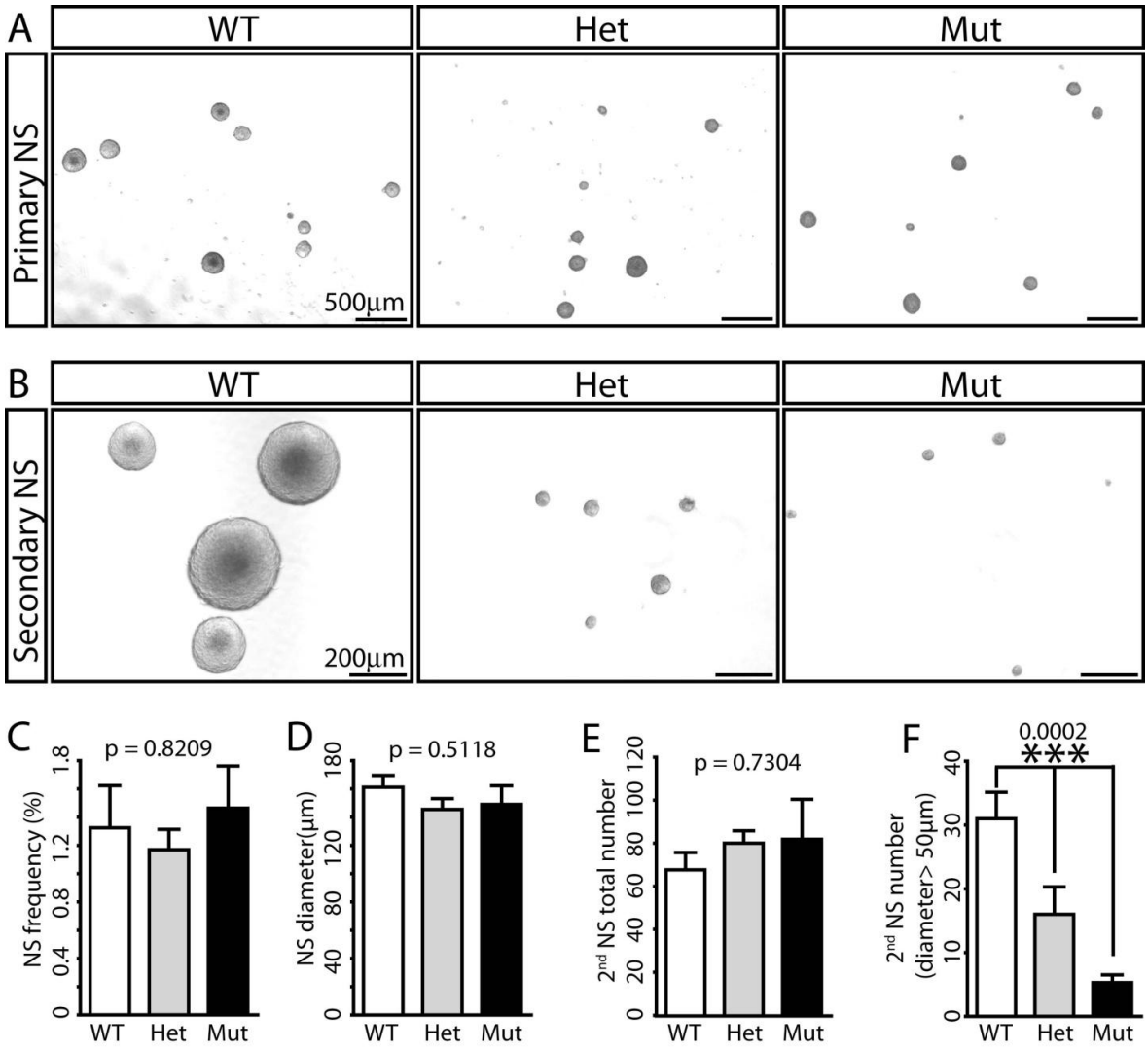

Figure 28. *Nf1* deficient neural stem/progenitor cells have reduced self-renewal capacity in vitro.

(A) *in vitro* neurosphere culture compared the primary neurosphere (NS) forming capacity between *Nf1* wildtype, heterozygous and *Nf1*^{hGFAP}KO neural progenitors, and no significant difference was found in the frequency and size of primary neurospheres (C, D). Scale bars, 500μ.

(B) Primary neurospheres derived from *Nf1* wildtype, heterozygous and *Nf1*^{hGFAP}KO progenitors were further passaged to assess the secondary sphere forming capacity. The frequency of secondary spheres was drastically reduced in *Nf1* heterozygous and *Nf1*^{hGFAP}KO neural progenitors (F). Of note, these *Nf1* heterozygous and *Nf1*^{hGFAP}KO cells could still form cell clusters in culture (E), but the size of these clusters was too small to be considered as secondary neurospheres. Scale bars, 200μ.

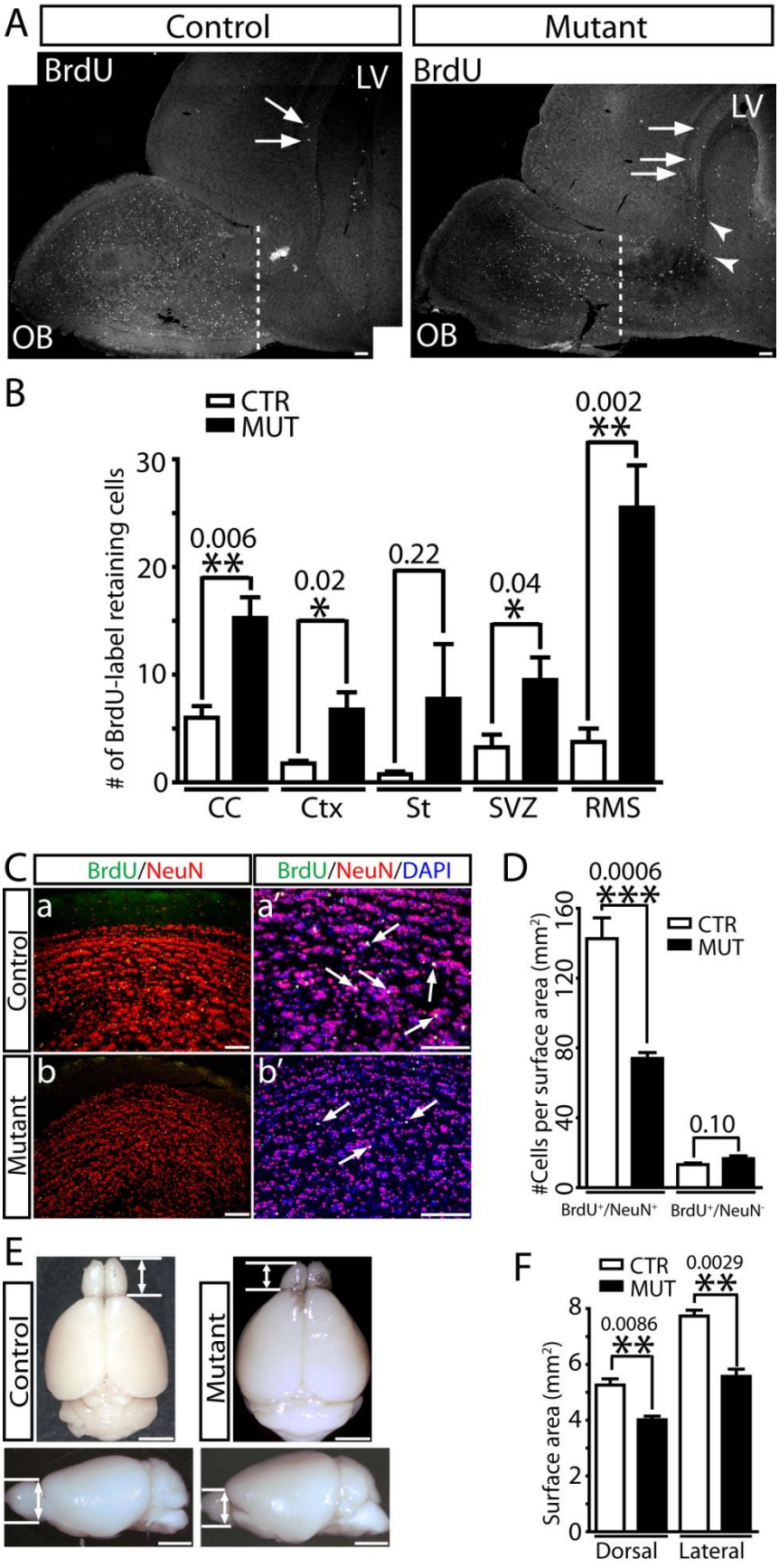
A
Control
Mutant
BrdU
LV
OB
B
CTR
MUT
# of BrdU-label retaining cells
0.006
0.02
0.22
0.04
0.002
CC
Ctx
St
SVZ
RMS
C
BrdU/NeuN
BrdU/NeuN/DAPI
Control
Mutant
a
a′
b
b′
D
#Cells per surface area (mm²)
0.0006
0.10
BrdU⁺/NeuN⁺
BrdU⁺/NeuN⁻
E
Control
Mutant
F
Surface area (mm²)
0.0086
0.0029
Dorsal
Lateral

Figure 29. Reduced neurogenesis in adult *Nf1*^{hGFAP}KO brain.
BrdU pulse-chase assay from P60-P90 was performed to label newly generated neurons and glia. (A) Low magnification view of the overall distribution of $BrdU^+$ cells in P90 brains. Arrows point to $BrdU^+$ cells in the CC and arrowheads mark the abnormal increase of $BrdU^+$ cells in the mutant RMS. Dashed line roughly compares OB size in control and mutants.
(B) Quantification of the $BrdU^+$ cells demonstrated a significant increase of $BrdU^+$ cells in the mutant SVZ/RMS/CC/CTX system.
(C) and (D) Neurogenesis in mutant OB is reduced by 50% evidenced by the quantification of $BrdU^+/NeuN^+$ cells (pointed by arrows). Of note, there was no significant difference in the $BrdU^+/NeuN^-$ populations.
(E) and (F) Whole mount analysis revealed that reduced neurogenesis in mutant results in reduced OB size.
Scale bars, 1 mm for (E) and 50μ for others.

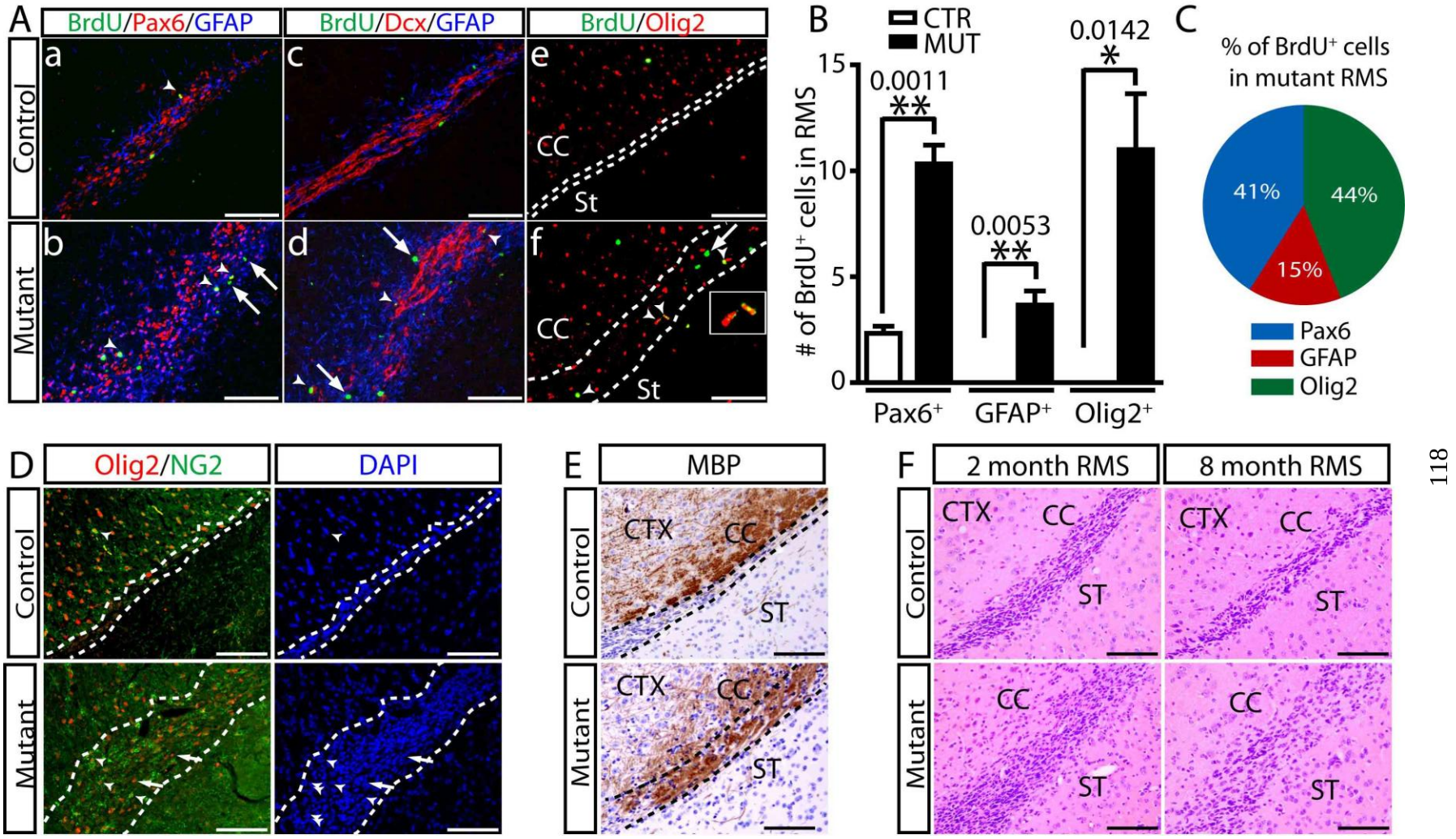
A
BrdU/Pax6/GFAP
BrdU/Dcx/GFAP
BrdU/Olig2
Control
Mutant
a
b
c
d
e
f
CC
St
B
CTR
MUT
# of BrdU+ cells in RMS
15
10
5
0
0.0011
**
0.0053
**
0.0142
*
Pax6+
GFAP+
Olig2+
C
% of BrdU+ cells in mutant RMS
41%
44%
15%
Pax6
GFAP
Olig2
D
Olig2/NG2
DAPI
Control
Mutant
E
MBP
CTX
CC
ST
F
2 month RMS
8 month RMS
CTX
CC
ST

Figure 30. Persistent glial differentiation in the RMS of adult *Nf1*^{hGFAP}KO brains.
(A)-(C) In the P60-P90 BrdU differentiation assay, there was a 9-fold increase of BrdU^{+} cells in the mutant RMS. Characterization of these BrdU^{+} cells was performed through double/triple-labeling with Pax6, DCX, GFAP and Olig2 (panel A). The number of BrdU^{+} cells that coexpressed Pax6, DCX, GFAP and Olig2 was quantified in (B). Unlike control RMS which only had a small number of BrdU^{+} cells that expressed Pax6, in the mutant RMS, 44%, 15% and 41% of BrdU^{+} cells expressed Olig2, GFAP and Pax6, respectively.
(D) Olig2/NG2 double-labeling revealed the presence of a large number of Olig2^{+}/NG2^{+} (labeled by arrowheads) in *Nf1*^{hGFAP}KO RMS.
(E) Mutant RMS exhibited high level of MBP, a marker for mature oligodendrocyte.
(F) Comparison between 2 month and 8 month old control and mutant RMS (H&E) demonstrated that over the time course *Nf1*^{hGFAP}KO RMS became a collection of loosely packed cells in contrast to the tightly packed neuroblast migratory chain in control RMS.
Dashed lines mark the border of RMS. Arrowheads label colocalizing cells and arrows represent noncolocalizing cells. Scale bars, 50μ.

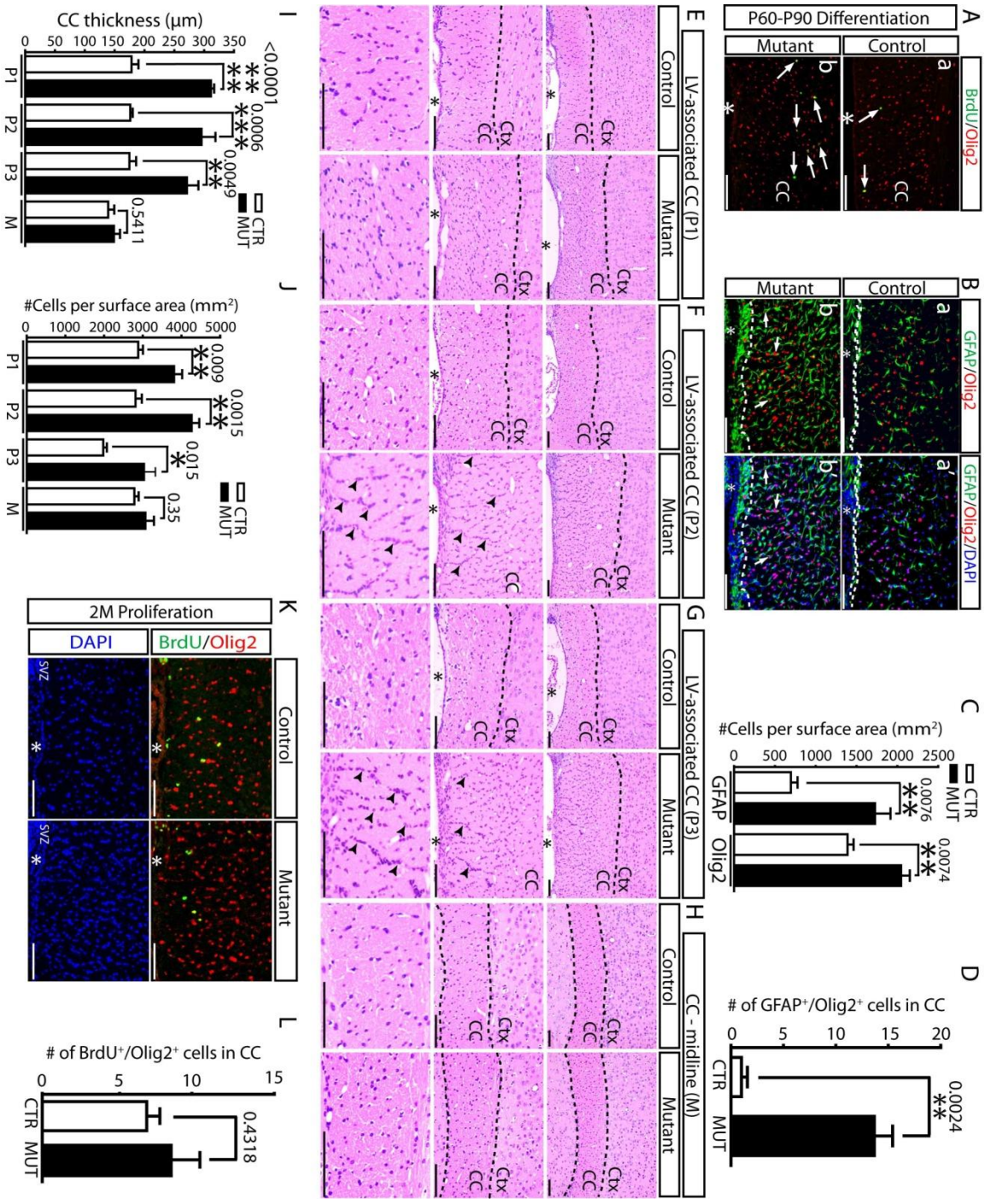
A
P60-P90 Differentiation
Mutant
Control
BrdU/Olig2
B
GFAP/Olig2
GFAP/Olig2/DAPI
C
#Cells per surface area (mm²)
GFAP
Olig2
CTR
MUT
0.0076
0.0074
D
# of GFAP⁺/Olig2⁺ cells in CC
0.0024
E
LV-associated CC (P1)
F
LV-associated CC (P2)
G
LV-associated CC (P3)
H
CC - midline (M)
Control
Mutant
Ctx
CC
I
CC thickness (µm)
P1
P2
P3
M
<0.0001
0.0006
0.0049
0.5411
J
#Cells per surface area (mm²)
0.009
0.0015
0.015
0.35
K
2M Proliferation
DAPI
BrdU/Olig2
SVZ
L
# of BrdU⁺/Olig2⁺ cells in CC
0.4318

Figure 31. Increased gliogenesis leads to structural defects in the CC of *Nf1*^{hGFAP}KO brains.

(A) In the P60-P90 BrdU differentiation assay, increased oligodendrogenesis, marked by Brdu/Olig2, was found in mutant CC. Arrows label Brdu^{+}/Olig2^{+} cells.

(B) and (C) Number and density of GFAP^{+} astrocytes and Olig2^{+} oligodendrocytes were dramatically increased in mutant CC. Of note, cells expressing both GFAP and Olig2 were also increased (D). Dashed lines roughly delineate the border of SVZ and LV. Arrowheads label colocalizing cells and arrows represent noncolocalizing cells.

(E)-(H) H&E–stained paraffin sections from 4 different histological planes. The thickness and cell density of CC were quantified and compared in (I) and (J). Aside from the midline position, enlargement of CC was found in Position 1-Position 3 sections. Arrows highlight cells that were clustered in the CC. Dashed lines roughly delineate the dorsal border of CC.

(K) and (L) 2 month BrdU proliferation assay. Local proliferation of Olig2^{+} cells was not increased in mutant CC based on the quantification (panel L) of BrdU/Olig2 double positive cells.

Scale bars, 50μ.

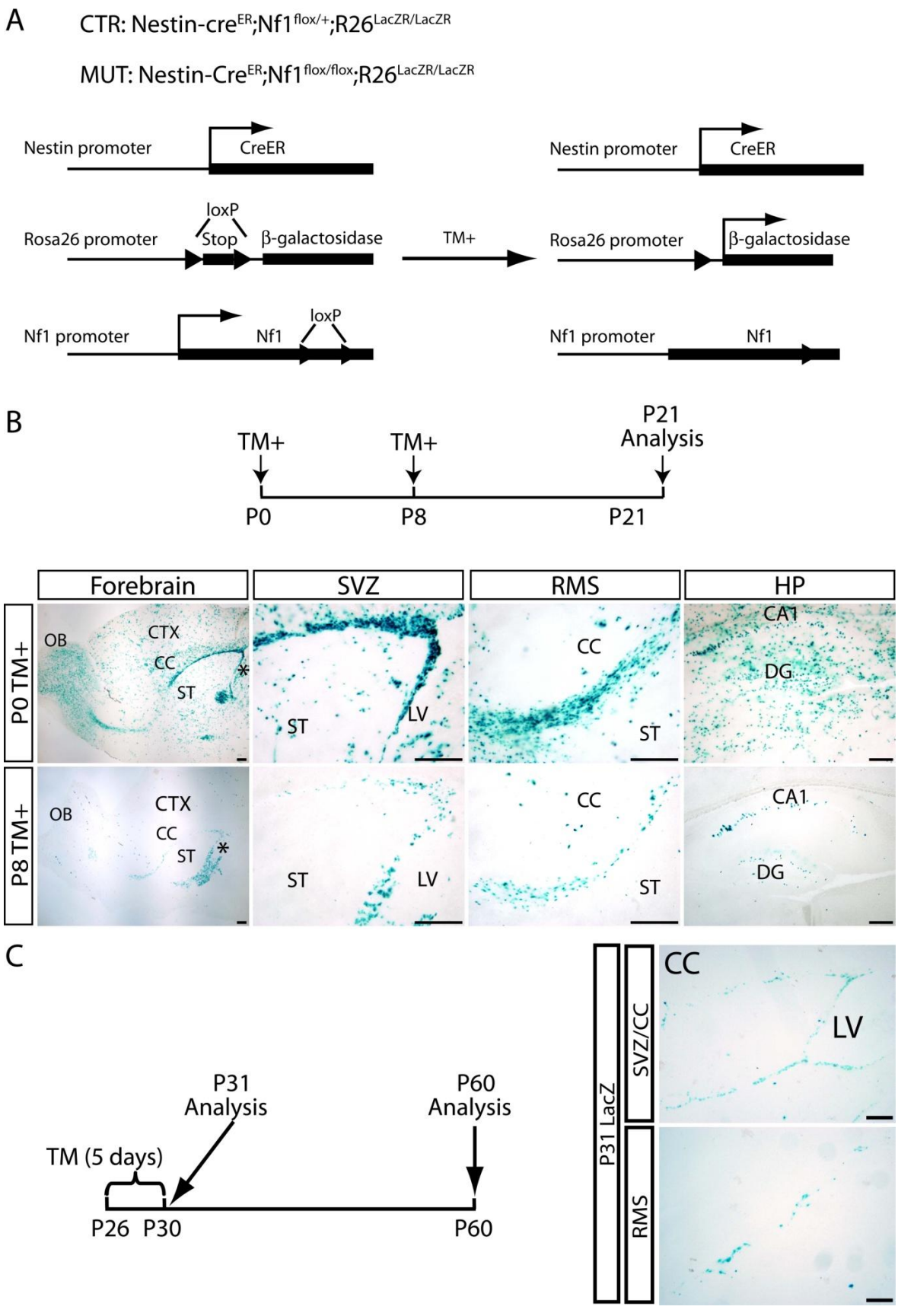
A
CTR: Nestin-cre^{ER};Nf1$^{flox/+}$;R26$^{LacZR/LacZR}$
MUT: Nestin-Cre^{ER};Nf1$^{flox/flox}$;R26$^{LacZR/LacZR}$
Nestin promoter
CreER
loxP
Rosa26 promoter
Stop
β-galactosidase
TM+
Nf1 promoter
Nf1
B
TM+
TM+
P21 Analysis
P0
P8
P21
Forebrain
SVZ
RMS
HP
P0 TM+
P8 TM+
OB
CTX
CC
ST
LV
CA1
DG
C
P31 Analysis
P60 Analysis
TM (5 days)
P26 P30
P60
P31 LacZ
SVZ/CC
RMS

Figure 32. Characterization of the Nestin-Cre^{ER} strain.
(A) Genetic configuration of the inducible mouse model and how tamoxifen (TM) induction leads to conditional inactivation of *Nf1* (see text for details).
(B) Control mice were induced at P0 or P8 and analyzed at P21. LacZ staining was performed on brain sections to label targeted cells. While P0.5 induction targeted a large number of cells in the brain, P8-induced recombinant cells were more restricted in SVZ/RMS/CC/OB system. Hippocampus area also exhibited robust recombination.
(C) Young adult mice were induced from P26-P30 and analyzed at P31, one day after the completion of TM induction. The cells undergoing Cre-mediated recombination revealed by LacZ staining were restrictedly distributed in the SVZ (upper panel) and RMS (lower panel), as well as SGL in the hippocampus, but not in any other brain regions.
Scale bars, 50μ.

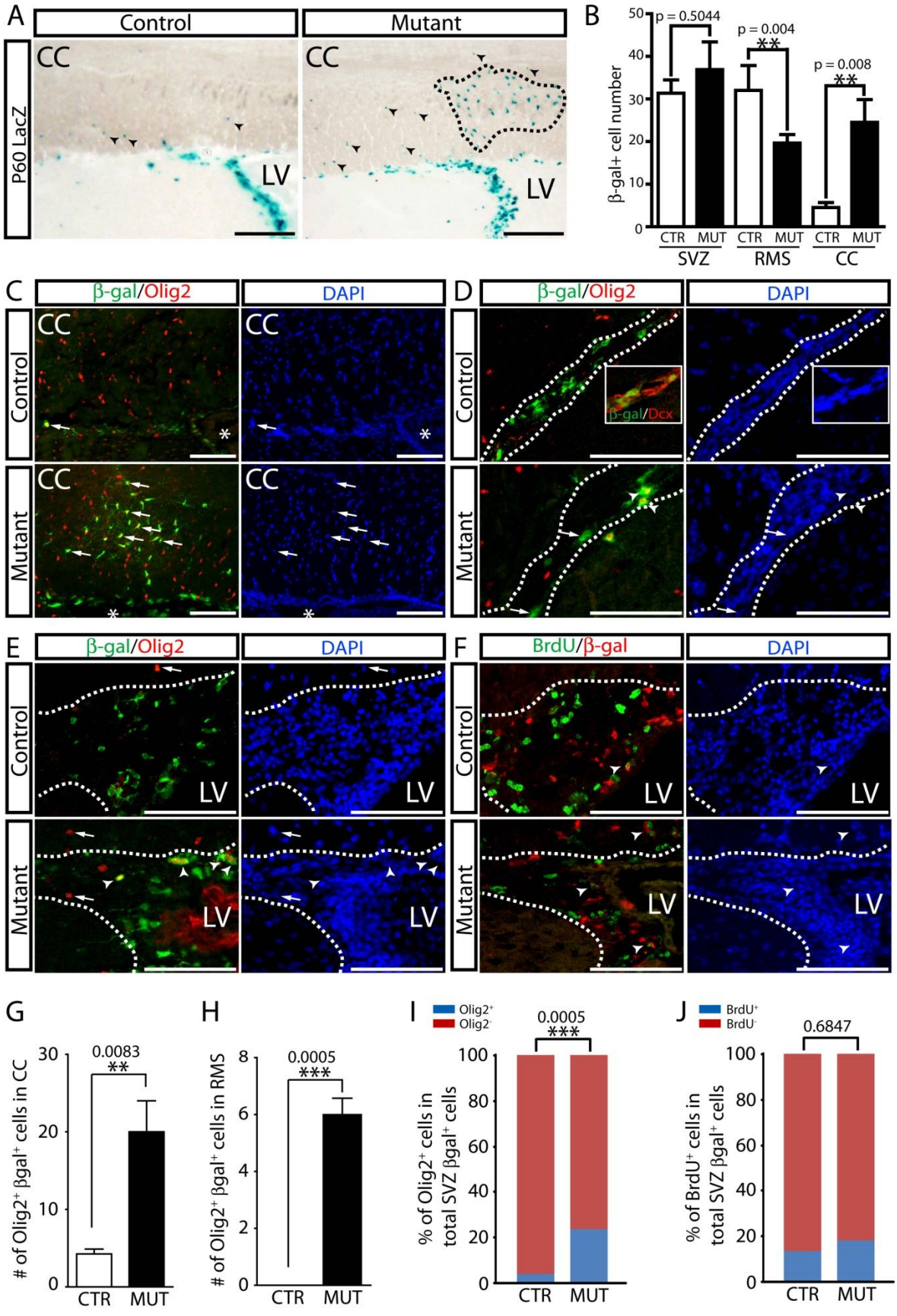
A
Control
Mutant
P60 LacZ
CC
LV
B
β-gal+ cell number
p = 0.5044
p = 0.004
p = 0.008
**
**
CTR MUT CTR MUT CTR MUT
SVZ RMS CC
C
β-gal/Olig2
DAPI
Control
Mutant
D
β-gal/Olig2
DAPI
β-gal/Dcx
E
β-gal/Olig2
DAPI
F
BrdU/β-gal
DAPI
G
# of Olig2⁺ βgal⁺ cells in CC
0.0083
**
H
# of Olig2⁺ βgal⁺ cells in RMS
0.0005
***
I
Olig2⁺
Olig2⁻
% of Olig2⁺ cells in total SVZ βgal⁺ cells
0.0005
***
J
BrdU⁺
BrdU⁻
% of BrdU⁺ cells in total SVZ βgal⁺ cells
0.6847

Figure 33. Acute inactivation of *Nf1* is sufficient to induce fate switch in the adult SVZ.
(A) LacZ staining of TM-induced control and mutant brains at P60, a month after P26-P30 TM induction. In control brains, only a small population of $LacZ^+$ cells was found in the overlying CC (Left panel). In contrast, $LacZ^+$ cells dramatically increased and formed clusters (marked by dashed lines) in the CC of TM-induced mutant brains (Right panel).
(B) Quantification of $\beta\text{-gal}^+$ cells in SVZ/RMS/ CC.
(C) The majority of $\beta\text{-gal}^+$ cells were $Olig2^+$ in both control and mutant CC. Arrows point to the colocalizing cells. Panel (G) is the quantification for the number of $\beta\text{-gal}^+$ /$Olig2^+$ cells in the CC.
(D) The number of $\beta\text{-gal}^+$ cells was reduced in mutant RMS, and many of the $\beta\text{-gal}^+$ cells ectopically expressed Olig2 instead of neuroblast marker Dcx (inset). Panel (H) is the quantification for the number of $\beta\text{-gal}^+$ /$Olig2^+$ cells in the RMS.
(E) The ratio of Olig2-expressing cells in the $\beta\text{-gal}^+$ cell compartment was increased in mutant SVZ. Panel (I) is the quantification.
(F) The proliferation rate of $\beta\text{-gal}^+$ cells marked by BrdU/β-gal in the SVZ was comparable between mutant and controls, quantified in (J).
Arrows label the non-colocalizing cells and arrowheads point to colocalizing cells. Dashed lines delineate the SVZ and/or RMS region. *, lateral ventricle. Scale bars, 50μ.

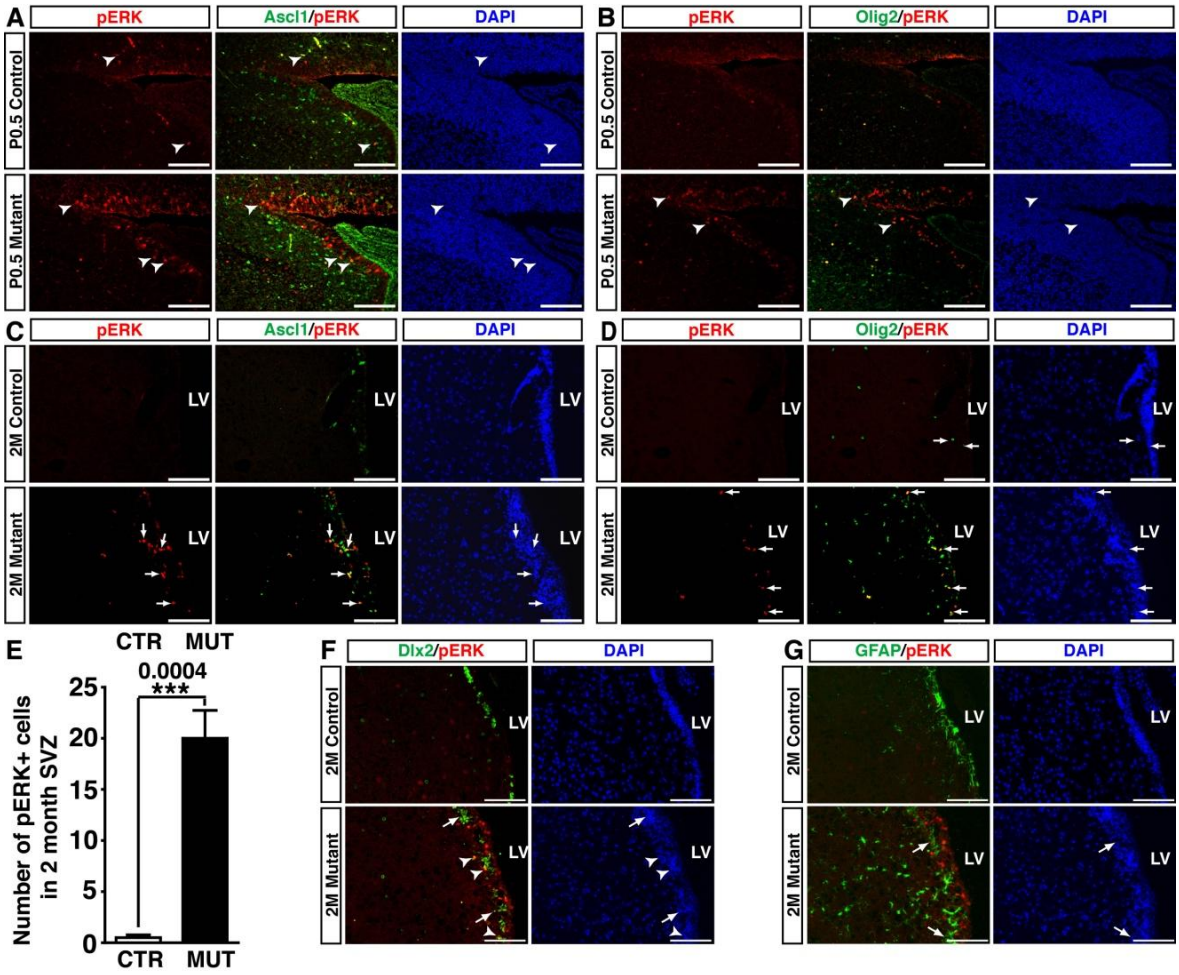

Figure 34. *Nf1*-deficiency leads to specific ERK activation in SVZ progenitors.
(A)-(B) Activation of ERK signaling was found in both control and mutant SVZ at P0.5 through p-ERK immunofluorescence. Mutant SVZ already contained more p-ERK^{+} cells, and many of them were expressing Ascl1 and/or Olig2.
(C)-(E) In 2 month old brains, p-ERK staining was barely detected in control SVZ, while in mutants, p-ERK^{+} cells persisted and were restricted to Ascl1^{+} and/or Olig2^{+} cells.
(F) and (G) The majority of Dlx2^{+} cells did not express pERK, and no pERK expression was found in GFAP^{+} cells.
Arrows label the non-colocalizing cells and arrowheads point to colocalizing cells. *, lateral ventricle. Scale bars, 50 μ.

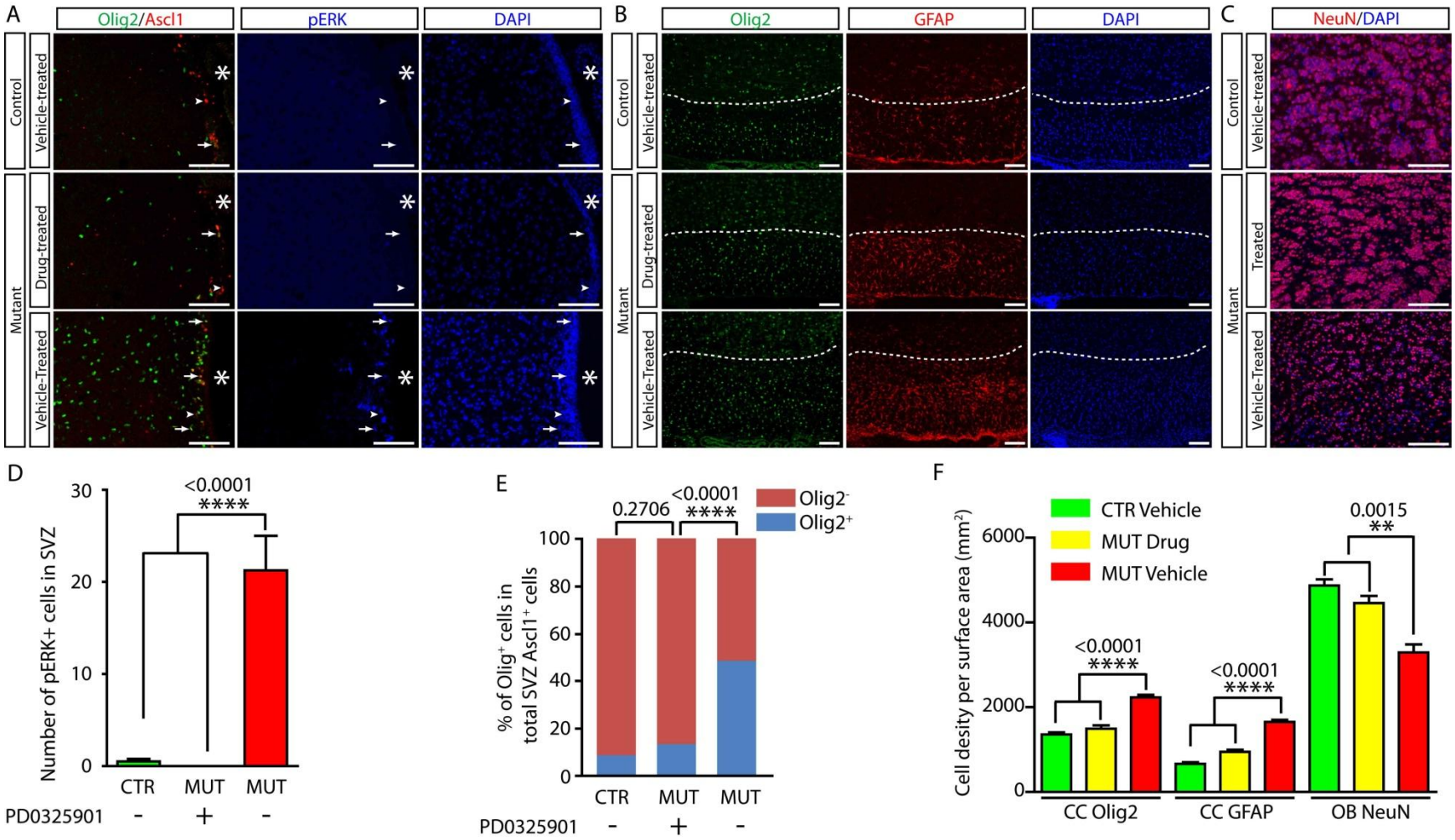
A
Olig2/Ascl1
pERK
DAPI
Control
Vehicle-treated
Mutant
Drug-treated
Vehicle-Treated
B
Olig2
GFAP
DAPI
C
NeuN/DAPI
Treated
D
Number of pERK+ cells in SVZ
<0.0001
****
CTR
MUT
MUT
PD0325901
E
% of Olig+ cells in total SVZ Ascl1+ cells
0.2706
<0.0001
****
Olig2-
Olig2+
F
Cell desity per surface area (mm2)
CTR Vehicle
MUT Drug
MUT Vehicle
0.0015
**
CC Olig2
CC GFAP
OB NeuN

Figure 35. MEK inhibitor treatment rescues the CC and OB phenotypes in *Nf1*^{hGFAP}KO mice through inhibition of ERK in SVZ progenitors.

Nf1^{hGFAP}KO mice were treated with MEK inhibitor PD0325901 from P0.5-P18, and compared to vehicle-treated control mice and *Nf1*^{hGFAP}KO mice.

(A) Triple labeling of p-ERK/Ascl1/Olig2 demonstrated that MEK inhibitor treatment inhibits ERK signaling in SVZ Olig2^{+}/Ascl1^{+} cells (quantified in D). Such inhibition of ERK signaling restored Olig2 expression to control level (quantified in E).

(B) After treatment, in the CC, the density of Olig2^{+} cells in MEKi-treated *Nf1*^{hGFAP}KO brains was rescued to the level of vehicle-treated controls; the density of GFAP^{+} cells, albeit not completely rescued, was significantly reduced compared to that of vehicle-treated mutants. Dashed lines mark the dorsal border of CC.

(C) In the OB, neuronal density was significantly increased after MEKi treatment.

(D) Quantification of GFAP^{+} and Olig2^{+} cells in the CC and NeuN^{+} cells in the OB. Statistical comparison was performed by Anova test.

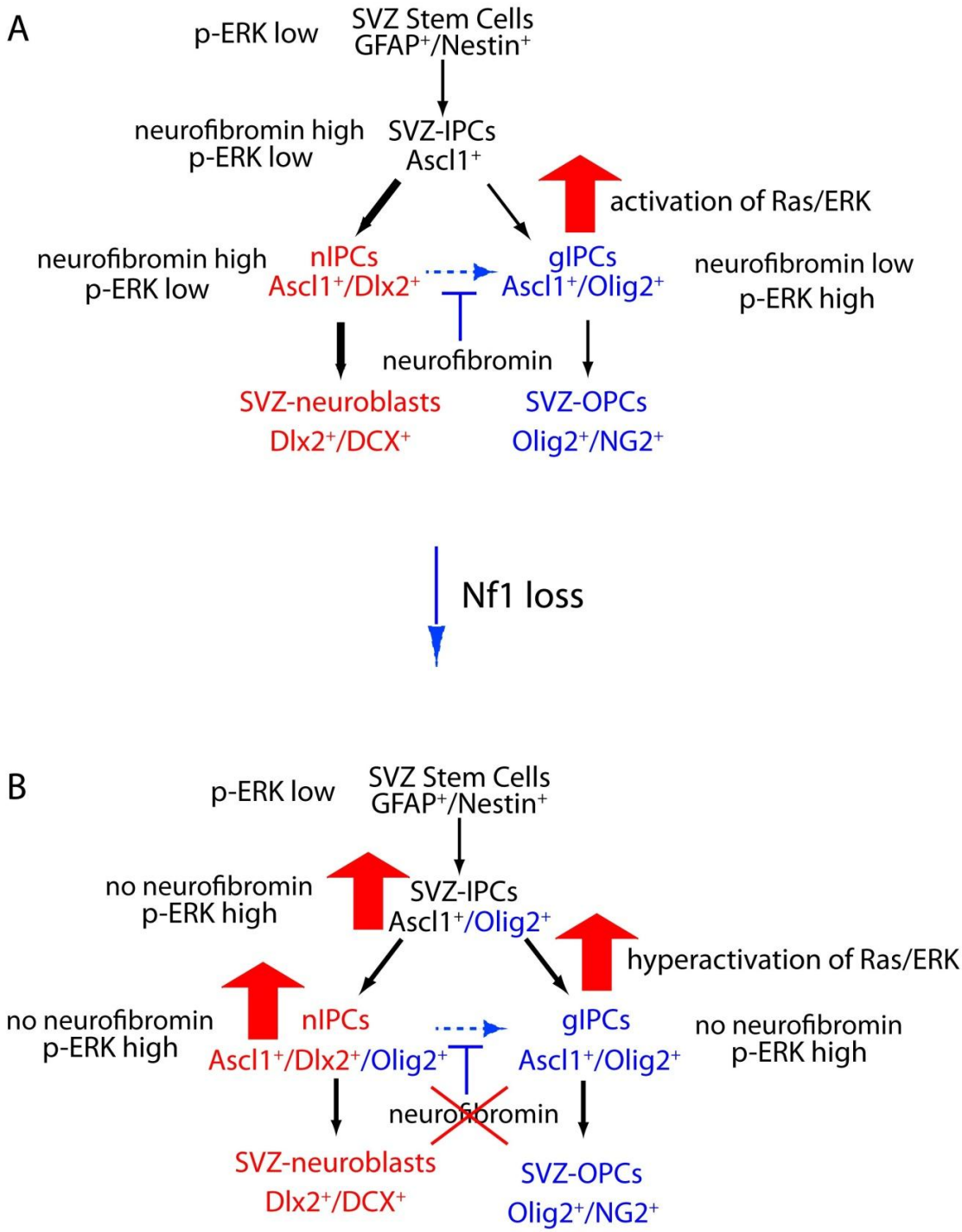
A
p-ERK low
SVZ Stem Cells
GFAP+/Nestin+
neurofibromin high
p-ERK low
SVZ-IPCs
Ascl1+
activation of Ras/ERK
neurofibromin high
p-ERK low
nIPCs
Ascl1+/Dlx2+
gIPCs
Ascl1+/Olig2+
neurofibromin low
p-ERK high
neurofibromin
SVZ-neuroblasts
Dlx2+/DCX+
SVZ-OPCs
Olig2+/NG2+
Nf1 loss
B
p-ERK low
SVZ Stem Cells
GFAP+/Nestin+
no neurofibromin
p-ERK high
SVZ-IPCs
Ascl1+/Olig2+
hyperactivation of Ras/ERK
no neurofibromin
p-ERK high
nIPCs
Ascl1+/Dlx2+/Olig2+
gIPCs
Ascl1+/Olig2+
no neurofibromin
p-ERK high
neurofibromin
SVZ-neuroblasts
Dlx2+/DCX+
SVZ-OPCs
Olig2+/NG2+

Figure 36. Proposed model of how neurofibromin regulates SVZ C cell fate specification in adult.
(A) In *Nf1* wildtype mice, the Ascl1^{+} cells are bipotent intermediate progenitors and have the potential to acquire a neuronal or glial fate. Upon commitment to glial intermediate progenitors (gIPCs), Ascl1^{+} cells downregulate *Nf1* and activate Ras/ERK signaling to promote Olig2 expression, while neuronal committed progenitors (nIPCs) maintain high level of *Nf1* to inhibit Ras/ERK signaling and prevent misexpression of Olig2.
(B) In *Nf1*^{hGFAP}KO brains, Ras/ERK signaling is dysregulated in Ascl1^{+} cells and nIPCs due to the loss of *Nf1*. Overactive Ras/ERK activity leads to expression of Olig2 in these cells and ultimately specify these cells to the glial linage.
Red arrows indicate the Ras/ERK signaling activation, red represents the neuronal lineage and blue represents the glial lineage.

3.5 References

Alberta JA, Park SK, Mora J, Yuk D, Pawlitzky I, Iannarelli P, Vartanian T, Stiles CD, Rowitch DH. 2001. Sonic hedgehog is required during an early phase of oligodendrocyte development in mammalian brain. *Mol Cell Neurosci* **18**: 434-441.

Ballester R, Marchuk D, Boguski M, Saulino A, Letcher R, Wigler M, Collins F. 1990. The NF1 locus encodes a protein functionally related to mammalian GAP and yeast IRA proteins. *Cell* **63**: 851-859.

Barrett SD, Bridges AJ, Dudley DT, Saltiel AR, Fergus JH, Flamme CM, Delaney AM, Kaufman M, LePage S, Leopold WR et al. 2008. The discovery of the benzhydroxamate MEK inhibitors CI-1040 and PD 0325901. *Bioorg Med Chem Lett* **18**: 6501-6504.

Bilican B, Fiore-Heriche C, Compston A, Allen ND, Chandran S. 2008. Induction of Olig2 precursors by FGF involves BMP signalling blockade at the Smad level. *PLoS One* **3**: e2863.

Campbell K, Gotz M. 2002. Radial glia: multi-purpose cells for vertebrate brain development. *Trends Neurosci* **25**: 235-238.

Chandran S, Kato H, Gerreli D, Compston A, Svendsen CN, Allen ND. 2003. FGF-dependent generation of oligodendrocytes by a hedgehog-independent pathway. *Development* **130**: 6599-6609.

Cichowski K, Jacks T. 2001. NF1 tumor suppressor gene function: narrowing the GAP. *Cell* **104**: 593-604.

Cui Y, Costa RM, Murphy GG, Elgersma Y, Zhu Y, Gutmann DH, Parada LF, Mody I, Silva AJ. 2008. Neurofibromin regulation of ERK signaling modulates GABA release and learning. *Cell* **135**: 549-560.

Dasgupta B, Gutmann DH. 2005. Neurofibromin regulates neural stem cell proliferation, survival, and astroglial differentiation in vitro and in vivo. *J Neurosci* **25**: 5584-5594.

Dubovsky EC, Booth TN, Vezina G, Samango-Sprouse CA, Palmer KM, Brasseux CO. 2001. MR imaging of the corpus callosum in pediatric patients with neurofibromatosis type 1. *AJNR Am J Neuroradiol* **22**: 190-195.

Friedman JM, Riccardi VM. 1999. *Neurofibromatosis : phenotype, natural history, and pathogenesis*. Johns Hopkins University Press, Baltimore.

Hack MA, Saghatelyan A, de Chevigny A, Pfeifer A, Ashery-Padan R, Lledo PM, Gotz M. 2005. Neuronal fate determinants of adult olfactory bulb neurogenesis. *Nat Neurosci* **8**: 865-872.

Hegedus B, Dasgupta B, Shin JE, Emnett RJ, Hart-Mahon EK, Elghazi L, Bernal-Mizrachi E, Gutmann DH. 2007. Neurofibromatosis-1 regulates neuronal and glial cell differentiation from neuroglial progenitors in vivo by both cAMP- and Ras-dependent mechanisms. *Cell Stem Cell* **1**: 443-457.

Hyman SL, Shores A, North KN. 2005. The nature and frequency of cognitive deficits in children with neurofibromatosis type 1. *Neurology* **65**: 1037-1044.

Ivkovic S, Canoll P, Goldman JE. 2008. Constitutive EGFR signaling in oligodendrocyte progenitors leads to diffuse hyperplasia in postnatal white matter. *J Neurosci* **28**: 914-922.

Jackson EL, Garcia-Verdugo JM, Gil-Perotin S, Roy M, Quinones-Hinojosa A, VandenBerg S, Alvarez-Buylla A. 2006. PDGFR alpha-positive B cells are neural stem cells in the adult SVZ that form glioma-like growths in response to increased PDGF signaling. *Neuron* **51**: 187-199.

Kessaris N, Jamen F, Rubin LL, Richardson WD. 2004. Cooperation between sonic hedgehog and fibroblast growth factor/MAPK signalling pathways in neocortical precursors. *Development* **131**: 1289-1298.

Kriegstein A, Alvarez-Buylla A. 2009. The glial nature of embryonic and adult neural stem cells. *Annu Rev Neurosci* **32**: 149-184.

Listernick R, Charrow J, Gutmann DH. 1999. Intracranial gliomas in neurofibromatosis type 1. *Am J Med Genet* **89**: 38-44.

Listernick R, Louis DN, Packer RJ, Gutmann DH. 1997. Optic pathway gliomas in children with neurofibromatosis 1: consensus statement from the NF1 Optic Pathway Glioma Task Force. *Ann Neurol* **41**: 143-149.

Lu QR, Sun T, Zhu Z, Ma N, Garcia M, Stiles CD, Rowitch DH. 2002. Common developmental requirement for Olig function indicates a motor neuron/oligodendrocyte connection. *Cell* **109**: 75-86.

Marshall CA, Novitch BG, Goldman JE. 2005. Olig2 directs astrocyte and oligodendrocyte formation in postnatal subventricular zone cells. *J Neurosci* **25**: 7289-7298.

Menn B, Garcia-Verdugo JM, Yaschine C, Gonzalez-Perez O, Rowitch D, Alvarez-Buylla A. 2006. Origin of oligodendrocytes in the subventricular zone of the adult brain. *J Neurosci* **26**: 7907-7918.

Merkle FT, Alvarez-Buylla A. 2006. Neural stem cells in mammalian development. *Curr Opin Cell Biol* **18**: 704-709.

Moore BD, 3rd, Slopis JM, Jackson EF, De Winter AE, Leeds NE. 2000. Brain volume in children with neurofibromatosis type 1: relation to neuropsychological status. *Neurology* **54**: 914-920.

Petryniak MA, Potter GB, Rowitch DH, Rubenstein JL. 2007. Dlx1 and Dlx2 control neuronal versus oligodendroglial cell fate acquisition in the developing forebrain. *Neuron* **55**: 417-433.

Pride N, Payne JM, Webster R, Shores EA, Rae C, North KN. 2010. Corpus callosum morphology and its relationship to cognitive function in neurofibromatosis type 1. *J Child Neurol* **25**: 834-841.

Rodriguez-Viciana P, Tetsu O, Tidyman WE, Estep AL, Conger BA, Cruz MS, McCormick F, Rauen KA. 2006. Germline mutations in genes within the MAPK pathway cause cardio-facio-cutaneous syndrome. *Science (New York, NY* **311**: 1287-1290.

Soriano P. 1999. Generalized lacZ expression with the ROSA26 Cre reporter strain. *Nat Genet* **21**: 70-71.

Zhou Q, Anderson DJ. 2002. The bHLH transcription factors OLIG2 and OLIG1 couple neuronal and glial subtype specification. *Cell* **109**: 61-73.

Zhu Y, Harada T, Liu L, Lush ME, Guignard F, Harada C, Burns DK, Bajenaru ML, Gutmann DH, Parada LF. 2005. Inactivation of NF1 in CNS causes increased glial progenitor proliferation and optic glioma formation. *Development* **132**: 5577-5588.

Zhuo L, Theis M, Alvarez-Maya I, Brenner M, Willecke K, Messing A. 2001. hGFAP-cre transgenic mice for manipulation of glial and neuronal function in vivo. *Genesis* **31**: 85-94.

Chapter IV Discussion

4.1 p53 and *Nf1* in glioma development

4.1.1 The sequential order and respective contribution of p53 and *Nf1* loss in glioma development

The objective of my thesis project is to understand the role of the tumor suppressors p53 and *Nf1* in neural stem cells and how loss of these tumor suppressors could independently and cooperatively transform neural stem cells into cancer cells. Our p53 glioma mouse models demonstrate that a p53-deficiency alone can efficiently induce malignant glioma formation in mice. Furthermore, in all instances in which *Nf1* is lost either simultaneously or subsequent to loss of p53 (Mut1, Mut3 and CKO3 in Table 1) (Mut1: hGFAPCre+; p53 KO/KO; *Nf1* flox/flox; Mut3: hGFAPCre+; p53 KO/+; *Nf1* flox/+; CKO3: hGFAPCre+; p53 flox/flox; *Nf1* KO/+), the rate of glioma formation was greatly enhanced (Zhu et al. 2005; Wang et al. 2009). This suggests that *Nf1*-deficiency cooperates with p53-deficiency to promote tumorigenesis. However, *Nf1* deficiency alone is insufficient for malignant transformation; $Nf1^{hGFAP}$KO mice could live up to a year without brain tumor development. More strikingly, as Zhu et al. demonstrated in their 2005 paper, when *Nf1*-deficiency is induced prior to loss of p53 glioma rarely arose (Mut2 on Table 1) (Mut2: hGFAPCre+; p53 KO/+; *Nf1* flox/flox) (Zhu et al. 2005). Together, these observations suggest that in order to efficiently promote gliomagenesis, p53 must be inactivated prior to or simultaneously with *Nf1*. The order of genetic mutations and tumor penetrance in different mouse models are summarized in Table 1. Such sequential order of p53 and *Nf1* inactivation is supported by Attolini et al. in 2010 who employed mathematic modeling to deduce the temporal sequence of genetic mutations based on genomic data of human glioblastoma (Attolini et al. 2010). These findings are consistent with the clinical observation that p53 mutations are among the

earliest genetic lesions in human gliomas (Maher et al. 2001; Ohgaki et al. 2004; Furnari et al. 2007). However, two central questions remain unaddressed: 1) in a p53 wildtype or heterozygous background, how *Nf1*-deficient cells are resistant to malignant transformation and 2) in a p53-deficient background, how Nf1-deficiency promotes gliomagenesis.

One potential explanation for why *Nf1*-deficient cells do not progress to malignancy is that additional oncogenic mutations are required for glioma transformation, and only p53 deficiency could provide a permissive environment for these cells to accumulate such mutations. However, this alone does not explain the stark contrast between models where *Nf1* is lost prior to p53 (Mut2) and simultaneous *Nf1* and p53 loss (Mut3) in terms of glioma penetrance. As shown in Figure 37A, via co-LOH, both Mut2 and Mut3 require only one genetic event to become p53/*Nf1* double deficient. Mut2 mice also have the additional option of acquiring loss of function mutations at the p53 locus. If the accumulation of additional oncogenic mutations in p53-deficient cells is the rate-limiting step for gliomagenesis, we would expect Mut2 and Mut3 to develop gliomas at a similar rate. In fact, while the tumor penetrance in Mut3 mice is 100%, only 1 out of 18 Mut2 mice develop brain tumors (Zhu et al. 2005). The huge difference in glioma incidence between Mut2 and Mut3 leads us to propose that in cells that have undergone loss of *Nf1* in the presence of wildtype p53, *Nf1*-deficiency must trigger a p53-mediated response(s) to eliminate the oncogenic potential of $Nf1^{-/-}$ cells (Mut2). Such p53-mediated response(s) are absent in cells that have undergone simultaneous loss of *Nf1* and p53 (Mut3). This model of cellular events makes the reasonable assumptions that *Nf1* heterozygosity does not elicit this p53 response and that the loss of the wildtype *Nf1* allele accompanied by the loss of p53 precludes any p53-mediated response. This can potentially resolve how *Nf1*-deficient cells are resistant to malignant transformation in the context of functional p53.

It has been well documented that p53 is activated in response to stress signals including DNA damage, oxidative stress and oncogenic mutations. The activation of p53 and its downstream transcriptional targets could result in one of three cellular responses:

transient cell-cycle arrest, permanent cell-cycle arrest (senescence) and apoptosis (Vogelstein et al. 2000; Junttila and Evan 2009; Kruse and Gu 2009; Vousden and Prives 2009). When cells suffer from low level stress or DNA damage, p53 induces transient cell-cycle arrest and activates DNA repair proteins to fix the damage. If DNA damage is severe or irreparable, p53 initiates senescence or apoptosis to remove these damaged cells. In *Nf1*-deficient brains, we did not observe any change in the incidence of apoptosis either during neonatal development or adulthood. Apoptosis is therefore unlikely to be the mechanism that protects *Nf1*-deficient SVZ cells from malignant transformation. A recent study in human glioma cell lines demonstrated that *Nf1* inactivation can induce a p53-dependent senescence response (McGillicuddy et al. 2009). However, our *in vivo* analysis demonstrated that *Nf1*-deficiency does not alter the proliferation rate of SVZ cells nor prevent differentiation, suggesting that a large number of $Nf1^{-/-}$ SVZ progenitors remain in the cell cycle and do not undergo cellular senescence. Our *in vitro* neurosphere assay also suggests that *Nf1-/-* SVZ progenitors normally proliferate and form primary neurospheres comparable to their WT counterparts. Alternatively, p53 may induce transient cell cycle arrest and restrict the number or length of cell cycles in *Nf1*-deficient progenitors, which would ultimately differentiate and become resistant to malignant transformation. In support of this hypothesis, we identified that the most dramatic difference between $Nf1^{-/-}$ and $Nf1^{+/+}$ SVZ progenitors is their ability to form secondary neurospheres. The ratio of the number of secondary neurospheres to primary neurospheres was dramatically reduced in $Nf1^{hGFAP}$KO cells compared to controls, which indicates that under culture conditions, $Nf1^{-/-}$ progenitors have reduced self-renewal capacity and can only undergo limited number of cell cycles. Consistently, p53 has been shown to be a negative regulator of neural stem cell self-renewal in neurosphere assays (Meletis et al. 2006). Based on these observations, we hypothesize that p53 eliminates the oncogenic potential of *Nf1-/-* progenitors by suppressing their self-renewal capacity through restriction of the number/length of cell cycles. We can directly test this hypothesis *in vivo* by comparing the number/length of cell cycles of $Nf1^{-/-}$ progenitors with $Nf1^{+/+}$ progenitors using a short-term BrdU pulse-chase experiment. Mice will be pulsed with BrdU once and analyzed 24 hours later. By using Ki67 as a marker for cells that remain in cell cycle, we could identify cells that exit the cell cycle after 24h as

$BrdU^+/Ki67^-$, and the cells that remain in or re-enter the cell cycle will be marked as $BrdU^+/Ki67^+$. The ratio of $BrdU^+/Ki67^-$ vs. $BrdU^+/Ki67^+$ represent a "cell cycle exit index (CCEI)" and reflects the relative fraction of cells that exit the cell cycle and begin to differentiate versus cells that remain in the cell cycle (Chenn and Walsh 2002). Based on our hypothesis, we predict that *Nf1*$^{-/-}$ progenitors are more likely to exit the cell cycle and have a higher CCEI value. In addition, if *Nf1*-deficiency leads to reduced self-renewal *in vivo*, we would expect to see a gradual depletion of SVZ neural progenitor cells in *Nf1*-deficient brains. The ideal system to test this is the Nestin-Cre^{ER} inducible model. By introducing *Nf1* mutation into a subset of adult neural stem/progenitor cells through tamoxifen-induced Cre activation, we could monitor the long-term fate of these *Nf1*$^{-/-}$ progenitors with the R26^{LacZ} reporter and determine whether they are more likely to be eliminated in the SVZ compared to *Nf1* heterozygous or wild type cells. To further determine whether reduced self-renewal of *Nf1*$^{-/-}$ progenitors is dependent on p53, we could analyze the Mut1 brains, which are p53/*Nf1* double-deficient, and investigate whether p53-deficiency could rescue the *in vivo* and *in vitro* self-renewal defects of *Nf1*$^{-/-}$ progenitors. More specifically, we could compare the CCEI of p53/*Nf1* double-deficient SVZ progenitors with *Nf1*$^{-/-}$ progenitors, and test their secondary-sphere-forming capacity in neurosphere assays. The proposed model is summarized in Figure 37B.

The second question to address is how loss of *Nf1*, in the context of *p53*-deficiency, accelerates glioma development. In the p53 model, we demonstrated that Olig2-expressing SVZ-C-like cells are the cell-of-origin for gliomas, and Ligon et al have demonstrated that Olig2 plays a critical role in promoting the proliferation of neural stem cells and malignant glioma cells through its inhibition of tumor suppressor p21 (Ligon et al. 2007). Our finding that *Nf1* regulates Olig2 expression specifically in SVZ-C cells leads us to hypothesize that ectopic activation of Olig2 could be the underlying mechanism for *Nf1*-deficiency to promote gliomagenesis. However, while *Nf1*-deficiency significantly expands the number of Olig2 $^+$ cells in the brain, many of these cells are well-differentiated oligodendrocytes, and Olig2$^+$ glial progenitors do not overproliferate. One possible explanation for this is the phosphorylation status of Olig2 in *Nf1*-deficient cells. Recent studies have identified that the proliferative function of Olig2 in glioma

cells is dependent on the phosphorylation of Olig2 triple-serine motif (Sun et al. 2011), and *Nf1*-deficiency may not promote phosphorylation of Olig2 at this specific site. One intriguing possibility is that in the *p53*-deficient background, either through blockade of p53-mediated response, or through accumulation of additional oncogenic mutations, Olig2 becomes phosphorylated at this triple-serine motif. Under such circumstances, *Nf1*-deficiency may provide a much larger pool of target cells available for malignant transformation by activating Olig2 overexpression in SVZ progenitors. This model of how *Nf1* may promote gliomagenesis can be tested using an antibody that specifically recognizes the phosphorylated form of Olig2 at this triple-serine motif.

In summary, my study on p53 and *Nf1* mouse models underscores the significance of the sequential order of genetic mutations in tumor development. This set of data opens up many directions toward the understanding of how these two tumor suppressors interact and synergistically promote gliomagenesis.

4.1.2 The uniqueness of our p53 $^{\Delta E5\text{-}6}$ glioma mouse model and its clinical implications

Our p53 $^{\Delta E5\text{-}6}$ mouse model is unique because, as opposed to existing GEM glioma mouse models that inactivate multiple tumor suppressors (Reilly et al. 2000; Zhu et al. 2005; Zheng et al. 2008), we introduce only the initiating mutation, allowing stochastic accumulation of additional oncogenic mutations. This model therefore more closely recapitulates the stepwise accumulation of oncogenic mutations in human tumor development (Maher et al. 2001). Another unique feature of our p53 $^{\Delta E5\text{-}6}$ model is that the expression of mutant p53 can be used as a marker to identify early glioma cells. Although advanced-stage p53$^{\Delta E5\text{-}6}$ gliomas are extremely heterogeneous histopathologically and molecularly, the p53$^{\Delta E5\text{-}6}$-positive glioma precursors are remarkably homogeneous in terms of lineage marker expression and are likely driven by the activation of limited number of signaling pathways. Further characterization of these early glioma cells at different stages of glioma development would allow us to pinpoint the sequential order of the activation of oncogenic pathways in an *in vivo* setting and identify genetic pathways that are critical for the glioma initiation, progression and

maintenance. For instance, our preliminary data demonstrate that $p53^{\Delta E5-6}$-expressing cells in the CC of 4.5-5 month old mice already have high level of ERK activation based on pERK immunofluorescence, suggesting that the activation of Ras/ERK signaling could be among the early genetic events that drive the initial expansion of glioma precursor cells (unpublished observation). Targeting these signaling pathways could be used as therapies to treat individuals who are genetically predisposed to glioma development and eliminate the tumor initiating cells in their brains. Finally, since $p53^{\Delta E5-6}$ mice provide a sensitive genetic background and can cooperate with oncogenic mutations (such as *Nf1*) to promote glioma development, this strain could be used to validate newly identified glioma genes and investigate their respective role in gliomagenesis. In addition, compound mutants may also generate a series of fast-growing GBM models that can be used for preclinical testing of therapies that target more specific oncogenic pathways.

4.1.3 Potential oncogenic activity of $p53^{\Delta E5-6}$ protein

In human cancers, TP53-associated tumors typically contain missense mutations in the TP53 gene rather than deletions of TP53 (Olivier et al. 2002). These mutant p53 proteins are highly expressed in endstage tumor cells, suggesting possible growth advantage for cells with missense mutations (Sigal and Rotter 2000). The oncogenic roles of mutant p53 alleles have been examined extensively in cell lines (Iwamoto et al. 1996; Gualberto et al. 1998; Li et al. 1998; Blandino et al. 1999; Murphy et al. 2000; Dong et al. 2007). Mouse models that inherit p53 mutations expressed at physiological levels have recently been generated to examine the activities of mutant p53 *in vivo* (Duan et al. 2002; Lang et al. 2004; Olive et al. 2004; Heinlein et al. 2008; Adorno et al. 2009). In these models, mice with p53 hotspot point mutations develop tumor spectrums and metastatic phenotypes different from those of mice with a p53-null allele. Mechanisms for this gain-of-function potential include increased genomic instability, increased cell migration and invasion and resistance to proapoptotic signals (Oren and Rotter 2010). Many gain-of-function effects of mutant p53 rely on its ability to bind and inactivate the p53 family members p63 and p73 (Gaiddon et al. 2001; Oren and Rotter 2010).

Although the same $p53^{\Delta E5-6}$ mutation is not found in human gliomas (Olivier et al. 2002), our mouse model phenocopies the histological features of human GBM and exhibits high level of $p53^{\Delta E5-6}$ accumulation in tumor cells. Previous studies reported no brain tumor formation in p53 germline knockout mice (Gil-Perotin et al. 2006; Meletis et al. 2006), and $p53^{-/-}$ mice in our colony with a similar genetic background to CKO1 and CKO2 mice do not develop brain tumors. This raises the question whether $p53^{\Delta E5-6}$ could have oncogenic activities similar to p53 missense mutations. The comparison of $p53^{\Delta E5-6}$, p53 hotspot point mutation (R172H) and p53 conditional null allele is an ongoing project in the lab carried out by Dr. Yinghua Li. His preliminary data suggest that mutant p53, compared to p53 conditional null, does increase the genetic instability and promote the survival of cells after irradiation. However, $p53^{\Delta E5-6}$, p53 R172H and p53 conditional null mice develop glioma at a similar rate and penetrance (personal communication). This could be due to the fact that our genetic targeting strategy using hGFAP-Cre is targeting too many cells in the brain, which masked the difference between mutant p53 and p53 conditional null in their tumorigenic capacity. Whether mutant p53 has oncogenic activity in gliomagenesis could be better tested in the Nestin-Cre^{ER} inducible system, which targets much fewer cells in adult brain and allows for the assessment of whether increased genetic instability/survival in a relatively minor population of cells could contribute to increased glioma penetrance.

4.2. *Nf1* in neural progenitor fate specification and cognitive deficits

4.2.1 Potential mechanism for the regulation of Olig2 expression by Neurofibromin

Multiple lines of evidence suggest that neurofibromin may inhibit Olig2 expression via negative regulation of receptor tyrosine kinases, specifically by suppressing the Ras/ERK signaling pathway. Ras acts as a major second messenger for receptor tyrosine kinases. Neurofibromin contains GTPase Activating Protein (GAP) related domain, which converts active Ras-GTP to inactive Ras-GDP. Erk/MAPK is an effector pathway of Ras, therefore inhibition of Ras by neurofibromin will also result in suppression of the Erk/MAPK pathway. There have been numerous studies that have linked Ras/ERK

activity to Olig2 expression. BMP/Smad signaling plays a crucial role in establishing dorsal neural identity and its inhibition is sufficient to generate OPCs both *in vitro* and *in vivo* (Mekki-Dauriac et al. 2002; Munoz-Sanjuan and Brivanlou 2002; Vallstedt et al. 2005; Bilican et al. 2008). Activation of the Sonic hedgehog (Shh) pathway, which opposes BMP signaling in ventral neural tube, can promote Olig2 expression in neocortical progenitor cells and induce oligodendrocyte progenitor production (Lu et al. 2002; Zhou and Anderson 2002). Kessaris et al. demonstrated that Shh activity is dependent on ERK signaling (Kessaris et al. 2004). In cultured dorsal spinal cord cells, fibroblast growth factor 2 (FGF2) induces Olig2 expression, which can be inhibited by a MEK inhibitor (Bilican et al. 2008). This observation suggests that FGF2-induced Olig2 expression depends on the Ras/ERK signaling pathway. In the forebrain, overexpression of growth factors, i.e. epidermal growth factor (EGF) or platelet-derived growth factor (PDGF), can lead to overproduction of $Olig2^+$ cells in SVZ and CC (Chandran et al. 2003; Jackson et al. 2006; Ivkovic et al. 2008). However, the specific cell type(s) that are responsive to EGF/PDGF overexpression have not yet been determined. In addition, these studies did not offer data to support any mechanisms that could account for the expansion of Olig2-expressing cells.

Our study demonstrates that *Nf1* regulates Olig2 expression in SVZ $Ascl1^+$ cells through Ras/ERK signaling, which plays an important role in SVZ progenitor fate specification and regulates the overall output of neurogenesis and gliogenesis. Consistently, we found that in control brains, the level of Ras/ERK signaling activation corresponds to the level of gliogenesis. Phosphorylated ERK levels, a readout for active Erk/MAPK activity, are very low in the adult brain where there is minimal gliogenesis in adult. In contrast, we found a number of $pERK^+$ cells colocalizing with Olig2 in the SVZ at early postnatal stages, the peak period of gliogenesis in the brain, suggesting a role for Ras/ERK signaling during the normal gliogenesis process. In addition, MEK inhibitor treatment of *Nf1*-deficient mice not only repressed Olig2 expression in SVZ progenitors, but also rescued the neuron-glial output in the brain, suggesting that *Nf1*-deficient phenotype is indeed caused by overactivation of Ras/ERK signaling. Based on these findings we propose the following model for the fate specification of $Ascl1^+$ SVZ cells: $Ascl1^+$ cells

are bipotent and can undergo specification to acquire either a neuronal or glial fate. Upon commitment to glial intermediate progenitors (gIPCs), Ascl1^{+} cells downregulate *Nf1* and activate Ras/ERK signaling to promote Olig2 expression, while neuronal committed progenitors (nIPCs) maintain high level of *Nf1* to inhibit Ras/ERK signaling and prevent misexpression of Olig2. In *Nf1*^{hGFAP}KO brains, Ras/ERK signaling transduction activity is dysregulated in Ascl1^{+} cells and nIPCs due to the loss of its negative regulator, *Nf1*. Overactive Ras/ERK activity leads to expression of Olig2 in these cells, ultimately resulting in a fate switch from the neuronal lineage to the glial lineage.

This model of how neurofibromin regulates the expression of Olig2 not only addresses important questions concerning neural progenitor fate specification, but also opens up many directions for follow-up studies. First, the relationship between Ras/ERK signaling and increased Olig2 expression in Ascl1^{+} cells has yet to be defined. A recent publication by Bilican et al. demonstrated that in dorsal spinal cord, FGF-induced ERK signaling counteracts BMP signaling by deactivating Smad1, the major effecter in the BMP signaling pathway. Upon activation, ERK phosphorylates the linker region of Smad1, preventing nuclear translocation and thus inhibits Smad1 transcriptional activity (Bilican et al. 2008). It is possible that this is a conserved mechanism for different types of progenitors in the CNS. Second, the upstream signal that activates Ras/ERK signaling cascade in SVZ cells is yet to be determined. As aforementioned, Shh signaling, as well as activation of RTK signaling through growth factors FGF/EGF/PDGF could all be likely candidates. Finally, how Ras/ERK activity is dynamically regulated in neuronal committed nIPCs and glial committed gIPCs still remains to be uncovered. One possible mechanism could be that these two cell populations have different neurofibromin levels. This could be achieved through differential transcriptional or post-transcriptional regulation of *Nf1* gene expression. However, based on the Alan Brain Atlas which provides the *in situ* hybridization data for *Nf1*, at mRNA level there is no evidence that different SVZ cells have different *Nf1* transcription (Lein et al. 2007). Alternatively, the level of neurofibromin could be regulated by protein degradation. One candidate molecule that regulates neurofibromin degradation is F-box and WD repeat domain-containing 7 (FBW7). FBW7 is a substrate-recognition component of the SKP1, CUL1

and F-box (SCF) complex, an E3 ubiquitin ligase. Dr. Yi Sun at the University of Michigan has recently provided *in vitro* evidence that FBW7 recognizes neurofibromin and targets neurofibromin for degradation through ubiquitination (personal communication). In addition, my colleague from the Zhu Lab, Dr. Huarui Zheng, found reduced number of $Olig2^{+}$ cells in FBW7 conditional knockout mice accompanied by increased *Nf1* expression (personal communication). These findings lead to the intriguing possibility that FBW7 specifically degrades neurofibromin in gIPCs to maintain high level of Ras/ERK signaling in these cells. Assessment of the protein level of FBW7 and neurofibromin in different progenitor cells will be key experiments to test this hypothesis. To perform cell-type specific analysis, it is necessary to introduce transgenic reporters to facilitate effective sorting of different population of SVZ cells. Previously published strains that carry Ascl1-GFP and Olig2-GFP reporters could be very useful in these experiments (Marshall et al. 2005; Parras et al. 2007).

4.2.2 Corpus callosum defect and NF1-associated learning disabilities

One unique feature of our mouse model is that *Nf1*^{hGFAP}KO mice exhibit an enlarged corpus callosum, a common structural abnormality found in the brains of a subset of NF1 patients with severe cognitive deficits. Importantly, as MEK inhibition rescued the enlarged corpus collusum and glial specification phenotype found in *Nf1*^{hGFAP}KO mice, a similar treatment during neonatal development might serve as a therapeutic strategy in NF1 patients to alleviate associated neurocognitive defects. These results may have a broader clinical implication in NCFC syndromes caused by germline mutations in the oncogenic Ras/ERK signaling pathway, which all have cognitive impairment as a common symptom (Rodriguez-Viciana et al. 2006).

The remaining questions include how an enlarged corpus callosum is related to learning disabilities and whether rescuing the structural defect could rescue the cognitive deficits. To address these questions, we need to first confirm that *Nf1*-deficient mice exhibit learning disabilities as seen in NF1 patients. However, *Nf1*^{hGFAP}KO mice are not the ideal model for behavioral analysis because they have hindlimb paralysis and thus cannot be subjected to behavioral analysis. The exact cause of such hindlimb paralysis is yet to be

determined. One notable observation is that in our Nestin-Cre^{ER} inducible model, when *Nf1*-deficiency is introduced into a restricted number of SVZ Nestin-expressing cells at P26-P30, we did not observe any hindlimb defects, suggesting that it is most likely a developmental phenotype caused by the widespread genetic recombination in CNS and PNS induced by hGFAP-Cre (Zhuo et al. 2001). Although we did find an increase of oligodendrocytes in the CC in these mice, the number of targeted cells is too small to recapitulate the enlarged CC phenotype in *Nf1*^{hGFAP}KO mice. Yet this opens up a possibility that there may exist a time point earlier than P26-P30 to induce differentiation, which targets a sufficient amount of cells in the brain to recapitulate the CC phenotype without causing hindlimb paralysis. This would allow us to analyze the behavioral alterations in *Nf1* mutant mice and determine whether they have learning disabilities. If so, we could treat these mice with MEK inhibitors and assess cognitive impairment with or without treatment.

Besides behavior studies, it is important to understand how an enlarged corpus callosum can lead to cognitive deficits. The corpus callosum is a thick band of neural fibers that connects the left and right cerebral hemispheres and facilitates interhemispheric communication by transferring motor, sensory, and cognitive information between the brain hemispheres (Raybaud 2010). To establish a structure-function relationship between enlarged corpus callosum and cognitive deficits, we need to determine whether the *Nf1*^{hGFAP}KO corpus callosum is structurally compromised for interhemispheric communication. We will first perform EM analysis on control and *Nf1*^{hGFAP}KO corpus callosum and specifically compare the number of axons and their myelination status. In the CNS, a single oligodendrocyte can ensheath and myelinate multiple axons. Myelination is critical for the quick and accurate transmission of electrical current from one nerve cell to the next, and demyelination could lead to a number of clinical symptoms including cognitive disruption such as speech impairment and memory loss (Jessen and Mirsky 2008). However, since *Nf1*^{hGFAP}KO corpus callosum has increased number of oligodendrocytes which can normally produce myelin (based on myelin basic protein MBP immunostaining), it is unlikely that cognitive defect in *Nf1*^{hGFAP}KO mice is due to demyelination. Rather, we would expect increased myelination in *Nf1*^{hGFAP}KO

corpus callosum and one possibility is that excessive myelination interferes with the integration and processing of information, ultimately resulting in diminished cognitive performance. Alternatively, it is equally possible that while *Nf1*-deficient oligodendrocytes could produce myelin, they could not properly entheath axons. This could be readily tested in EM ultrastructural analysis. Further, we will perform electrophysiological analysis to directly compare the signal transmission capacity of axons in wildtype and $Nf1^{hGFAP}$KO corpus callosum.

4.3. Summary

In this thesis, I used genetically engineered mouse models to investigate the role of the tumor suppressor genes *Nf1* and p53 in the regulation of neural stem/progenitor cell function. My study has made significant insights into basic developmental biology and glioma development. These mouse models could provide valuable tools for future studies to explore the mechanism underlying gliomagenesis and NF1-associated learning deficits and could be used for preclinical trials to treat these diseases.

Table 1. Summary of p53/*Nf1* glioma models

Mouse models	**Genetic configuration**	**Sequential order of genetic mutations**	**Glioma penetrance**	**Tumorigenesis rate**
Mut1	hGFAPCre+; p53 KO/KO; *Nf1* flox/flox	Loss of **p53** in germline **first**, followed by tissue specific inactivation of *Nf1*	high	fast
CKO3	hGFAPCre+; p53 flox/flox; *Nf1* KO/+	Tissue specific inactivation of **p53 first** in a *Nf1* HET background, then loss of the *Nf1* WT allele through **LOH**	high	fast
Mut3	hGFAPCre+; p53 KO/+; *Nf1* flox/+	Loss of the WT chromosome through **Co-LOH**; **concurrent loss of p53 and *Nf1***	high	slow
Mut2	hGFAPCre+; p53 KO/+; *Nf1* flox/flox	Tissue specific inactivation of ***Nf1* first** in a p53 HET background, then loss of the p53 WT allele through **Co-LOH**	extremely low	slow
CKO1 and CKO2	hGFAPCre+; p53 KO/flox or flox/flox	Tissue specific inactivation of **p53** in a *Nf1* WT background	high	slow
$Nf1^{hGFAP}$CKO	hGFAPCre+; *Nf1* flox/flox	Tissue specific inactivation of ***Nf1*** in a p53 WT background	none	none

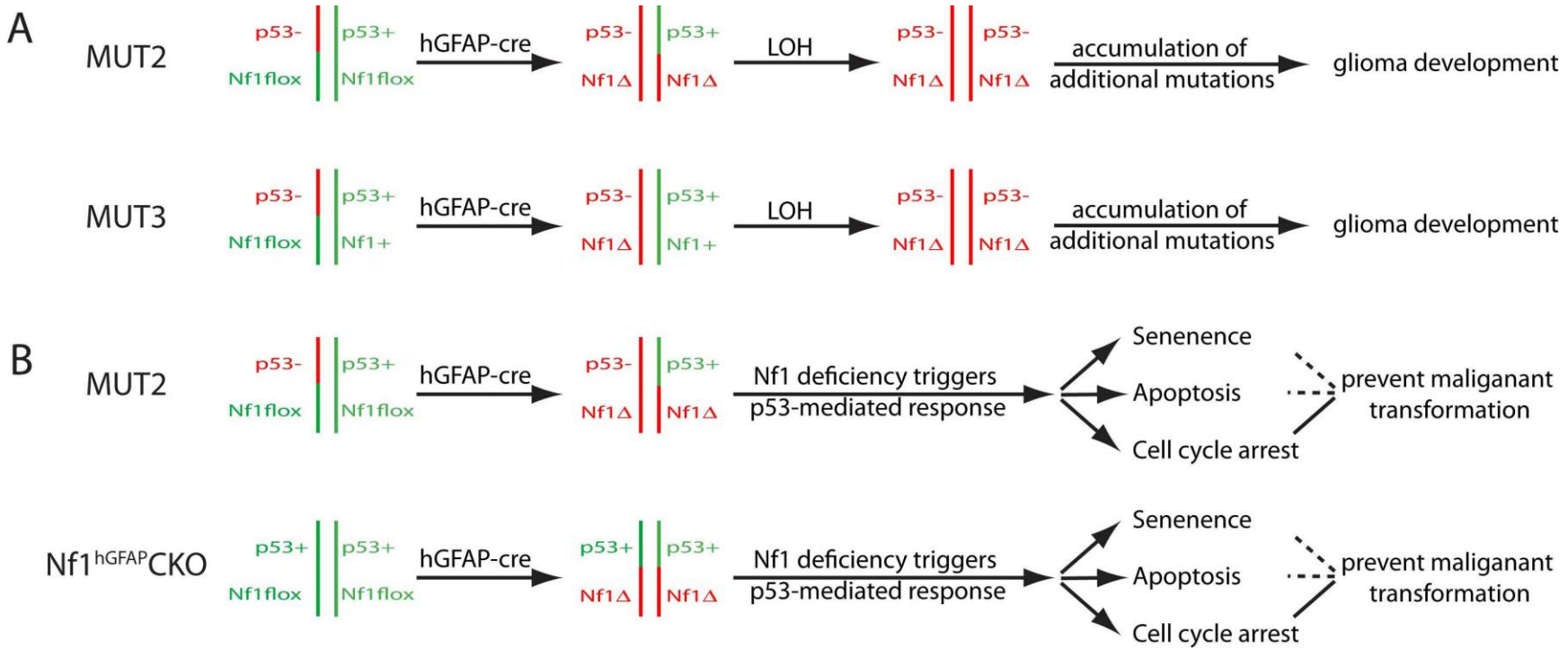
A
MUT2
p53-
Nf1flox
p53+
Nf1flox
hGFAP-cre
p53-
Nf1Δ
p53+
Nf1Δ
LOH
p53-
Nf1Δ
p53-
Nf1Δ
accumulation of
additional mutations
glioma development
MUT3
p53-
Nf1flox
p53+
Nf1+
hGFAP-cre
p53-
Nf1Δ
p53+
Nf1+
LOH
p53-
Nf1Δ
p53-
Nf1Δ
accumulation of
additional mutations
glioma development
B
MUT2
p53-
Nf1flox
p53+
Nf1flox
hGFAP-cre
p53-
Nf1Δ
p53+
Nf1Δ
Nf1 deficiency triggers
p53-mediated response
Senenence
Apoptosis
Cell cycle arrest
prevent maliganant
transformation
Nf1hGFAPCKO
p53+
Nf1flox
p53+
Nf1flox
hGFAP-cre
p53+
Nf1Δ
p53+
Nf1Δ
Nf1 deficiency triggers
p53-mediated response
Senenence
Apoptosis
Cell cycle arrest
prevent maliganant
transformation

Figure 37. Proposed model for genetic events that occur during glioma development in different mouse models. (A) Illustration why Mut2 and Mut3 mice have equal chance to develop gliomas if accumulation of additional mutations is the rate-limiting step of gliomagenesis. (B) Proposed model for the tumor prevention machinery in Mut2 and *Nf1*^{hGFAP}CKO mice.

4.4 References

Adorno M, Cordenonsi M, Montagner M, Dupont S, Wong C, Hann B, Solari A, Bobisse S, Rondina MB, Guzzardo V et al. 2009. A Mutant-p53/Smad complex opposes p63 to empower TGFbeta-induced metastasis. *Cell* **137**: 87-98.

Attolini CS, Cheng YK, Beroukhim R, Getz G, Abdel-Wahab O, Levine RL, Mellinghoff IK, Michor F. 2010. A mathematical framework to determine the temporal sequence of somatic genetic events in cancer. *Proc Natl Acad Sci U S A* **107**: 17604-17609.

Bilican B, Fiore-Heriche C, Compston A, Allen ND, Chandran S. 2008. Induction of Olig2 precursors by FGF involves BMP signalling blockade at the Smad level. *PLoS One* **3**: e2863.

Blandino G, Levine AJ, Oren M. 1999. Mutant p53 gain of function: differential effects of different p53 mutants on resistance of cultured cells to chemotherapy. *Oncogene* **18**: 477-485.

Chandran S, Kato H, Gerreli D, Compston A, Svendsen CN, Allen ND. 2003. FGF-dependent generation of oligodendrocytes by a hedgehog-independent pathway. *Development* **130**: 6599-6609.

Chenn A, Walsh CA. 2002. Regulation of cerebral cortical size by control of cell cycle exit in neural precursors. *Science* **297**: 365-369.

Dong P, Tada M, Hamada J, Nakamura A, Moriuchi T, Sakuragi N. 2007. p53 dominant-negative mutant R273H promotes invasion and migration of human endometrial cancer HHUA cells. *Clin Exp Metastasis* **24**: 471-483.

Duan W, Ding H, Subler MA, Zhu WG, Zhang H, Stoner GD, Windle JJ, Otterson GA, Villalona-Calero MA. 2002. Lung-specific expression of human mutant p53-273H is associated with a high frequency of lung adenocarcinoma in transgenic mice. *Oncogene* **21**: 7831-7838.

Furnari FB, Fenton T, Bachoo RM, Mukasa A, Stommel JM, Stegh A, Hahn WC, Ligon KL, Louis DN, Brennan C et al. 2007. Malignant astrocytic glioma: genetics, biology, and paths to treatment. *Genes Dev* **21**: 2683-2710.

Gaiddon C, Lokshin M, Ahn J, Zhang T, Prives C. 2001. A subset of tumor-derived mutant forms of p53 down-regulate p63 and p73 through a direct interaction with the p53 core domain. *Mol Cell Biol* **21**: 1874-1887.

Gil-Perotin S, Marin-Husstege M, Li J, Soriano-Navarro M, Zindy F, Roussel MF, Garcia-Verdugo JM, Casaccia-Bonnefil P. 2006. Loss of p53 induces changes in the behavior of subventricular zone cells: implication for the genesis of glial tumors. *J Neurosci* **26**: 1107-1116.

Gualberto A, Aldape K, Kozakiewicz K, Tlsty TD. 1998. An oncogenic form of p53 confers a dominant, gain-of-function phenotype that disrupts spindle checkpoint control. *Proc Natl Acad Sci U S A* **95**: 5166-5171.

Heinlein C, Krepulat F, Lohler J, Speidel D, Deppert W, Tolstonog GV. 2008. Mutant p53(R270H) gain of function phenotype in a mouse model for oncogene-induced mammary carcinogenesis. *Int J Cancer* **122**: 1701-1709.

Ivkovic S, Canoll P, Goldman JE. 2008. Constitutive EGFR signaling in oligodendrocyte progenitors leads to diffuse hyperplasia in postnatal white matter. *J Neurosci* **28**: 914-922.

Iwamoto KS, Mizuno T, Ito T, Tsuyama N, Kyoizumi S, Seyama T. 1996. Gain-of-function p53 mutations enhance alteration of the T-cell receptor following X-irradiation, independently of the cell cycle and cell survival. *Cancer Res* **56**: 3862-3865.

Jackson EL, Garcia-Verdugo JM, Gil-Perotin S, Roy M, Quinones-Hinojosa A, VandenBerg S, Alvarez-Buylla A. 2006. PDGFR alpha-positive B cells are neural stem cells in the adult SVZ that form glioma-like growths in response to increased PDGF signaling. *Neuron* **51**: 187-199.

Jessen KR, Mirsky R. 2008. Negative regulation of myelination: relevance for development, injury, and demyelinating disease. *Glia* **56**: 1552-1565.

Junttila MR, Evan GI. 2009. p53--a Jack of all trades but master of none. *Nat Rev Cancer* **9**: 821-829.

Kessaris N, Jamen F, Rubin LL, Richardson WD. 2004. Cooperation between sonic hedgehog and fibroblast growth factor/MAPK signalling pathways in neocortical precursors. *Development* **131**: 1289-1298.

Kruse JP, Gu W. 2009. Modes of p53 regulation. *Cell* **137**: 609-622.

Lang GA, Iwakuma T, Suh YA, Liu G, Rao VA, Parant JM, Valentin-Vega YA, Terzian T, Caldwell LC, Strong LC et al. 2004. Gain of function of a p53 hot spot mutation in a mouse model of Li-Fraumeni syndrome. *Cell* **119**: 861-872.

Lein ES Hawrylycz MJ Ao N Ayres M Bensinger A Bernard A Boe AF Boguski MS Brockway KS Byrnes EJ et al. 2007. Genome-wide atlas of gene expression in the adult mouse brain. *Nature* **445**: 168-176.

Li R, Sutphin PD, Schwartz D, Matas D, Almog N, Wolkowicz R, Goldfinger N, Pei H, Prokocimer M, Rotter V. 1998. Mutant p53 protein expression interferes with p53-independent apoptotic pathways. *Oncogene* **16**: 3269-3277.

Ligon KL, Huillard E, Mehta S, Kesari S, Liu H, Alberta JA, Bachoo RM, Kane M, Louis DN, Depinho RA et al. 2007. Olig2-regulated lineage-restricted pathway controls replication competence in neural stem cells and malignant glioma. *Neuron* **53**: 503-517.

Lu QR, Sun T, Zhu Z, Ma N, Garcia M, Stiles CD, Rowitch DH. 2002. Common developmental requirement for Olig function indicates a motor neuron/oligodendrocyte connection. *Cell* **109**: 75-86.

Maher EA, Furnari FB, Bachoo RM, Rowitch DH, Louis DN, Cavenee WK, DePinho RA. 2001. Malignant glioma: genetics and biology of a grave matter. *Genes Dev* **15**: 1311-1333.

Marshall CA, Novitch BG, Goldman JE. 2005. Olig2 directs astrocyte and oligodendrocyte formation in postnatal subventricular zone cells. *J Neurosci* **25**: 7289-7298.

McGillicuddy LT, Fromm JA, Hollstein PE, Kubek S, Beroukhim R, De Raedt T, Johnson BW, Williams SM, Nghiemphu P, Liau LM et al. 2009. Proteasomal and genetic inactivation of the NF1 tumor suppressor in gliomagenesis. *Cancer Cell* **16**: 44-54.

Mekki-Dauriac S, Agius E, Kan P, Cochard P. 2002. Bone morphogenetic proteins negatively control oligodendrocyte precursor specification in the chick spinal cord. *Development* **129**: 5117-5130.

Meletis K, Wirta V, Hede SM, Nister M, Lundeberg J, Frisen J. 2006. p53 suppresses the self-renewal of adult neural stem cells. *Development* **133**: 363-369.

Munoz-Sanjuan I, Brivanlou AH. 2002. Neural induction, the default model and embryonic stem cells. *Nat Rev Neurosci* **3**: 271-280.

Murphy KL, Dennis AP, Rosen JM. 2000. A gain of function p53 mutant promotes both genomic instability and cell survival in a novel p53-null mammary epithelial cell model. *FASEB J* **14**: 2291-2302.

Ohgaki H, Dessen P, Jourde B, Horstmann S, Nishikawa T, Di Patre PL, Burkhard C, Schuler D, Probst-Hensch NM, Maiorka PC et al. 2004. Genetic pathways to glioblastoma: a population-based study. *Cancer Res* **64**: 6892-6899.

Olive KP, Tuveson DA, Ruhe ZC, Yin B, Willis NA, Bronson RT, Crowley D, Jacks T. 2004. Mutant p53 gain of function in two mouse models of Li-Fraumeni syndrome. *Cell* **119**: 847-860.

Olivier M, Eeles R, Hollstein M, Khan MA, Harris CC, Hainaut P. 2002. The IARC TP53 database: new online mutation analysis and recommendations to users. *Hum Mutat* **19**: 607-614.

Oren M, Rotter V. 2010. Mutant p53 gain-of-function in cancer. *Cold Spring Harb Perspect Biol* **2**: a001107.

Parras CM, Hunt C, Sugimori M, Nakafuku M, Rowitch D, Guillemot F. 2007. The proneural gene Mash1 specifies an early population of telencephalic oligodendrocytes. *J Neurosci* **27**: 4233-4242.

Raybaud C. 2010. The corpus callosum, the other great forebrain commissures, and the septum pellucidum: anatomy, development, and malformation. *Neuroradiology* **52**: 447-477.

Reilly KM, Loisel DA, Bronson RT, McLaughlin ME, Jacks T. 2000. Nf1;Trp53 mutant mice develop glioblastoma with evidence of strain-specific effects. *Nat Genet* **26**: 109-113.

Rodriguez-Viciana P, Tetsu O, Tidyman WE, Estep AL, Conger BA, Cruz MS, McCormick F, Rauen KA. 2006. Germline mutations in genes within the MAPK pathway cause cardio-facio-cutaneous syndrome. *Science (New York, NY* **311**: 1287-1290.

Sigal A, Rotter V. 2000. Oncogenic mutations of the p53 tumor suppressor: the demons of the guardian of the genome. *Cancer Res* **60**: 6788-6793.

Sun Y, Meijer DH, Alberta JA, Mehta S, Kane MF, Tien AC, Fu H, Petryniak MA, Potter GB, Liu Z et al. 2011. Phosphorylation state of Olig2 regulates proliferation of neural progenitors. *Neuron* **69**: 906-917.

Vallstedt A, Klos JM, Ericson J. 2005. Multiple dorsoventral origins of oligodendrocyte generation in the spinal cord and hindbrain. *Neuron* **45**: 55-67.

Vogelstein B, Lane D, Levine AJ. 2000. Surfing the p53 network. *Nature* **408**: 307-310.

Vousden KH, Prives C. 2009. Blinded by the Light: The Growing Complexity of p53. *Cell* **137**: 413-431.

Wang Y, Yang J, Zheng H, Tomasek GJ, Zhang P, McKeever PE, Lee EY, Zhu Y. 2009. Expression of mutant p53 proteins implicates a lineage relationship between neural stem cells and malignant astrocytic glioma in a murine model. *Cancer Cell* **15**: 514-526.

Zheng H, Ying H, Yan H, Kimmelman AC, Hiller DJ, Chen AJ, Perry SR, Tonon G, Chu GC, Ding Z et al. 2008. p53 and Pten control neural and glioma stem/progenitor cell renewal and differentiation. *Nature* **455**: 1129-1133.

Zhou Q, Anderson DJ. 2002. The bHLH transcription factors OLIG2 and OLIG1 couple neuronal and glial subtype specification. *Cell* **109**: 61-73.

Zhu Y, Guignard F, Zhao D, Liu L, Burns DK, Mason RP, Messing A, Parada LF. 2005. Early inactivation of p53 tumor suppressor gene cooperating with NF1 loss induces malignant astrocytoma. *Cancer Cell* **8**: 119-130.

Zhuo L, Theis M, Alvarez-Maya I, Brenner M, Willecke K, Messing A. 2001. hGFAP-cre transgenic mice for manipulation of glial and neuronal function in vivo. *Genesis* **31**: 85-94.